THE
PHYSICAL REVIEW
A journal of experimental and theoretical physics established by E. L. Nichols in 1893

SECOND SERIES, VOL. 64, NOS. 7 AND 8 OCTOBER 1 AND 15, 1943

The Width of X-Ray Diffraction Lines From Cold-Worked Tungsten and α-Brass*

CHARLES S. SMITH†
AND
E. E. STICKLEY**
University of Pittsburgh, Pittsburgh, Pennsylvania
(Received August 7, 1943)

The x-ray line width from specimens of cold worked α-brass and tungsten has been measured as a function of Bragg angle and of x-ray wave-length. The results are in agreement with a microstress theory of broadening. In α-brass the line width is found to depend on crystallographic direction in a systematic manner while with tungsten it does not. Both observations are explained on the basis of the elastic properties of the materials.

INTRODUCTION

ONE of the most striking phenomena connected with the cold working of polycrystalline metals is the broadening, in certain cases, of the x-ray diffraction lines. Thus, when well-annealed α-brass is cold worked by rolling to a 30 percent reduction in area, the width of the 420 diffraction line increases from 3×10^{-3} radian, to 30×10^{-3} radian, the width being defined as the full angular width at half-maximum intensity.

This x-ray phenomenon has received a great deal of scattered attention in the literature for a period of 25 years without a clear-cut decision being reached as to the cause of the broadening. At least two mechanisms present themselves as explanations of the broadening: the microstress theory and the particle size theory. The microstress theory pictures a system of internal stresses in the metal. In a general way these stresses are supposed to be random in direction, magnitude, and sign, and uniform only over distances very small compared with the dimensions of the sample. Such a system of stresses will produce a corresponding system of strains and hence random variations from crystal to crystal of any given interplanar spacing. Random variation of interplanar spacing will produce a broad x-ray diffraction line from the polycrystalline material. The particle size theory presumes that in the process of cold work, crystal fragmentation proceeds so far that the resulting small crystals have low resolving power. The width of the lines is then given by the Scherrer formula as $B=0.89\lambda\sec\theta/L$, where L is an average crystal dimension, λ is the x-ray wave-length, and θ is the Bragg angle.

It is difficult to show by a direct independent method either the existence in the metal of such a system of internal stresses, or the existence of crystals smaller than 2000A. This dimension is that which is just small enough to cause detectable broadening.[1] The weight of the opinion in the

* The work on tungsten reported here is part of a thesis presented by E. E. Stickley to the University of Pittsburgh in partial fulfillment of the requirements for the degree of Doctor of Philosophy, June, 1942.

† Now with the Department of Physics, Case School of Applied Science, Cleveland, Ohio.

** Now with the Pittsburgh Plate Glass Company, Creighton, Pennsylvania.

[1] B. E. Warren, J. App. Phys. 12, 375 (1941).

literature, influenced by many indirect observations, has inclined toward the former point of view.

The x-ray observations themselves are capable of direct discrimination between these two theories, if numerous quantitative measurements are made and if their dependence on the Bragg angle θ, and the x-ray wave-length λ is examined.

Dehlinger[2] has suggested the test involving the data themselves. If the broadening is caused by small particle size, the breadth B should be proportional to sec θ or if comparable data of different x-ray wave-lengths is available, to $\lambda \sec \theta$. If a microstress mechanism is responsible the breadth should be proportional to tan θ and independent of x-ray wave-length, as logarithmic differentiation of the Bragg law will show.

The present work was originally an attempt to apply the Dehlinger test to α-brass. The systematic effects which are described appeared at once and the explanation in terms of elastic anisotropy presented itself. This explanation in turn suggested the experiments on tungsten. The work is discussed in the reverse order for the sake of convenience.

EXPERIMENTAL PROCEDURE

A side reflection focusing camera of 100-mm diameter was used in this work. This camera has the advantage that geometrical contributions to the line width can be computed and thus patterns, made of different materials and with different wave-lengths, can be made comparable. The camera was capable of registering effectively reflections from $\theta = 30°$ to $\theta = 80°$, a region which contains the majority of lines useful for the present purpose. A back reflection camera, which would be preferable from the point of view of precision, proved incapable of registering enough lines, as might be anticipated.

All patterns were made with $K\alpha$ radiation reflected from a self-focusing NaCl monochromator.[3] The use of crystal monochromated radiation is considered by the authors to be a "must" in work of this sort. It is only with such radiation that the background fluorescent scattering from the sample, caused by the continuous radiation from the x-ray tube, can be eliminated. A low background is absolutely necessary in order to secure significant width values from microphotometer readings. The self-focusing feature of the monochromator provides a wide horizontal angular distribution of radiation, all of which can be utilized in a camera of the focusing type, keeping exposures down to reasonable values. The x-ray tubes were of the common demountable hot filament type. Cu, Ni, Co, and Fe targets were used in the work on brass, while only Cu, Ni, and Fe were used on tungsten. From 400 to 1000 watts input was used, depending on the target. Exposures were about four hours. An important intensity factor with the softer radiations is the window of the x-ray tube. It was found, quite fortuitously, that the aluminium foil in which pre-war x-ray film was wrapped is satisfactory for windows. This foil is 0.0004 in. thick and is entirely without pinholes. The red paper if left on provides a convenient method for handling the foil.

The film which was used in these experiments was Eastman no-screen x-ray film. It is necessary to use the single-coated film because the x-ray beam in focusing cameras does not strike the film at normal incidence. This film, by test, has a linear density exposure relation for densities less than one. Thus the maximum density of all lines must be less than one, and further analysis of the precision of half-intensity width measurements by the photographic method showed that for best results the maximum density of the line should be held to the range of from 0.15 to 0.85. The x-ray diffraction lines used in these experiments varied in intensity, most markedly because of the multiplicity factor. In order to bring all lines on a given film to a common density level, aluminum absorbers were placed immediately in front of the film at the position of the strong lines. This procedure raised the relative intensity of the 400 and 222 lines and materially reduced the number of exposures necessary. Standard and uniform film treatment was used throughout.

The α-brass which was used here was ordinary 30 Zn 70 Cu material which was cold rolled to a 30 percent reduction in area from the well-annealed state. For use with the focusing camera a cylindrical surface on the specimen of 100-mm diameter is necessary. This surface was obtained

[2] P. Dehlinger, Zeits. f. Metallk. **31**, 231 (1939).
[3] C. S. Smith, Rev. Sci. Inst. **12**, 312 (1941).

by machining and the machined area was then etched electrolytically to a depth of about 0.005 in. The redeposition of copper could be visually detected by its color and was avoided by simple adjustment of the etching technique.

The tungsten, which was used was a section of an ingot prepared in the ordinary commercial way.[4] The ingot had been fused at the center and was obviously large grained. The diffraction pattern of the material in the condition in which it was received consisted of speckled lines. The problems of cold working the tungsten and of preparing a 100-mm diameter surface were solved simultaneously by grinding the surface with a fine 100-mm diameter wheel.

REDUCTION OF THE DATA

The films produced by the above process were microphotometered with a Hilger non-recording microphotometer of a type commonly used in spectrochemical analysis. The widest available scanning slit, approximately 0.1 mm, was used to reduce the otherwise prominent graininess fluctuations. The procedure used follows: The galvanometer deflection was adjusted to a standard δ_0 on either side of the line being measured. The line was scanned and the galvanometer deflection δ_m corresponding to maximum density was determined. The galvanometer deflection corresponding to half-maximum density was then computed by the relation $\delta_{\frac{1}{2}}=(\delta_0\delta_m)^{\frac{1}{2}}$. The two film positions corresponding to $\delta_{\frac{1}{2}}$ were then read off the scale and drum provided. Distances on the film could be read with a least count of 0.005 mm, which with lines one to six millimeters wide is more than good enough.

The measurements on each line were repeated several times with the film in slightly different positions perpendicular to the scanning direction. The reproducibility of width values on a given line on a given film was rarely worse than 1 percent. The same line measured on different films did not reproduce so well, differences of 10 percent being found. At least two and more often four and five films were available for each line. The average deviation from the mean among films carrying the same diffraction line may be set at a 5 percent maximum.

The result of the microphotometry is an average width for each line expressed in millimeters. For a 100-mm diameter camera this is quickly converted to B_m, the measured breadth expressed in radians, by dividing by 100. Consideration shows that the widening effect of oblique incidence on the film is just compensated by the correspondingly shortened specimen-film distance.

The measured breadth B_m is the result of a number of factors only one of which is cold work. These other factors are, in the present case, the natural wave-length width of the x-ray lines, the added widening caused by the presence of the α_2 component of the radiation and the width due to the finite size of the slit in the x-ray camera. In making these corrections it is important to note that they must be made as squared terms as pointed out by Warren.[1] The squared law for corrections may be verified by assuming that each element of an initial error curve distribution of intensity having width B_s is spread out into an error curve distribution having width B_c. Integration yields a new error curve distribution of width B_T where $B_T^2=B_s^2+B_c^2$. As will be noted a modified square law is valid for another type of distribution also.

The angular breadth, B_α, of an x-ray diffraction line which is due to the natural wave-length width of the α_1 component can be written $B_\alpha=2(\Delta\lambda_{\alpha_1}/\lambda)\tan\theta$, where $\Delta\lambda_{\alpha_1}$ is the half-maximum natural wave-length width which can be obtained from double crystal spectrometer data.[5]

The $\Delta\lambda_{\alpha_1}$ values all run about $\frac{1}{2}XU$ which gives a correction B_α^2 of from 1 to 10×10^{-6} radian^2. This correction is negligible compared with B_m^2 which ran from 100 to 3000×10^{-6} radian^2 but it was included for completeness.

The necessary correction $B_{\alpha_1\alpha_2}$ for the presence of the α_2 component of the doublet was determined by a graphical method developed by Warren.[6] In arriving at this correction the assumption is made that the intensity of the α_2 line is just one-half the intensity of the α_1 line. The

[4] The tungsten was obtained through the courtesy of Mr. W. P. Sykes, Cleveland Wire Works, General Electric Company, Euclid, Ohio.

[5] A. H. Compton and S. K. Allison, *X-Rays in Theory and Experiment* (D. Van Nostrand, New York, 1935), p. 745.

[6] This correction for doublet broadening, which is unpublished, was presented by B. E. Warren at the Gibson Island Symposium, July 28, 1941 in a paper entitled "Theory and Practise of Particle Size Determination."

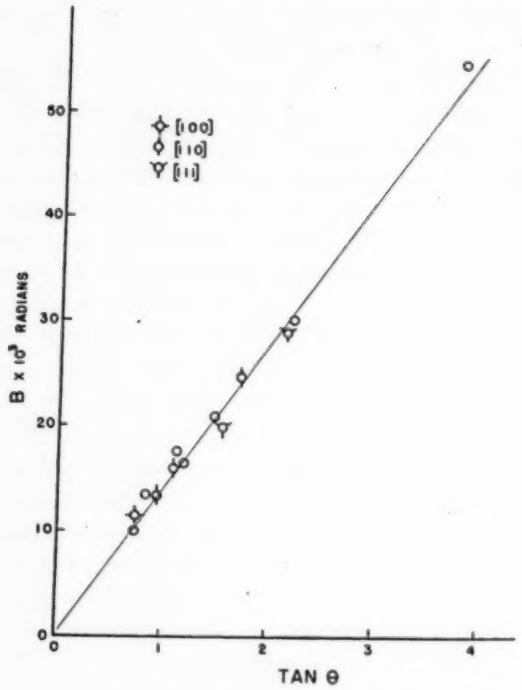

FIG. 1. Reduced breadth plotted against the tangent of the Bragg angle for tungsten. The data for the principal crystallographic directions are indicated.

lines are further assumed to possess error curve intensity distribution with some arbitrary width B_e. The separate curves are plotted a number of times with the two components separated by varying amounts S. The composite curve is drawn in each case by adding ordinates, and the width B_g at half the maximum intensity of the composite curve is measured. When the B_g^2 values are plotted against S^2 a linear relation results, giving $B_g^2 = B_e^2 + (1.225S)^2$. The necessary correction will be denoted by $B^2_{\alpha_1\alpha_2} = (1.225S)^2$ where S must be taken to be the angular separation of the doublet components

$$S = 2(\Delta\lambda_{\alpha_1\alpha_2}/\lambda) \tan\theta.$$

The final correction is then

$$B^2_{\alpha_1\alpha_2} = [2.45(\Delta\lambda_{\alpha_1\alpha_2}/\lambda) \tan\theta]^2.$$

The wave-length separation of the two doublet components is practically constant at $4XU$ for all wave-lengths. This correction is therefore large, $B^2_{\alpha_1\alpha_2}$ being roughly 20 percent of B_m^2 in all cases. It is interesting to note the $B^2_{\alpha_1\alpha_2}$ will be very much larger for short wave-length radiation such as Mo$K\alpha$ than it is for long wave-length radiation such as Fe$K\alpha$; in this case, $B^2_{\alpha_1\alpha_2}$ is 7 times larger.

It must be emphasized that this method of correcting for the α_2 component is valid only if the two components are completely unresolved, as was the case in these experiments.

The correction B_s made necessary by the finite width of the camera slit was the most troublesome one in the present work. The NaCl monochromator may be adjusted to focus the $K\alpha$ radiation to a rather narrow beam at the focal point, but within this narrow beam the α_1 and α_2 components will be relatively displaced because of the small wave-length difference. In order to make sure that the intensity of the $K\alpha_1$ line was just twice that of the $K\alpha_2$ line it was necessary to use a larger slit, about one-half millimeter wide and two millimeters high, than would have been necessary otherwise. Both the width and the height of the slit must be considered in this correction.

The height of the slit may introduce a widening on two counts, the permitted height of parallel rays and the vertical divergence allowed. It was felt that the use of the crystal monochromators and the resulting large distance between the tube focal spot and the camera slit reduced the widening due to vertical divergence to a negligible amount.

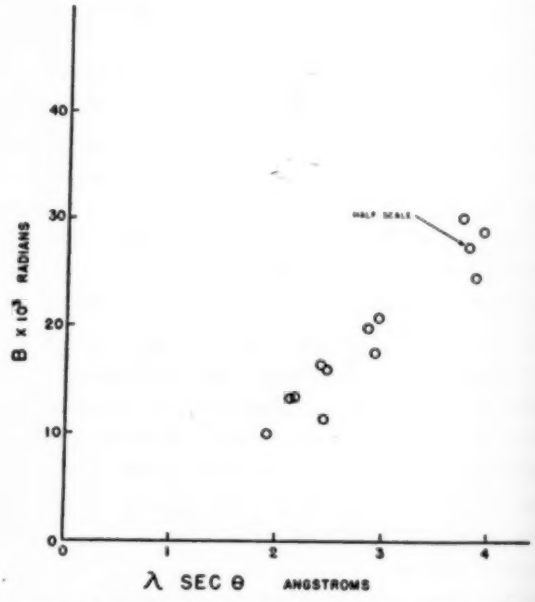

FIG. 2. Reduced breadth plotted against the function $\lambda \sec\theta$ for tungsten.

The width due to a finite height of parallel rays is important only in regions of θ near to 0° or 90°, and where the sample-film distance is small. This correction, for example, vanishes at $\theta=45°$ where angle of opening of the cone of diffracted radiation is 90°. In the side reflection camera the sample to film distances are large except in just the region $\theta \gtrless 45°$. Furthermore, this type of slit height width can usually be detected visually, the lines being wider at the ends than in the center. For these reasons the entire correction due to the height of the slit was neglected.

A correction appropriate to the width of the slit was deduced by a graphical method. This was first done for the case of the error introduced into the measurements by the finite microphotometer slit width. This problem is mathematically just the reverse of the problem for the camera slit width, and results in exactly the same form of correction. For convenience the derivation of the correction is explained in terms of the microphotometer slit width. If a diffraction line of any given form of density distribution and of width B is scanned with a slit of finite width ω, an observed density distribution will result which will be of slightly different analytical form and which will certainly have width B' greater than B. It was assumed that the lines dealt with here had the shape of error curves of width B_e. With the help of tables of $2/\sqrt{\pi}\int_0^x \exp(-x^2)dx$ the distribution which results from scanning an error curve with a slit of width ω can be computed. The new distribution can be plotted and the width B_θ measured. This was done for a series of ω values and the resulting widths were plotted as B_θ^2 against ω^2. A straight line of the form $B_\theta^2=B_e^2+0.45\omega^2$ closely agrees with the points for $\omega<0.3B_e$. This relation therefore gives $B_s^2=0.45\omega^2$.

In the case of the microphotometer slit $\omega=0.1$ mm while the measured breadth of the lines was 1 mm or greater. The maximum correction of 0.5 percent in the squared terms was neglected. In the case of the camera slit, quantities must be expressed in angular measure and ω can easily be shown to be the angle subtended by the slit at the sample. The average sample-slit distance was 50 mm. In the work on tungsten a 0.50-mm slit was used and in the work on brass a 0.40-mm slit. The squared corrections that were applied were therefore 45×10^{-6} radian^2 and 29×10^{-6} radian^2, respectively. This correction is of course a constant. The order of magnitude of this correction was checked by diffraction patterns made of large grained powdered material. It must be admitted that this correction is unsatisfying on several counts. It is a constant correction, however, and is not large enough to affect any conclusions drawn from the present experiments.

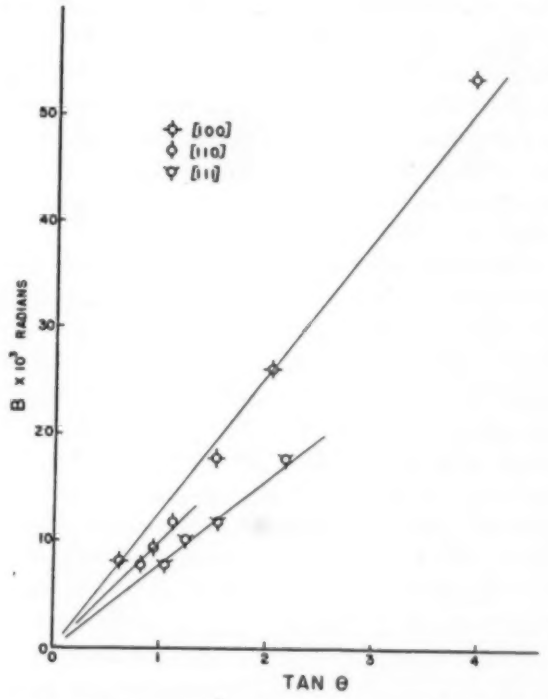

FIG. 3. Reduced breadth plotted against tan θ for the three principal crystallographic directions in α-brass.

In summary, then, the measured widths were corrected by the relation $B_m^2=B^2+B_a^2+B_{\alpha_1\alpha_2}^2+B_s^2$ where B is the width due to cold work alone.

RESULTS

The reduced data for tungsten are plotted in Fig. 1 against tan θ and in Fig. 2 against λ sec θ. In Fig. 1 the data fall on a straight line drawn through the origin within ±5 percent. In the λ sec θ plot, not only is the scatter of the data noticeably greater, but any straight line presumed to represent the data would necessarily have a negative intercept on the B axis. Such a negative intercept is of course impossible physically; furthermore, of the two important corrections

made to the data, B_s is not large enough to eliminate this situation and $B_{\alpha_1\alpha_2}$, if reduced or neglected would worsen the situation. These results show that the data are proportional to tan θ and are not proportional to λ sec θ.

The data from tungsten include the following reflections: (211), (220), (310), (222), and (321) with Cu$K\alpha$ radiation; (211), (220), (310), and (222) with Ni$K\alpha$ radiation; and (200), (211), (220), and (310) with Fe$K\alpha$ radiation. The data from planes (100), (110) and (111) are indicated in Fig. 1. In the cubic system these planes are normal to the principal crystallographic directions [100], [110], and [111], respectively. It is evident from Fig. 1 that B does not depend on the crystallographic direction of the reflecting planes by an amount more than the experimental error.

The data for brass included reflections from the following planes: (311), (222), (400), (331), and (420) with Cu$K\alpha$ radiation; (220), (311), (222), (400), and (331) with Ni$K\alpha$ radiation; (220), (311), (222), and (400) with Co$K\alpha$ radiation; and (200), (220), (311), and (222) with Fe$K\alpha$ radiation. It may be noted that the (200) and (400) planes are both normal to the [100] direction. On a tan θ plot similar to Fig. 1 these data scatter considerably compared with those for tungsten, but inspection shows that the scatter is systematic depending particularly on the crystallographic direction normal to the reflecting planes. Figure 3 shows the data for the principal directions, [100], [110], and [111], while Table I shows values of $B/\tan\theta$ for all reflections. For each crystallographic direction B is proportional to tan θ to within a ± 10 percent deviation from the individual mean and the systematic trend among the various directions is unmistakable. The values of the orientation function Γ are included in Table I for reference below.

It is evident from comparison of Figs. 1, 2, and 3 that the data for α-brass, taken as a whole or taken one direction at a time, are not proportional to λ sec θ.

TABLE I. Values of $B/\tan\theta$ in units of 10^{-3} radian and of the orientation function Γ for different crystallographic directions in α-brass.

Line	Radiation	$B/\tan\theta$	Direction	Γ
200	Fe	13.09	[100]	0.000
400	Cu	11.65		
	Ni	12.72		
	Co	13.49		
Average		12.74		
420	Cu	10.91	[210]	0.160
311	Cu	11.05	[311]	0.157
	Ni	10.55		
	Co	10.72		
	Fe	11.41		
Average		10.93		
220	Ni	9.40	[110]	0.250
	Co	10.00		
	Fe	10.45		
Average		9.95		
331	Cu	9.23	[331]	0.274
	Ni	9.65		
Average		9.44		
222	Cu	7.44	[111]	0.333
	Ni	8.15		
	Co	7.55		
	Fe	8.07		
Average		7.80		

DISCUSSION

The results for cold-worked tungsten show that the breadth of the x-ray diffraction lines is proportional to tan θ and is not proportional to λ sec θ. These results are consistent with a microstress mechanism of broadening and are inconsistent with a particle size mechanism. It may be concluded on the basis of this result alone that particle size makes no significant contribution to the breadth in the case of tungsten and that the microstress picture may be accepted as a simple explanation of the facts.

The results for α-brass are similarly inconsistent with a particle size theory, but they are consistent with a microstress picture only if this picture is capable of explaining the systematic effect observed with the brass and of explaining simultaneously its absence in the case of tungsten. Such an explanation may be found in the elastic properties of the two materials.

Cubic crystals are in general anisotropic in their elastic properties. The Young's modulus, defined as the ratio of normal force per unit area to deformation in the direction of the force per unit of length in the same direction, is given by,

$$1/E = A - B\Gamma \qquad (1)$$

for a cubic crystal. In this equation A and B are constants of the material, and Γ is the orientation function given by $\Gamma = \gamma_1^2\gamma_2^2 + \gamma_2^2\gamma_3^2 + \gamma_3^2\gamma_1^2$, where

γ_1, γ_2, and γ_3 are the direction cosines of the specimen axis with respect to the cubic crystal axes.[7] For α-brass of composition 72 percent Cu, 28 percent Zn, A is 19.4×10^{-13} cm^2 dyne^{-1} and B is 41.6×10^{-13} cm^2 dyne^{-1}. The modulus in the [111] direction is then a maximum and the modulus in the [100] direction is the minimum with a ratio of $E_{[111]}/E_{[100]}=3.5$. For tungsten $A=2.573\times10^{-13}$ cm^2 dyne^{-1} and $B=0$. This latter value means that tungsten is elastically isotropic, the only known example of a crystalline material which is so.[8]

A given system of microstress in a metal will produce a system of strains, the magnitude of which will depend on the elastic properties of the material. In an anisotropic material one would expect the strain magnitude to be a function of crystallographic direction since the modulus is a function of crystallographic direction. Since the breadth of a diffraction line, from this point of view is simply a measure of the strain magnitude one would expect the breadth to be a function of the crystallographic direction, and further, inspecting Eq. (1), a function which monotonically decreases with increasing Γ. In Table I this may be seen to be the case within the errors of experiment for α-brass.

Tungsten, which was chosen for these experiments because of its elastic isotropy, shows no dependence of breadth on direction in agreement with the above point of view.

The above conclusions are semi-quantitative only, the results being only in the predicted sequence for α-brass and exhibiting no sequence for tungsten as expected. It is not possible to make quantitative conclusions from the present experiments since the details of the stress distribution are unknown. It is not correct to predict that the breadths should be quantitatively proportional to tan θ/E for an anisotropic material, where E is given by Eq. (1). The modulus in Eq. (1) is the stress strain ratio for a single crystal under a uniaxial stress, i.e., with free boundaries, which is certainly not the case for the crystals in the interior of a massive piece of cold-worked polycrystalline metal. As a simple example it may be pointed out that a single cubic crystal under hydrostatic pressure would exhibit strain which would be independent of Γ.

Some work reported in a recent letter by Stokes, Pascoe, and Lipson[9] is of interest in connection with the above. These workers have studied the breadth of diffraction lines from copper *filings* and have found that the quantity $EB/\tan\theta$ is a constant for their data, or in other words, that the breadth is proportional to tan θ/E, where E is presumably computed from Eq. (1). It is quite conceivable that Eq. (1) might apply to the crystals in a filing more rigorously than to crystals in a massive piece of metal and this is probably the explanation of their result. Moreover the present writers cannot check the modulus values quoted in this letter, finding $E_{[100]}$ high by 10 percent and $E_{[111]}$ low by the same amount. The conclusion that $EB/\tan\theta$ is constant would thus be incorrect by 20 percent. The constants A and B in Eq. (1) may have come from different sources however. In any event it seems in order to comment that experiments on the connection between elastic properties and breadth may prove a profitable way in which to study the microstress distribution as a function of the method of cold work.

Elastic anisotropy and its relation to the well-known method of x-ray stress analysis has been discussed at length in the German literature.[10,11] A definite effect is claimed but it is apparently not large enough to cause trouble in stress measurements on aluminum and steel, to which the method is usually applied.

The difference between the α-brass and tungsten found in the present experiments might very possibly be accounted for on grounds other than that of the elastic properties. The materials differ in two important respects: They are of different crystal structure and they have been cold worked by quite different methods. The writers can find no obvious explanation based on either of these two differences. Experiments with controlled crystal structure and controlled cold-work method can decide this point.

The present data for tungsten and α-brass are not strictly comparable quantitatively because

[7] E. Schmid and W. Boas, *Kristallplastizität* (Julius Springer, Berlin, 1935), p. 23.
[8] See reference 7, page 200.
[9] R. S. Stokes, K. J. Pascoe, and H. Lipson, Nature **151**, 137 (1943).
[10] R. Glocker, Zeits. f. tech. Physik **19**, 289 (1938).
[11] H. Moeller and G. Martin, Mitt. Kaiser-Wilhelm Inst. Eisenforsch, Duesseldorf **21**, 213 (1939).

TABLE II. Comparison of root-mean-square strains with maximum strains.

	$\Delta d/d$	U.T.S./E
Tungsten	12×10^{-3}	12×10^{-3}
α-brass	5	7
Permalloy	4	3

the method and amount of cold work is different in the two cases. However, since Haworth[12] has shown that the breadth rapidly approaches a limiting value with increasing amounts of cold work an attempt has been made to compare these data with those of Haworth on Permalloy. For this purpose a microstress mechanism is assumed to be responsible for the broadening in all cases and the root-mean-square strain $\Delta d/d$ is computed by help of the relation given by Haworth, $(\Delta d/d)^2=0.55(B/\tan\theta)^2$. The r.m.s. strain may be compared with the maximum strains computed by dividing the ultimate strength by the modulus. Handbook values were used in the latter case. Table II shows the results of doing this.

The rough agreement of the two columns of Table II and the order in which the $\Delta d/d$ values arrange themselves may be considered to be further support for the microstress mechanism.

It is interesting to see what conclusions result when the evidence in favor of a microstress mechanism recorded here is disregarded and a particle size theory is assumed. If the reduced breadths for tungsten are introduced directly into the Scherrer formula and an average computed from all the data the number resulting is 140A. α-brass yields a value of 180A while the data of Stokes, Pascoe, and Lipson for copper yield 310A. These values are so small that they are hardly credible.

There is other evidence that the major portion of cold-work broadening is due to strains in the metal. This evidence has been summarized elsewhere.[13] The possibility of broadening mechanisms other than the two examined here cannot be ruled out by the present results.

CONCLUSIONS

The results of measurements of x-ray line width in cold-worked tungsten and α-brass are in agreement with a microstress theory of broadening and are in disagreement with a particle size theory. The former hypothesis explains the observed dependence of the breadth on the Bragg angle and on the x-ray wave-length; it explains in a simple manner the systematic dependence of breadth on Miller indices found with α-brass and it explains the absence of this effect in tungsten; the mechanism yields reasonable quantitative results for the strains presumed to be present in the metal.

ACKNOWLEDGMENT

The authors have had several interesting discussions with Professor C. S. Barrett of the Carnegie Institute of Technology during the course of the present work. They wish to express their appreciation for his interest in these experiments.

[12] F. E. Haworth, Phys. Rev. **52**, 613 (1937).

[13] F. Niemann and S. T. Stephenson, Phys. Rev. **62**, 330 (1942).

Further Measurements on the Disintegration Curve of Mesotrons

NORRIS NERESON AND BRUNO ROSSI
Cornell University, Ithaca, New York
(Received July 26, 1943)

Further measurements have been made on the disintegration curve of mesotrons. An extensive set of data gives a mean lifetime of 2.15±0.07 microseconds as calculated from the differential disintegration curve.

1. EXPERIMENTAL PROCEDURE

THE authors of the present paper have recently described a method for the experimental determination of the disintegration curve of mesotrons and have given a preliminary account of the results obtained.[1] The method has been since improved and a new and more extensive set of data has been taken. A summary of the new results is presented here.

The experimental arrangement, which is similar in principle to that used in the previous experiment, is schematically represented in Fig. 1. The three counters L are in parallel, and so are the four counters B and the five counters M. Counters A_1, A_2, and B feed into the "time circuit" T; this circuit gives a pulse whose amplitude is a function of the time delay between a coincidence A_1A_2 and the subsequent pulse of B. Counters L, A_1, A_2, B, and M feed into an anticoincidence circuit C, which records the anticoincidences LA_1A_2B-M, i.e., the coincidences between LA_1A_2 and B which are not accompanied by a pulse in M. The recording circuit R operates a pen writing instrument in such a way that the pulse from the time circuit is recorded only when it is accompanied by a pulse from the anticoincidence circuit.

The events which one desires to record are of the following type. A mesotron traverses the counters L, A_1, and A_2, is stopped in the absorber A, and then disintegrates giving rise to an electron which discharges one of counters B. The amplitude of the pulse from the time circuit, as recorded by the pen writing instrument, gives a measure of the life span of the mesotron in the absorber.

In addition to the records representing disintegration events, records will be obtained whenever showers or other spurious effects discharge L, A_1, A_2, B, and fail to discharge M. In these cases counters A_1, A_2, and B are discharged almost exactly at the same time. However, small delays may be recorded because of the spontaneous time lags of counters. Previous experiments have shown that the time lags of counters hardly ever exceed 0.8 μsec. Thus, no spurious delays due to time lags of counters will be recorded if all delays less than 0.8 μsec. are disregarded in the data.

As discussed in the paper previously quoted[1] errors may arise on account of "chance coincidences" between two spurious events, between a spurious event and a real disintegration event, or between two real disintegration events. The number of these coincidences has been greatly reduced in the present experiment as compared with the previous one through a more careful design of the circuits. Actually, if we confine ourselves to delays larger than 0.8 μsec., we can say that out of every 1000 events recorded as disintegrations, only six on the average are due

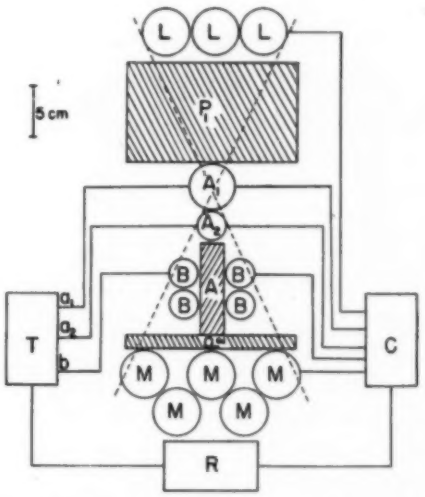

FIG. 1. Experimental arrangement used in the determination of the disintegration curve of mesotrons.

[1] B. Rossi and N. Nereson, Phys. Rev. **62**, 417 (1942).

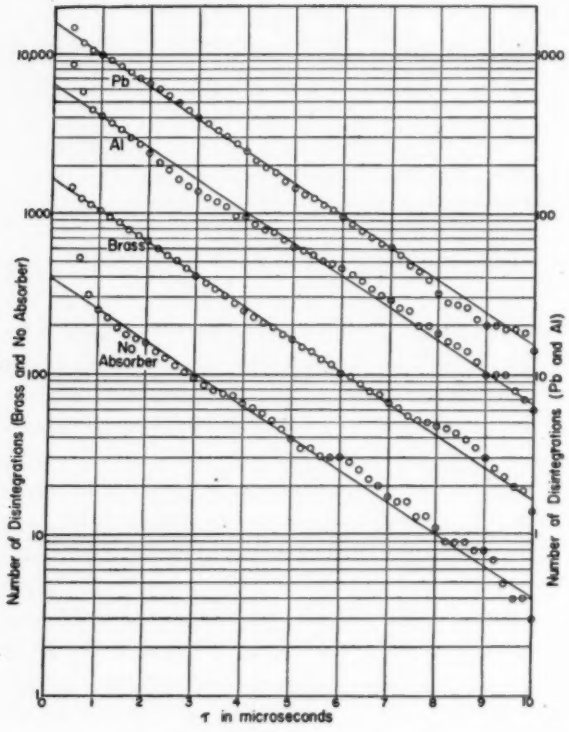

FIG. 2. Integral disintegration curves of mesotrons obtained with lead, aluminum, brass, and no absorber in A.

to chance coincidences, while ten of the records are slightly modified by overlapping between true and spurious events, and six disintegrations may be expected to be missed on account of overlapping between disintegration events. These numbers are very small and thus the errors caused by chance coincidences can be disregarded.

2. EXPERIMENTAL RESULTS

The combined measurements represent about 4000 hours of observation distributed over a period of seven months during which a total of approximately 3000 decay electrons emitted with a delay larger than 0.8 μsec. were recorded. During the measurements the time circuit was calibrated twice a week with artificial pulses whose time separation was determined by a quartz oscillator.[1] The deviations between consecutive calibrations never exceeded 0.1 μsec., while the maximum variation of the calibration curve at any one point during the entire seven-month period was 0.2 μsec.

Measurements were taken with absorbers of lead (1303 hours), brass (937 hours), and aluminum (452 hours) in A. In all cases the size of the absorber was 25.5×8×2.3 cm. Measurements were also taken with no absorber (1302 hours). The results are presented in the form of integral disintegration curves in Fig. 2. Actually, all delays up to 15 μsec. (the resolving time of the anticoincidence circuit) were recorded in the experiment but the points corresponding to delays above 10 μsec. have rather large statistical errors and are not presented here. In these graphs the ordinates give on a logarithmic scale the number of mesotrons whose life span τ in the absorber is larger than the corresponding abscissa. Except for the points below 0.8 μsec., the experimental points for the three absorbers fall on practically straight lines which all show about the same slope. This indicates that mesotrons decay exponentially and that the average lifetime is the same in the different absorbers as, of course, one would expect. The deviations of the points obtained with the aluminum absorber from a straight line are larger than those for the lead or brass absorbers since fewer disintegration events were observed for aluminum. The measurements with no absorber are also subject to rather large statistical fluctuations. However, the corresponding curve is again approximately a straight

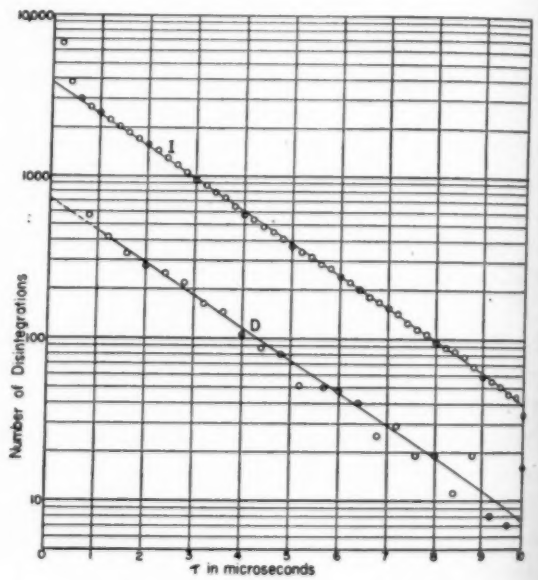

FIG. 3. Differential (D) and integral (I) disintegration curves of mesotrons obtained from the combined data of the lead, brass, and aluminum absorbers. The straight line through the experimental points for the differential curve is drawn according to the method of least squares.

line parallel to the other three, indicating that most of the events recorded with no absorber are disintegrations of mesotrons stopped in the walls of the counters or in the permanent lead absorber P_2.

The results obtained with lead, brass, and aluminum are combined into a single differential disintegration curve in Fig. 3 (lower curve). In this figure the number of mesotrons whose life is between τ and $\tau+\Delta\tau$ is plotted on a logarithmic scale against $\tau+\Delta\tau/2$, where $\Delta\tau$ is chosen as 0.4 μsec. A straight line has been fitted to the experimental points corresponding to delays larger than 1 μsec. by the method of least squares. The equation of this line gives for the mean lifetime of mesotrons the following value:

$$\tau_0 = 2.15 \pm 0.07 \ \mu\text{sec.},$$

where the error indicated represents the standard statistical error. The same value is obtained when only experimental points lying in the regions from 1 to 8 and 1 to 6 μsec. are used to determine the equation of this line. The corresponding combined integral curve is also plotted in Fig. 3; a straight line having a slope corresponding to the above lifetime is drawn through the experimental points.

The previous measurements[1] gave $\tau_0 = 2.3 \pm 0.2$ μsec. The difference between the two values of τ_0 is well within the statistical error. The new value, of course, is much more accurate.

Straight lines with slopes corresponding to $\tau_0 = 2.15$ μsec. are also drawn through the experimental points in Fig. 2. The intersections with the ordinate axis gives the total numbers of disintegration electrons recorded. These numbers divided by the total time of observation are listed under n in Table I. The difference $n-n_0$ between the values of n with a given absorber and with no absorber represents the number of decay electrons per hour coming out of the absorber and recorded by counters B.

Table I also lists under N the number of anticoincidences LA_1A_2-M per hour recorded with each of the three absorbers and with no absorber. By subtracting the anticoincidences recorded with no absorber, N_0, from the anticoincidences recorded with a given absorber, N, one obtains the average number of mesotrons stopped per hour by the particular absorber

TABLE I. Summary of the experimental results. N is the number of anticoincidences LA_1A_2-M per hour, and n is the number of disintegration electrons recorded per hour (extrapolated value).

	N	$N-N_0$	n	$n-n_0$	$\frac{n-n_0}{N-N_0}$
Lead	40 ± 2	17 ± 2	1.20 ± 0.03	0.90 ± 0.04	0.05 ± 0.01
Brass	40 ± 2	17 ± 2	1.76 ± 0.04	1.46 ± 0.05	0.09 ± 0.01
Aluminum	29 ± 1	6 ± 1	1.43 ± 0.06	1.13 ± 0.06	0.19 ± 0.03
No absorber	23 ± 1	—	0.30 ± 0.02	—	—

(second column). The last column of Table I gives the "yield," namely, the ratio $(n-n_0/(N-N_0)$ between the number of decay electrons recorded and the total number of mesotrons stopped.

The ratios between the numbers $N-N_0$ of the mesotrons stopped in the three absorbers correspond very closely to the theoretical predictions, based upon the theory of ionization losses of mesotrons in matter (see especially the paper by Rossi and Greisen[2]). The yield $(n-n_0)/(N-N_0)$ appears to be a rapidly decreasing function of the atomic number. This is exactly what one would expect because the range of the disintegration electrons decreases rapidly as the atomic number is increased.

In aluminum the average range of the disintegration electrons, which have an energy of about 40 Mev, is approximately 6 cm. Since the thickness of the absorber is 2.3 cm, it may be assumed that almost all of the disintegration electrons produced in the aluminum come out of the absorber. If all mesotrons stopped in the absorber disintegrated, the average "yield" in the case of aluminum should be approximately equal to $\frac{1}{4}\pi$ times the average solid angle subtended by counters B from the point where the disintegration occurred. From a rough evaluation of this solid angle, one estimates a yield of about 0.5 while the experimental value of $(n-n_0)/(N-N_0)$ is about 0.2. This would seem to indicate that only half of the absorbed mesotrons undergo disintegration, in agreement with the results of Rasetti.[3]

The authors take pleasure in expressing their thanks to Mr. F. Chromey, who helped in running the measurements and evaluated most of the records.

[2] B. Rossi and K. Greisen, Rev. Mod. Phys. **13**, 240 (1941).
[3] F. Rasetti, Phys. Rev. **60**, 198 (1941).

The Beta-Ray Spectrum of Antimony (124)

E. B. HALES,* *University of Illinois, Urbana, Illinois*

AND

E. B. JORDAN, *Bennington College, Bennington, Vermont*

(Received June 8, 1943)

The continuous beta-ray spectrum of antimony^{124} has been investigated with a 180° type of spectrometer. The spectrum consists of two components, the end points of which are: 0.74±0.03 Mev and 2.45±0.07 Mev. The difference between these end points, 1.71±0.07 Mev, agrees with the known value of the hard gamma-ray from Sb^{124}. In addition, internal conversion lines, probably due to the decay of a long-lived Te isotope present in the source, have been observed. These lines correspond to gamma-ray energies of 0.23 Mev and 0.61 Mev. In conclusion, a possible energy level scheme representing this transition is discussed.

I. INTRODUCTION

THE magnetic spectrometer is the only instrument which can be used for making precise, direct measurements on the energy or momentum distribution of beta-rays. In those cases in which gamma-rays are associated with a detectable number of internal conversion electrons, it is also valuable as an instrument for determining the relative intensities and energies of the K, L, and M conversion lines. These gamma-ray energies, as well as the maximum beta-particle energies in beta-ray spectra, are among the most important constants to be determined in a systematic study of the properties of the radioactive nuclei.

II. THE SPECTROMETER

The beta-ray spectrometer used in this experiment was the usual π radian type of instrument.

The magnet yoke and windings were parts of an old Edison bipolar generator, kindly loaned to us by the Electrical Engineering Department. The yoke was fitted with a pair of rectangular pole pieces, 30.5 cm×25.4 cm×25.4 cm, made of dense iron. The pole faces on either side of the air gap were polished until they were plane to about 0.001". With an air gap of one and one-half inches, and with the plane faces parallel to each other, the magnetic field was constant within one-quarter of one percent over an area slightly more than 18 cm^2.

Cast bronze was used for the frame of the vacuum chamber. Although this material was porous and had to be sealed with Glyptal or some similar substance before evacuation, it could be cast to the approximate size and shape of the finished chamber. This choice of material and method of handling saved many hours of shop work in building this part of the instrument.

The top and bottom covers of the vacuum chamber were brass plates made to fit exactly into milled brass "steps" in the frame casting. This arrangement was made vacuum tight by sealing the edges with Glyptal.

A sturdy cylindrical post was soldered to the center of the bottom cover of the chamber. The set of radial arms which carried the slit system was fastened to this post by a single screw. The slits were thus held rigidly in place. However, they could all be removed as a unit, and the slit holder could be placed in a lathe for the adjustment of slit widths and positions. The slit jaws were adjusted to the proper positions by sliding them along radial arms which acted as supports.

Although not used in the present experiment, an arrangement consisting of a long cylindrical rod, notched near its lower end and ground and polished to fit a porthole in the casting, permits the quick insertion of sources which have a short lifetime. Very little air is admitted into the chamber while inserting a source, and within a minute after it has been put into place, the pumps restore the vacuum to better than 10^{-4} mm of mercury.

By means of another vacuum-tight rod and porthole arrangement, a stop may be moved back and forth into and out of the path of the beam. It is thus possible to determine the

* Now at the Radiation Laboratory, Massachusetts Institute of Technology, Cambridge, Massachusetts.

background counting rate of the counter for any particular field setting.

In the present experiment, the distance between the source and the nearest point on the counter was approximately 12 cm. The region in between was filled with lead in order to absorb scattered radiation and to reduce the background due to possible gamma-rays from the source.

All slit edges, the top and bottom of the chamber, and all other parts exposed to the beta-ray beam were painted a large number of times with Aquadag. The resulting coat of carbon was dense, coherent, and about one-half mm thick. This carbon was applied to reduce the scattering of the beta-particles by the metal parts. For the same reason, the slits were made of aluminum plates with slightly beveled edges.

The completed chamber was mounted in a vertical plane between the magnet pole faces. These pole faces were held firmly against the chamber covers by a brass yoke which completely surrounded the pole pieces.

In order to measure the magnetic field, a small flip coil, connected to a ballistic galvanometer, was mounted within the chamber. The field measurements were estimated to be accurate within one percent.

III. THE BETA-RAY COUNTERS AND RECORDING DEVICES

The Geiger-Mueller counters employed were the alcohol-filled type first described by Trost.[1] After evacuation, they were filled with a mixture of gases with the following partial pressures measured in centimeters of mercury: helium 5 cm; argon 5 cm; ethyl alcohol 1 cm.

The counter cylinders were made of aluminum which was oxidized by several hours immersion in a 30 percent solution of hydrogen peroxide. Counters prepared in this way had a counting region which extended over several hundred volts. The counting efficiency for gamma-rays increased slowly over this region. This was probably due to an increase in the active volume of the counter, which occurred in the fringing electric field near the ends of the counter cylinder. The counting efficiency for beta-rays was constant over the counting region.

Space limitations required that the counter be quite small. The cylinder was about one and one-half inches long and five-eighths inch in diameter. Such a counter had a relatively small background produced by stray radiation. The beta-rays entered through a slit in the counter cylinder, which was covered by a thin (0.0008″) Cellophane window.

The stabilized high voltage supply for the Geiger-Mueller counter was based on a design due to Ashworth and Mouzon.[2]

The input circuit was a single stage resistance-coupled amplifier which served to amplify, invert the phase, and limit the amplitude of the voltage pulses from the Geiger-Mueller tube. The scaling circuit was based on a design reported by Stevenson and Getting.[3] The positive pulses from the input circuit were fed into a scale-of-eight circuit. The first scale-of-two had an adjustable bias to reject voltage pulses smaller than true counting pulses delivered by the input circuit. The pulses from the last scale-of-two were applied to an output circuit which operated a mechanical recorder. The circuits were shown to operate properly for more than 40,000 regularly spaced pulses per second. In the case of random counts, the upper limit of the counting rate without losses was not definitely known, but was shown, experimentally, to be far greater than any counting rates encountered in spectrometer work.

IV. EXPERIMENTAL PROCEDURE

Since the source investigated was known to be weak and to be a relatively strong gamma-ray emitter, the geometrical arrangement chosen was such as to get a reasonably strong beta-ray beam without sacrificing too much resolution. The beam was defined by four slits, the mean radius of which was 7.475 cm. The maximum and minimum radii were 7.575 cm and 7.375 cm, respectively.

The gamma-ray background was always measured at a magnetic field strength closely corresponding to the field strength at which the spectrum reading was made.

A reasonable statistical accuracy required that some of the counting times be as long as twelve

[1] A. Trost, Zeits. f. tech. Physik **16**, 407 (1935).

[2] J. A. Ashworth and J. C. Mouzon, Rev. Sci. Inst. **8**, 127 (1937).

[3] E. C. Stevenson and I. A. Getting, Rev. Sci. Inst. **8**, 414 (1937).

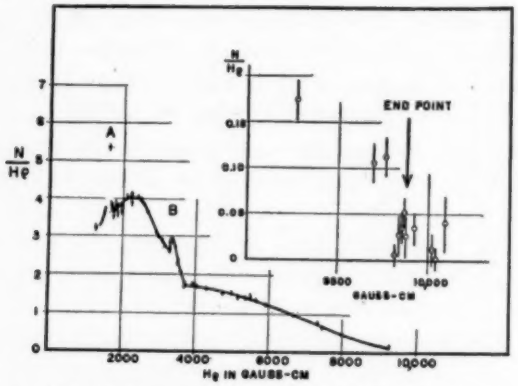

FIG. 1. The beta-ray spectrum of Sb^{124}. The curve is plotted with arbitrary ordinates.

hours. The difficulty of maintaining uniform conditions over so long a period required that certain criteria be set up for acceptable data. If the counting voltage showed any detectable change during the run, the reading was rejected. For ordinary points in the continuous beta-ray spectrum, the reading was accepted if the magnetic field strength decreased less than one-quarter of one percent. In such a case the mean field strength was used. In the case of measurements near the end point of the continuous spectrum, or near an internal conversion line, the reading was rejected if any decrease in the magnetic field was detected. All readings were adjusted for decay of the source by correcting them to a standard time.

V. THE BETA-RAY SPECTRUM OF ANTIMONY[124]

Deuteron bombardment of antimony gives rise to a large number of radioactive isotopes. Sb^{122} and Sb^{124} are formed from the two stable isotopes Sb^{121} (56 percent) and Sb^{123} (44 percent) by a (d, p) reaction.[4] The periods associated with these two radioactive isotopes have been identified by producing them in a number of different ways.[5] The average of the values reported for the half-life of Sb^{122} is 61 hours[4, 6–10] and that of Sb^{124} is 60 days.[4] Both isotopes emit hard gamma-rays.

In addition to the radio-antimony isotopes, a number of tellurium isotopes are also formed by deuteron bombardment; Te^{121} is formed by a $(d, 2n)$ reaction, and has a half-life of 125 days.[11] There is some evidence[12] that it is a positron emitter giving rise to several gamma-rays.[11, 12] Other tellurium isotopes which are probably formed at the same time are those having mass numbers 122, 124, and 123; the first two by a (d, n) reaction and the latter by a $(d, 2n)$ process. Although these isotopes occur as stable in nature, there is good evidence[12] that two of them, $Te^{122, 124}$ are formed in excited states by the deuteron reaction, yielding gamma-rays having energies of 82.0 kev and 88.3 kev. Other gamma-rays which are emitted by the separated tellurium fraction, and whose origins are not definitely known, have energies of 136, 157.3, 210.8, and 615 kev.[12] A period of 30 days has been assigned to the composite gamma-ray activity.

The present investigation was undertaken in cooperation with Professor Goldhaber. A source produced by deuteron bombardment of antimony was prepared for him by Dr. Kamen. A fraction of this source, in the form of a powder scraped from the surface, was attached to a copper foil, 0.001″ thick, by pouring on a very small amount

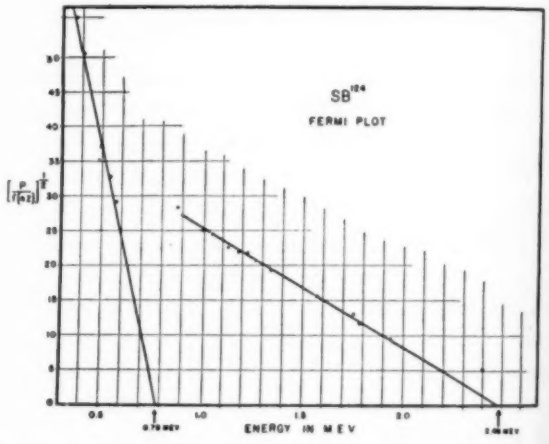

FIG. 2. Fermi plot of the beta-ray spectrum of Sb^{124}. The $f(nZ)$ function is for large Z. The end points agree closely with those determined by inspection.

[4] J. J. Livingood and G. T. Seaborg, Phys. Rev. **52**, 135 (1937).
[5] J. J. Livingood and G. T. Seaborg, Phys. Rev. **55**, 414 (1939).
[6] Amaldi, d'Agostino, Fermi, Pontecorvo, Rasetti, and Segrè, Proc. Roy. Soc. **A149**, 522 (1935).
[7] J. J. Livingood and G. T. Seaborg, Phys. Rev. **50**, 435 (1936).
[8] W. Y. Chang, M. Goldhaber, and R. Sagane, Nature **139**, 962 (1937).
[9] M. L. Pool, J. M. Cork, and R. L. Thornton, Phys. Rev. **52**, 239 (1937).
[10] A. C. G. Mitchell, L. M. Langer, and P. W. McDaniel, Phys. Rev. **57**, 1107 (1940).
[11] G. T. Seaborg, J. J. Livingood, and J. W. Kennedy, Phys. Rev. **57**, 363 (1940).
[12] C. V. Kent and J. M. Cork, Phys. Rev. **62**, 297A (1942).

of vinylite dissolved in methyl ethyl ketone. The surface density of the source, including all materials, was estimated to be 30 mg/cm^2.

More than seventy days after the sample was bombarded, measurements were started on the continuous (negative electron) spectrum of Sb^{124}. The beta-ray activity of Sb^{122} was, by this time, reduced to approximately one part in two hundred million. The only other long lived activities present were those due to a 30-day gamma-ray[12] and to the 125-day Te^{121} activity. Since the latter decays either by K-electron capture or by positron emission, there were no beta-rays due to these activities except possibly those due to internally converted gamma-rays. In addition, measurements made at the momentum intervals specified by 3170 gauss-cm (0.57 Mev) and 5680 gauss-cm (1.26 Mev) gave half-lives of 59 days and 62½ days, respectively.

All relative numbers of counts were reduced to a standard time on the assumption that the 60-day half-life given by Livingood and Seaborg is correct.

Figure 1 is a plot of the relative number of counts per momentum interval against the corresponding momenta specified in gauss-cm. The probable errors in the relative numbers are given approximately by the lines through the points. A greatly magnified drawing of the end-point region is shown in the upper right-hand corner. Figure 1 clearly indicates that the continuous spectrum consists of two components.

The end points were determined both by inspection and by the Fermi plots. The two sets of values are in good agreement. Allowance was made for the fact that the last beta-rays to enter the counter were grazing the inner slit jaw. The upper end point did not include a small tail on the observed curve. The end points assigned were 3800±100 gauss-cm and 9720±200 gauss-cm. These probable errors are due largely to the magnetic field calibration. They would be about one-half as large on the basis of internal consistency alone. These end points correspond to energies of 0.74±0.03 Mev and 2.45±0.07 Mev.

The difference between these end points, 1.71±0.07 Mev, agrees with the known value of the energy of the hard gamma-ray of Sb^{124}. Using the absorption method, Mitchell, Langer, and McDaniel[10] obtained a value of 1.82±0.05 Mev for this gamma-ray. More recent measurements by Scharff-Goldhaber and Klaiber[13] gave a value of 1.75±0.02 Mev.

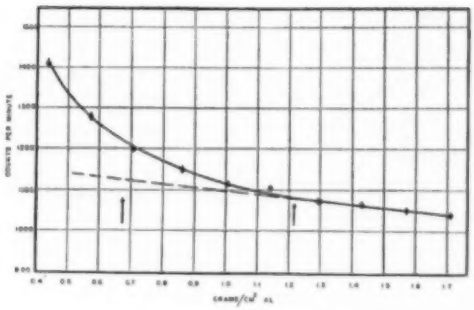

FIG. 3. Absorption in aluminum of beta-rays of Sb^{124}.

In addition, an internal conversion line corresponding to a gamma-ray energy of ~0.23 Mev was observed. Since the spectrometer was not adapted for making accurate measurements of line profiles, only the peak position (A) is indicated. This line appeared to have a half-life greater than 60 days. There is also an indication of another internal conversion line at 0.61 Mev (see point B, Fig. 1).

These values are in good agreement with those of two of the internally converted gamma-rays reported by Kent and Cork[12] as emanating from the separated tellurium fraction. They obtained the values 0.211 Mev and 0.615 Mev.

The half-life of Sb^{124} and the end-point energy of the continuous spectrum are such that a transition corresponding to the higher energy group is highly forbidden; consequently, to plot it according to the simple Fermi theory has no particular significance. When this is done, however, a straight line is obtained over a long portion of the curve (Fig. 2). The $f(n, Z)$ function used in making this plot was the Fermi function for large Z.

VI. ENERGY LEVEL SCHEME AND DISCUSSION

Livingood[7] made absorption measurements on the beta-ray spectrum of antimony forty-four days after the source was formed, when only the longest period remained. He found that 2 mm of aluminum cut out all of the activity, and from the shape of the absorption curve (log plot),

[13] G. S. Klaiber and G. Scharff-Goldhaber, Phys. Rev. 61, 733A (1942).

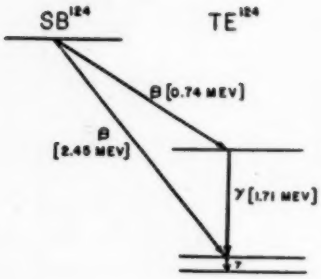

FIG. 4. Proposed energy level diagram for the levels of Te^{124} observed in the disintegration of Sb^{124}.

concluded that there was only a single distribution of electrons present.

Later, Mitchell, Langer, and McDaniel[10] reported single absorption and coincidence absorption measurements on Sb^{124}. They also concluded that Sb^{124} has a simple beta-ray spectrum and from single absorption measurements found the end point to be 1.53 ± 0.05 Mev.

In order to try to understand these discrepancies (end-point energy obtained by the authors $=2.45\pm0.07$ Mev; spectrum complex), the source was removed from the beta-ray spectrometer and single counter absorption measurements were made. The curve is shown in Fig. 3. Although the gamma-ray background was fairly intense, it is apparent that the point of tangency is approximately 1.22 grams/cm² of aluminum. This corresponds to an end-point energy of $\sim$2.5 Mev, which, within the probable error of the absorption measurement, is in good agreement with the beta-ray spectrometer value. The arrow at the left indicates where the point of tangency would have to be to give the value obtained by Mitchell, Langer, and McDaniel.

Although the methods of preparing the sources were different, this could not, in accordance with our present knowledge of these reactions, account for the reported differences in the character of the beta-ray spectrum.

In addition to single absorption measurements, the above-mentioned authors[10] also determined the number of beta-gamma coincidences, per beta-ray recorded, as a function of the thickness of aluminum between the source and the beta-ray counter. A thick absorber (0.6 cm Al) prevented all beta-rays from reaching the gamma-ray counter. When plotted as a function of the thickness of the aluminum absorber, the number of beta-gamma coincidences per recorded beta-ray was found to be independent of the energy of the beta-rays over a range extending from zero to 0.4 g/cm² Al ($\sim$.96 Mev).

From these results, Mitchell, Langer, and McDaniel concluded that the beta-ray spectrum of Sb^{124} was simple and that the resulting Te^{124} nucleus was left in an excited state.

It is difficult to correlate these results with those reported by the authors. If we assume that the level scheme is that shown in Fig. 4, for which there is considerable evidence, the beta-gamma coincidence ratio would be;

$$R=K_1/(1+(N_2/N_1))+K_2.$$

K_1 and K_2 are, for all practical purposes, constant, and N_2/N_1 is the ratio of the number of beta-particles in the high energy spectrum to the number in the low energy spectrum which are recorded for a given absorber thickness. This ratio R decreases rapidly with absorber thickness until the end point of the low energy spectrum is reached, and thereafter remains constant. The initial decrease should show up plainly in a coincidence experiment.

A second level was included in the energy level diagram (Fig. 4), since a second low energy gamma-ray (0.069 Mev by absorption measurements) has been reported by Mitchell, Langer, and McDaniel. In addition, they found gamma-gamma coincidences decreasing with a 60-day half-life and showed that this low energy gamma-ray was involved in the coincidences.

This level scheme, however, does not account for the preponderance of gamma-gamma coincidences per gamma-ray compared with the number of beta-gamma coincidences per recorded beta-ray. Mitchell, Langer, and McDaniel found this ratio to be 1.35.

For the level scheme shown in Fig. 4, the theoretical value of this ratio is less than one even if the counter sensitivities vary greatly with gamma-ray energy.

VII. ACKNOWLEDGMENTS

This research was supported in part by a grant from the Graduate School Research Fund. We are grateful for the continued interest of Professor Goldhaber and for the many suggestions made by the technicians, Charles Van Holland and Ernest Englund, Sr., who constructed the instrument.

Absorption Spectrum of N_2 in the Extreme Ultraviolet[1]

R. EDWIN WORLEY*
Department of Physics, University of California, Berkeley, California
(Received July 8, 1943)

The absorption spectrum of N_2 that corresponds to excited states in the range 12.2 – 17.0 ev has been investigated at large dispersion. Data are presented for a very extensive Rydberg series of bands, which are interpreted and correlated with previous observations. The ionization potential of N_2 corresponding to the series limit is 15.577 volts. Absorption beyond this point is complete for a path of ~0.5 mm atmos. From λ995 to λ815 the spectrum is well developed at ~0.2 mm atmos. Here most of the absorption is due to bands that show an open rotational structure which could usually be analyzed to give values of $B' - B''$. Several such bands above λ920 are correlated with the known states b and b'. In general the internuclear distance, r_e', was found to increase with energy, up to values 40 percent larger than for the normal state. Vibrational constants are unexpectedly small ($\omega'/\omega'' < \frac{1}{3}$), and the ratio ω'/B' is about half the nearly constant value (Birge-Mecke rule) found for all the lower states of N_2. There is some evidence that the coupling in a few of the more excited states represents a transition toward Hund's case d'.

INTRODUCTION

STUDIES of absorption in the extreme ultraviolet have furnished valuable information on the higher electronic states of diatomic molecules, but the existing data are still meager. My own investigation of the N_2 bands in the region λλ1015–730 has led to a number of interesting results, the details of which have not previously been published.

For purposes of orientation, the electronic scheme of the singlet states of nitrogen is given in Fig. 1. The a state was discovered from Lyman's[2] early measurements of the ultraviolet spectrum in 1911, and with the extension of this work in 1928 by Birge and Hopfield,[3] the states b, b', and c were added. In 1930, Hopfield[4] reported the absorption bands analyzed in this paper and gave data on two Rydberg series of bands at shorter wave-lengths. Both series, one in absorption and one in emission, have since been observed by others,[5] and the absorption series was interpreted by Mulliken[6] so as to give a spectroscopic value of the ionization potential of N_2. New ground state progressions reported in 1934 by Watson and Koontz[7] were designated d, e, g, f, and h, but of these Tschulanowsky[8]

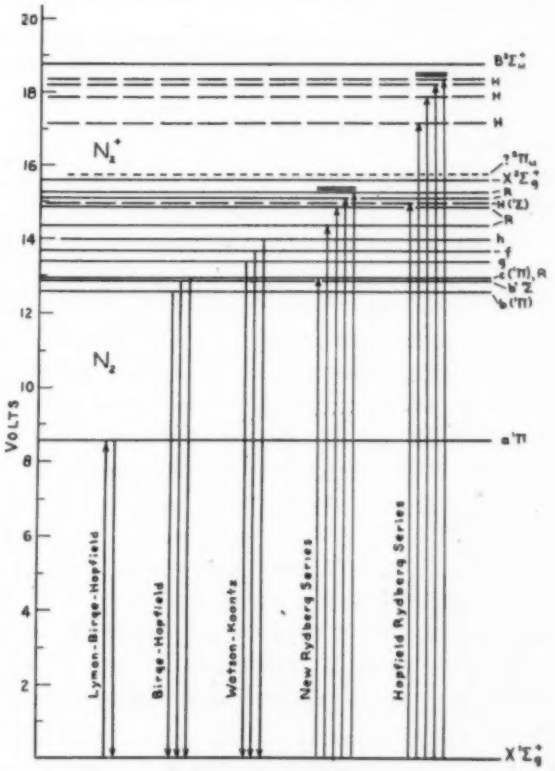

FIG. 1. Rydberg terms, and previously known singlet states, of N_2. The excited terms corresponding to the progressions of Fig. 2 lie between 12.5 and 15.3 ev (Fig. 4).

[1] For further details, see R. E. Worley, Thesis, University of California, 1940. The present article includes revisions and supplemental material.
* Now at the University of California at Los Angeles, on leave from San Diego State College.
[2] T. Lyman, Astrophys. J. **33**, 98 (1911).
[3] R. T. Birge and J. J. Hopfield, Astrophys. J. **68**, 257 (1928).
[4] J. J. Hopfield, Phys. Rev. **35**, 1133 (1930); **36**, 789 (1930). Cf. also ref. 3, p. 274.
[5] T. Takamine, T. Suga, and Y. Tanaka, Sci. Pap. Inst. Phys. Chem. Res. Tokyo **34**, 854 (1938).
[6] R. S. Mulliken, Phys. Rev. **46**, 144 (1934).
[7] W. W. Watson and P. G. Koontz, Phys. Rev. **46**, 32 (1934).
[8] W. M. Tschulanowsky, Bull. Acad. Sci. U.S.S.R. Classe d. sci. math. et nat., p. 1313 (1935). The results are briefly tabulated in ref. 1, p. 68a. Cf. also, W. M. Tschulanowsky and S. I. Gassilewitsch, Physik. Zeits. Sowjetunion **12**, 83 (1937).

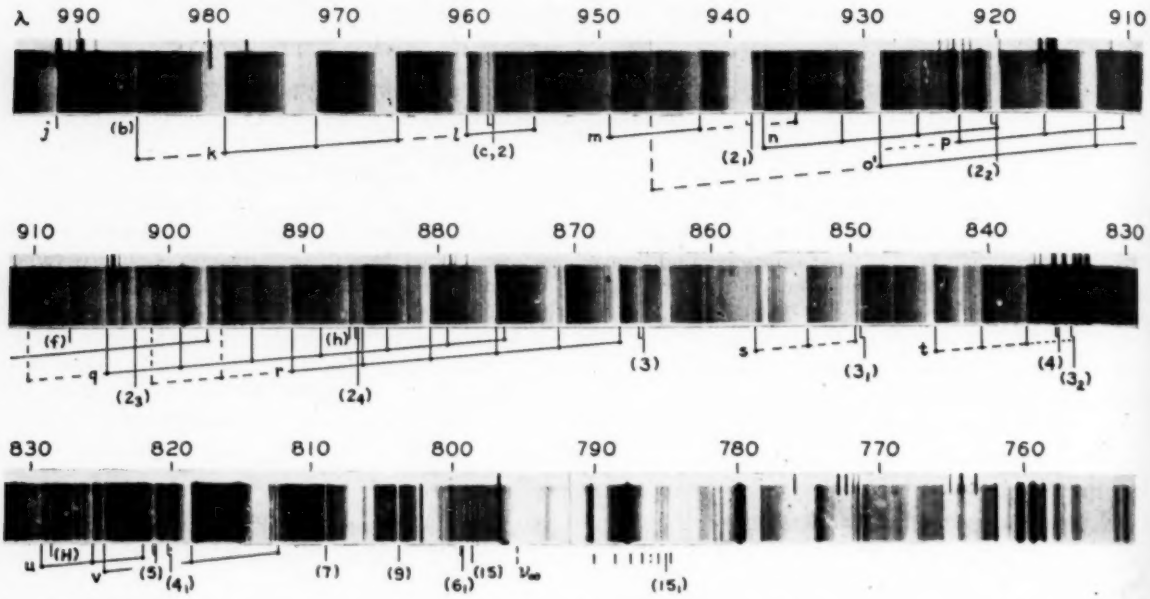

FIG. 2. Far ultraviolet absorption spectrum of N_2 (positive, 5.7×). Bands that have been grouped in progressions are joined by sloping lines. Rydberg bands of the main series ($v'=0$) are shown by parenthesized integers; subscripted integers refer to bands having $v'>0$.

ascribed d and e to the vibrational levels $v'=2$ and 3 of state b'. The Σ nature of this state was also established by Tschulanowsky, while the Π character of the a state is indicated by several investigations.[7, 9]

The first result of the present study was the announcement of a new Rydberg series[10] converging to the normal state of N_2^+. Some of the Rydberg terms are shown in Fig. 1, and it is now found that the lowest is the c state of Birge and Hopfield. Numerous bands that do not form obvious series of the Rydberg type will for convenience be referred to as "non-Rydberg." Several of these are interpreted as transitions to vibrational terms of states b and b', but the majority involve new electronic states. The partial rotational analysis obtained for many of the bands will be considered after discussing the Rydberg series.

EXPERIMENTAL

Apparatus

The vacuum spectrograph employed a three-meter grating of aluminized speculum, ruled 15,000 lines to the inch, and mounted at a grazing angle of 7.0°. This arrangement gave a dispersion of better than 2A/mm in the region investigated. The instrument was focused with precision, and correct grating apertures[11] were provided. An improved Lyman discharge tube used as source of the continuum has been described elsewhere,[12] but it may be noted here that the design largely avoids the usual mechanical difficulties, and that it was feasible to use a narrow slit (~0.02 mm) as required for good resolution.

Nitrogen used for absorption was prepared from sodium azide,[13] and stored in a large glass tank. Before an exposure, the spectrograph was thoroughly flushed, and the gas was then passed through in a slow, steady stream. As helium (purified) was generally used in the discharge tube, this gas was also present in the spectrograph. A condensed discharge through tank helium,

[9] E. T. S. Appleyard, Phys. Rev. **41**, 254 (1932). Cf. also G. Herzberg and H. Sponer, Zeits. f. physik. Chemie **26**, 1 (1934), footnote p. 2.

[10] R. E. Worley and F. A. Jenkins, Phys. Rev. **54**, 305 (1938). The indicial lines above Fig. 1 of this reference are in error. These higher members of the series are shown well, also, on a plate taken by other workers (reference 25), who used a helium source.

[11] R. O. Anderson and J. E. Mack, J. Opt. Soc. Am. **24**, 292 (1934), with the earlier papers listed therein. References to slit illumination are included.

[12] R. E. Worley, Rev. Sci. Inst. **13**, 67 (1942).

[13] Erich Tiede, Ber. d. D. Chem. Ges. **49**, 1742 (1916). I found it safe to decompose powdered azide with a low bunsen flame, if the azide was held in a nearly horizontal Pyrex tube (2-mm wall), protected from the main system by elbows filled with glass wool.

which contained traces of argon in air, provided a good comparison spectrum.[12]

Plate Material

Data for the initial report of the new Rydberg series were taken from exposures made with an earlier form of discharge tube,[14] with nitrogen in the source as well as in the receiver, and the reduction was based on a few lines of O II and O V that appeared with the continuum. The subsequent improvement in technique netted a distinct gain in actual resolution and permitted a more accurate reduction of the data. Both Ilford Q II and Hilger Schumann plates were employed, but most of the final measurements are taken from a single Schumann plate of unusually fine definition, reproduced in Fig. 2. The equivalent path of N_2 in this case was about 0.2 mm atmos., or one two-thousandths of the path used by Birge and Hopfield[3] in photographing the $a-X$ absorption bands. The spectrum shows no trace of contamination by O_2,[15] and very few atomic absorption lines of significant intensity are present. Absorption by helium in the source so weakened the continuum below λ505 that its 2nd order caused no obscuration in the region studied.

A comparator with a least count of 1μ was used to measure all plates, and the reduction was effected by linear interpolation between values of λ calculated quadratically for each millimeter. A final correction was based on the comparison spectrum of the individual plate.[1] In view of the care taken, it is probable that the absolute error for absorption lines rarely exceeds 0.02A,[1] while the relative error was about a tenth as great in favorable cases. The uncertainty in the relative position of band heads was about 0.01A, as judged from the consistency of two sets of readings.

RESULTS

Measurements of band heads, and of regions of diffuse absorption, were carried out for the range λλ1015–734. Except for higher members of the main Rydberg series (Table II), these results are collected in Table I. An arbitrary symbol in the first column designates the group to which a band is assigned, while eye estimates of intensities (0 to 15) are given in the second. The third and fourth columns contain λ_{vac} and ν_{vac}, respectively. As explained later, it was in many cases possible to obtain $-C=B''-B'$ from the rotational structure [Eqs. (1) and (3)]. This value, and the ratio $r'/r''=(B''/B')^{\frac{1}{2}}$, are given in columns five and six.[16] Incidental remarks appear in the last column. Here the letters V and X refer, respectively, to longer (violet) and shorter (x-ray) wave-lengths, while the symbols (d), d, and dd represent increasing degrees of diffuseness of band heads. Data beyond the Rydberg series limit are arranged somewhat differently, as explained in the table. Most bands beyond $R_1(16)$, and those indicated by a dagger, were recently measured at the Mt. Wilson Laboratory, on a comparator kindly made available by Dr. A. S. King.

RYDBERG SERIES

Very striking in Fig. 2 is the group of closely spaced, converging bands, lying between λ801 and the O II emission line λ797. These are the higher members of the series, whose limit at λ795.8 is indicated by ν_∞. With the identification of its first five members—raising the number of reliably measured bands to over twenty—this molecular Rydberg series is the most extensive thus far reported. The bands are all shaded toward longer wave-lengths, and are characterized by absence of resolved rotational structure. Lower members—indicated by Rydberg integers, m, in parentheses—show two heads of about equal intensity, but these draw together and are unresolved beyond $m\sim 8$. Where measurable, both heads are listed in Table I [$R_0(m)$ and $R_0'(m)$], and their separation $\Delta\nu_h$ is given in Table II. In the latter table, wave numbers of the more prominent short wave-length heads are listed for all observed members of the series.

With the new data it was possible to improve slightly the value of the series limit ν_∞ and to derive a Ritz formula to fit all but a few heads

[14] H. P. Knauss and S. S. Ballard, Phys. Rev. **48**, 796 (1935).

[15] The strong O_2 band λ983.1, faintly present on some of the earlier plates, is clearly absent. [Cf. W. C. Price and George Collins, Phys. Rev. **48**, 714 (1935).]

[16] Cf. ref. 37. An inferior digit in column five usually indicates an average deviation of at least 5 units in the last place.

TABLE I. Absorption bands of nitrogen, λλ1015–734 (Plate *B*59).

Group	Int.	λ(*A*)	ν(cm⁻¹)	$B''-B'$	r'/r''	Remarks
i	0^-	1015.37	98,486	—	—	Rotational structure not discernible.
—	0	08.95	9,113	—	—	Center of narrow, unshaded band. (N_2?)
i	0	08.52	9,155	—	—	Head (partially masked). Open rotational structure.
i	0^+	01.74_6	9,826	—	—	Head. Open rotational structure.
—	00	00.16_3	9,984	—	—	Faint, narrow band, shaded *V*. (N_2?)
—	0^-	994.23	100,580	—	—	Center of narrow, unshaded band. (N_2?)
		Preceding bands, from Plate *B*45 (higher pressure). Absent from Plate *B*59.				
j	2^+	991.853	100,821.4	0.54_5	1.17_3	
b, *k*	2	85.649	1,456.0	0.58	1.19	
k	10	78.87	2,158	0.58_5	1.19	(*d*) (Cf. Table IV.)
k	15	72.0_7	$2,87_3$	0.59	1.19	*dd*. Interpolated from Pl. *B*69 (lower pressure). (Cf. Table IV.)
k	12	965.63	3,559	0.580	1.187	(*d*) (Cf. Table IV.)
k(*l*)	7	0.206	104,144.4	0.508	1.158	
c $R_0'(2)$	3	958.625	$316._1$	0.077	1.020	$B''-B'$, estimated from $\Delta\nu_A$.
c $R_0(2)$	2	8.170	365.6			
k(*l*)	2	5.076	703.7	0.52	1.16	
m	2	949.221	105,349.6	0.63	1.21	
[*o'*]	1	6.123	694.5	—	—	
m	3	2.386	106,113.6	0.64	1.21^+	
$R_1(2)$	8	938.57	545	—	—	(*d*)
..	—	8.314	574.1	—	—	Strong blend in λ937.7. (Reference line.)
n	2	7.654	649.2	0.81	1.30	Apparent head. (Cf. Table IV.)
..	0	7.20	70_0	—	—	Center of narrow, unshaded band on Pl. *B*45. (N_2?)
[*m*]	1	5.147	935.1	—	—	
n	1^-	1.727	107,327.6	0.83^-	1.31^-	
o'[*p*]	6	928.876	657.0	—	—	(*d*)
n	1	5.926	108,000.0	0.80_5	1.29_5	(*d*)
p	2	2.746	372.2	0.78_5	1.28_4	
—	$\frac{1}{2}$	0.73_2	609	—	—	Faint head (?).
$R_2'(2)$?	$\frac{1}{2}$?	0.46	641	—	—	Questionable (overlaid).
$R_2(2)$; *n*	3^+?	0.04_1	$690._8$	—	—	Overlaid by λ919.8.
—	1^+?	919.846	713.9	—	—	
p	3	6.416	109,120.8	0.78	1.28	
o'	5	2.622	574.4	—	—	(*d*)
p[*q*]	1^-	0.475	832.8	—	—	
f	1	907.453	110,198.5	—	—	
q	2	4.731	530.1	0.88	1.34	
—	1	3.637	664.0	—	—	
$R_3(2)$	2	2.578	793.7	—	—	
[*r*]	1^-	1.352	944.5	—	—	
q	2	899.196	111,210.5	0.90	1.35	
o'	3	7.185	459.8	—	—	
[*r*]	1^+	6.192	583.3	—	—	(*d*)
q	1	3.863	873.9	0.92	1.36	
r	2	0.949	112,239.8	0.92_0	1.36_3	
q	$\frac{1}{2}$	888.81	51_0	—	—	Head very indistinct.
h	2	6.694	778.5	—	—	
$R_4'(2)$?	0^+	6.24_6	$835._3$	—	—	Line-like (questionable).
$R_4(2)$	$\frac{1}{2}$	6.030	863.0	—	—	Line-like.
r	2	5.657	910.5	—	—	
q	$\frac{1}{2}$	3.90_6	$113,134._2$	0.9_4	1.38^-	
..	—	2.966	254.7	—	—	Strong blend in λ880.7. (Reference line.)
r	4	0.723	543.1	0.93_5	1.37_2	(*d*) Rotational perturbation at λ882.5 (text)
q	$\frac{1}{2}$	879.47	705	—	—	
r	3^+	5.869	114,172.3	0.94_5	1.37_9	(*d*)
q	$\frac{1}{2}$	5.24	254			
r	3?	1.40?	758	0.94⁻?	1.37	Obscured by λ870.7. (Cf. Table IV.)
—	1^+?	0.744	844.3	—	—	
r	3	866.761	115,372.1	0.91^+	1.36	(*d*) Seemingly overlies another band.
$R_0'(3)$	1	5.324	563.6	—	—	
$R_0(3)$	1	5.060	598.9	—	—	
—	1	3.171	851.9	—	—	
—	1^-	0.511	116,210.1	—	—	
(*s*)	2^+	856.98	689	0.88	1.34	Head indistinct. (Cf. Table IV.)
—	2^-?	6.004	821.8	—	—	Overlapped by λ853.2.
(*s*)	5	3.190	117,207.2	0.93_5	1.37	(*d*)
(*s*)	4	849.714	686.6	1.03?	1.44?	*d*, overlaid by λ849.3.
$R_1'(3)$	1^+	9.302	743.7	—	—	

TABLE I (*Continued*)

Group	Int.	λ(A)	ν(cm⁻¹)	$B''-B'$	r'/r''	Remarks
—	1^+	846.930	118,073.5	—	—	
(*t*)	3^+	3.972	487.3	0.8_3?	1.31?	
..	—	2.860	643.7	—	—	Last *V* line, region of irregular absorption.
..	—	2.05_5	757.1	—	—	*V* edge of complete absorption.
..	—	1.873	782.8	—	—	*X* edge, same. (Band head?)
(*t*)	3	0.552	969.4	—	—	
(*t*)	2^+	837.314	119,429.5	0.95_0	1.38_2	
$R_0'(4)$	1?	5.16₀	737.8	—	—	Obscured by O III emission line.
$R_0(4)$		4.951	767.6	—	—	
?	$\frac{1}{2}^+$	4.52	829†	—	—	*V* edge, O II line. Open rotational structure at ~λ836 indicates head near this entry.
$R_2'(3)$?	$\frac{1}{2}$	4.11	888	—	—	Head indistinct.
—	$\frac{1}{2}$	2.00	120,192	—	—	
(*u*)	1^-	829.293	584.6	0.92	1.36	
H	1	8.550	692.8	—	—	
?	$\frac{1}{2}$	6.20	121,036†	—	—	Questionable head.
—	$\frac{1}{2}$	5.97_9	068.6	Questionable (overlaid).		
(*u*)	1?	5.64_6	117.2	Open but confused structure, associated with one or both heads.		
—	1?	5.575	127.7			
..	—	5.223	179.4	Line-like absorption.		
(*v*)	1	4.76_4	246.8	*X* edge of narrow band. Weak absorption extends to preceding "line."		
—	$\frac{1}{2}$	3.36	454	Interpolated from Pl. *B*45. (Open rotational structure.)		
(*u*)	0	2.12	636	Interpolated from Pl. *B*45.		
$R_0'(5)$	$\frac{1}{2}$	1.240	767.1			
$R_0(5)$	$\frac{1}{2}$	1.110	786.4			
$R_1'(4)$	$\frac{1}{2}^-$	0.234	916.4			
$R_1(4)$?	0^+	0.04_8	944.4			
—	3^+	818.66	122,151	*V* head interpolated from Pl. *B*69 (lower pressure). If single band, rotational structure is compact.		
(*v*)		8.534	169.6			
..	—	5.689	595.7	Line-like absorption.		
—	4?	3.6_2	90₀	Interpolated from Pl. *B*69 (lower pressure). Indication of rotational structure near λ814.5.		
[$R_0(6)$]	—	3.515	923.3	Calc. position. Overlaid.		
?	1^-?	3.33	952	Narrow band (?). Overlaid.		
—	1?	3.02_9	996.8	Narrow band (?).		
..	—	2.755	123,038.3	Center, narrow band (unshaded).		
(*v*)	1	2.366	097.2	*X* edge, narrow band.		
..	—	0.84	329†	Line-like absorption.		
..	—	0.312	409.3	Line-like absorption.		
$R_0'(7)$	1^-	808.96₇	614.4	Poorly resolved.		
$R_0(7)$		8.90₉	623.3			
—	5	6.43	124,004	*d*. Questionable traces of rotational structure near λ807.5.		
[$R_0(8)$]	—	5.901	084.7	Calc. position. Overlaid.		
?	2	5.72₅	111.8	Probable head.		
—		5.605	130.3	Definite head.		
..	—	4.484	303.3	Line-like absorption.		
$R_0(9)$	1^+	3.81_3	407.2			
$R_0(10)$	—	2.33	637	*V* edge of O IV emission line.		
$R_0(11)$	—	1.21	811	Overlaid by diffuse absorption.		
$R_0(12)$	$\frac{1}{2}^+$?	0.352	945.0	Tail, overlaid by diffuse absorption.		
$R_0(13)$	$\frac{1}{2}^+$	799.681	125,049.8			
$R_1'(6)$?	0^+	9.47	083			
$R_1(6)$	0^+	9.38_0	096.9			
$R_0(14)$	$\frac{1}{2}$?	9.155	132.2	Tail, overlaid by $R_1(6)$.		
$R_0(15)$	$\frac{1}{2}^-$	8.723	199.8			

For $R(16)$ to $R(26)$, see Table II. Following these bands on Plate *B*59 (Fig. 2) is a short region of strong, diffuse absorption, with a slight rise in background at ~126,030 cm⁻¹. Weaker, general absorption extends a great distance toward shorter wave-lengths, with a weak maximum at ~λ720. Above λ734 a number of structureless bands, many of them with diffuse heads but nearly all shaded to longer wave-lengths, are in evidence.

The following wave numbers refer to heads (*X* edges) of such bands, except as otherwise noted. The very narrow, faint bands that are members of the $v'=1$ Rydberg series are designated "$R_1(m)$." A rough estimate of the width of broad bands is given in the first column, and an index of completeness of absorption (1 to 5) is entered in the second. Bands that are in evidence on Plate *B*69 (lower pressure) are indicated by an asterisk. When they were measured only on this plate, the fact is indicated by a leading entry "*B*69," under "Remarks." Band widths and intensities refer always to plate *B*59.

TABLE I (*Continued*)

Width (cm^{-1})	Absorp. (*B59*)	$\nu(cm^{-1})$	Remarks
—	—	125,789*	*B69*, line-like absorption (traces).
—	—	126,113*	*B69*, line-like absorption.
—	(4)	306*	*B69*, strong band. (Possible 2nd head, ~40 cm^{-1} toward *V*.)
—	—	437*	*B69*, narrow band. (Cf. next entry.)
—	3	454	*d*, *B59*. Indistinct edge of seemingly continuous absorption.
—	—	481.1	Narrow band.
—	—	579.4	$R_1(9)$.
150	5	698.7*	*d*. Extends to O IV 790.2; 790.1 is absent. (Diffuse on *B69*.)
—	—	741.0	Faint, narrow band.
—	—	816.0	$R_1(10)$.
—	—	987.8	$R_1(11)$.
—	—	127,118.9	$R_1(12)$.
120	4	251*	*d*. (Diffuse on *B69*.)
—	—	306.1	$R_1(14)$.
—	—	373.7	$R_1(15)$.
—	—	428.7	$R_1(16)$.
80	3⁻	517	*dd*. This and next head, questionable.
50	3⁻	603*	*dd*. (Strong, but diffuse, on *B69*.)
60	3⁻	732	*dd*.
—	—	128,054*	*B69*, distinct head.
200	3	100	*d*. Masks previous head.
20⁻	2	157	Center of narrow, diffuse band.
200	2	462*	Head (*V* edge of 3rd order C IV 259.47). (Weak on *B69*.)
(220)	(4)	94_2*	*B69*, strong band.
>140	3	129,082*	*d*. Masks previous band. (Faint, narrow, on *B69*.)
—	—	105	Faint, line-like absorption in wing of O V 774.5.
—	—	129	Sharp, line-like absorption, super-posed on O V 774.5 ("self-reversed" appearance).
(240)	(2)	581*	*B69*, head. (*V* edge of 4th order O V 192.91.)
—	—	651*	*B69*, head (?). (*V* edge of 4th order O V 192.80.)
40	1	980*	Center, diffuse band. (Very faint on *B69*.)
80	2⁺	130,249*	*d*. (Very faint on *B69*.)
160	4	606	*V* edge (absent on *B69*).
		768*	*d*. *X* edge of same band. (Sharp, 15 cm^{-1} smaller, on *B69*.)
		878	Diffuse *V* edge.
160	3	984*	*B69*, weak head (sharp).
		131,034	Diffuse *X* edge.
—	—	069	Narrow band (sharp head).
—	—	44_4*	*B69*, head (?).
>230 (?)	5	477	Head, or *V* edge of O V 760.44. Absorption extends to O V 762.00; obscures O V 761.13.
—	—	543	Fine, line-like absorption (traces); "splits" O V 760.23.
>70 (?)	3	625	Sharp head (precedes edge of O V 759.44).
>80 (?)	3	910*	Sharp head.
60	3⁻	132,135*	
100	2⁻	373	Questionable (sharp, but overlaid).
(200)	(2)	59_0*	*B69*, diffuse head.
>70	2⁻	657	Masks previous entry.
40	2	791*	(Very faint on *B69*.)
120	2	133,002*	(Traces, 100 cm^{-1} toward *V*, on *B69*.)
<10	—	076	Center, very narrow band.
20⁻	1⁺	118	Head, narrow band.
30	2	202	Head.
<10	—	240	Center, very narrow band.
100	2	37_0	Questionable head (overlaid).
>130	2⁺	508*	Sharp head.
—	0⁺	572	*V* edge of weak absorption.
100	2	688*	*V* edge, stronger absorption.
		792*	Head (*V* edge of 2nd order O III 373.80).
70	3	967*	*d*. Contrast, very poor beyond this point.
220	3	134,400	Head (?).
30	2	498	*V* edge (?).
		530	*X* edge.
—	—	671	Line-like absorption, traces.
—	—	723	Line-like absorption, traces.
10	—	775	Center, narrow band.
120 (?)	1	860	*d*. Head (?).
—	2⁻	975	*d*. *V* edge (?).
>80 (?)	2⁻	$135,61_0$*	Head (?). (Very faint on *B69*.)
>120 (?)	2	136,169*	Head. (Very faint on *B69*.)

within the accuracy of measurement.[17] The residuals shown in Table II under $\nu^{obs}-\nu^{calc}$ were obtained from

$$\nu^{calc}=125{,}665.8-R/(m+0.3450 \\ -0.1000/m-0.100/m^2)^2,$$

with $m=2, 3, \cdots$ and $R=109{,}735$ cm^{-1}. Inasmuch as the measurements on lower members do not represent band origins, the small discrepancies in these cases are of no consequence.

The region of continuous absorption that follows the series limit, Fig. 2, corresponds to unquantized photo-ejection of an electron from N_2, and the limit itself gives, very precisely, an ionization potential of N_2. Its value, namely, 125,666 cm^{-1}=15.577 volts,[18] agrees perfectly with the ionization potential obtained less directly by Mulliken.[6] He pointed out that the upper terms of Hopfield's absorption series very likely approach the $^2\Sigma_u^+$ state of N_2^+ as a limit (evaluated below), and that subtraction of the electronic energy of the $^2\Sigma_u^+\rightarrow{}^2\Sigma_g^+$ emission system[19] of N_2^+ should accordingly give the position of the $^2\Sigma_g^+$ state of N_2^+ relative to the ground state of N_2. The result, in this case, is 151,247 −25,566=125,681 cm^{-1} or 15.579 ev. The limit of the new series represents the *lowest* ionization potential of N_2, if, as is believed, $^2\Sigma_g^+$ is the normal state of N_2^+.[20]

This state, $^2\Sigma_g^+$, is reached from $X^1\Sigma_g^+$ of N_2 by removal of a $\sigma_g 2p$ electron,[21c,22] whose excitation therefore gives rise to the Rydberg terms. These should be of Π type, as the double-headed aspect of the first few bands may be attributed to the presence of R and Q branches. The excited orbitals appear then to be $np\pi$ (Rydberg notation), with $n=3, 4, 5\cdots$, since $3p\pi$ is the lowest orbital to which $\sigma_g 2p$ (i.e., $3s\sigma$) could be excited and yet give a firmly-bound Π state. Thus it is probable that these Rydberg terms are of the form

$$KK(\sigma_g 2s)^2(\sigma_u 2s)^2(\pi_u 2p)^4(\sigma_g 2p) \\ \cdot(np\pi)^1\Pi_u, \quad n=3, 4, 5, \cdots.$$

No *series* of levels having the corresponding configuration $3s3p^2np$ is reported for the united atom Si I (below), but a single $3p^3D$ term is listed by Kiess.[23] Since the effective quantum number is of the same magnitude as for the first of the above molecular terms, the level $n=3(m=2$, Table II) is the lowest one to be expected in N_2.

As previously mentioned, this lowest Rydberg term has been identified as the c state of Birge and Hopfield,[3] who obtained the heads (0−0 band) by extrapolation. My direct measurements give a value 30 cm^{-1} smaller for the R head, but sensibly the same result for the Q head. The long wave-length (Q) heads of the $c-X$ emission bands were found by Birge and Hopfield to give the best fit in an ω_v formula, and this circumstance, together with the appearance of the bands, led them to favor type II for state c. The fact that the two heads in each absorption band draw rapidly together with increasing n is doubtless due to uncoupling of the orbital mo-

TABLE II. Heads of the new Rydberg series.*

m	ν^{obs}	$\nu^{obs}-\nu^{calc}$	$\Delta\nu_k$	m	ν^{obs}	$\nu^{obs}-\nu^{calc}$
2	104,365.6	−4.4	49.5	14	125,132.2	+0.2
3	15,598.9	+6.4	35.3	15	199.8	+0.5
4	19,767.6	−1.1	(30)	16	254.9	+0.2
5	21,786.4	−3.6	19.3	17	300.7	−0.1
6	(Table I)	—	—	18	339.0	−0.5
7	23,623.3	+0.6	8.9	19	371.9	−0.5
8	(Table I)	—	—	20	400.8	+0.2
9	24,407	+1.1	—	21	424.1	−0.7
10	4,637	(−1.2)	—	22	445.6	−0.3
11	4,811	(−0.7)	—	23	465.0	+0.6
12	4,945.0	+0.3	—	24	480.7	+0.1
13	5,049.8	+1.0	—	25	494.4	−0.5
				26	506.4	(−1.2)

* The bands for m=6, 8, 10, and 11 occur in regions of strong and seemingly diffuse absorption, but in the last two cases approximate wave numbers can be given (cf. Table I). The second head for m=4 is obscured by an emission line (O III). At m=9 (remeasured), the appearance still suggests two heads, but they are unresolved.

[17] The procedure was to first compute μ, in the Rydberg denominator, from the reliable measurements on bands for which it was sensibly constant (m=12 to 25), and for which the position of a band origin should, as shown below, be indistinguishable from that of its head. The value of μ so found (0.342) then led to a very consistent set of values of ν_∞ (a.d.∼0.3 cm^{-1}). However, in order to include the lower members of the series, the variation in μ has been expressed in a three-constant form, found by graphical approximation.

[18] The revised conversion factor is used. [R. T. Birge, Rev. Mod. Phys. **13**, 233 (1941).]

[19] M. Fassbender, Zeits. f. Physik **30**, 73 (1924). D. Coster and F. Brons, Zeits. f. Physik **73**, 747 (1932).

[20] One cannot altogether exclude the possibility that $^2\Pi_u$, known to be near $^2\Sigma_g^+$, is the normal state. (Cf. the brief remarks relative to $^2\Pi_u$, several paragraphs below, and again under *Absorption*, λλ*818–800*.)

[21] R. S. Mulliken, Rev. Mod. Phys. (a) **2**, 60 (1930); (b) **3**, 89 (1931); (c) **4**, 1 (1932).

[22] G. Herzberg, *Molecular Spectra* (Prentice-Hall, New York, 1939).

[23] C. C. Kiess, J. Research Nat. Bur. Stand. **21**, 185 (1938) [R.P. 1124].

mentum of the excited electron from the resultant momentum of the molecular core. Such a transition from case b' to case d' coupling is exemplified by the $(np\pi)^3\Pi \rightarrow (2s\sigma)^3\Sigma$ Rydberg bands of He_2.[24] By analogy, the heads of the higher members of the present series should give the positions of band origins very closely.

It is not surprising that Birge and Hopfield reported $c-X$ bands only in emission, as their spectrogram of the $a \leftarrow X$ system shows almost complete absorption below λ1020. When account is taken of the much smaller equivalent absorption path used in my case and of the difference in dispersion and in the number of bands observed (cf. third paragraph below), the transition probability for $c \leftarrow X$ appears to exceed that for $a \leftarrow X$ by a factor of 10^3 or 10^4. A reliable comparison however can hardly be made without photographing both systems on the same instrument, preferably at normal incidence.

Tanaka and Takamine[25] have reported several $v'=1$ bands of the new Rydberg series, and from them obtained a mean value of 2171 cm^{-1} for $\Delta G'(\frac{1}{2})$, as compared to 2175 cm^{-1} for the limiting state $^2\Sigma_g^+$ of N_2^+. I have subsequently identified several of the $v'=1$ bands on my own plates, but at the pressure used many of those with $m>4$ are overlaid by diffuse absorption.[26] My own data on these bands, indicated in Table I by the symbol $R_1(m)$, lead to the values of $\Delta G'(\frac{1}{2})$ shown in Table III. The intervals for $m=6$, 10, and 11 are based on computed heads for $v'=0$, but the last four and most reliable entries are seen to agree excellently with the expected value.

In contrast to the $v'=0$ bands, the appearance of the $v'=1$ bands for $m=3$, 4, and 6 (unobscured) shows that in these cases the R head becomes prominent only for $m>4$. Hence for $m=3$ and 4, the interval $\Delta G'(\frac{1}{2})$ has been formed with the Q head of the $v'=0$ band, rather than with the R head. Similarly, a weak band at λ834.1, if interpreted as a Q head for $m=3$, $v'=2$, gives 2144 cm^{-1} for $\Delta G'(\frac{3}{2})$, as compared to 2143 cm^{-1} for N_2^+.

The case of $m=2$, state c, is of special interest. The Q head for $v'=1$ could not be measured, but if the R head is again prominent, an intense band at λ938.6, Fig. 2, is just at the position expected for $v'=1$. In addition, heads are found corresponding to $v'=2$, 3, and 4, while for 2 and 4 there is indication of a Q head as well. The values of $\Delta G'$ (R heads) given by the five bands thus identified[27] would be 2180, 2146, 2103, and 2069 cm^{-1}. From these values, and from the $\Delta\nu_4$ interval for $v'=0$ (Table II), it has been possible to estimate ω_e and B_e, and so to plot the potential curve of state c (Fig. 4). r_0 is found to be the same as for $^2\Sigma_g^+$ of N_2^+, and to differ only slightly from r_0''—a situation ideal for the development of an extensive Rydberg series.

Professor Mulliken has reminded me that in addition to the Rydberg terms just discussed, which converge to $^2\Sigma_g^+$ of N_2^+, one may expect others that converge to $^2\Pi_u$, believed to lie slightly above $^2\Sigma_g^+$.[21] According to Mulliken's estimate[21] of 1.15A for r_e of $^2\Pi_u$, the strongest bands should have $v'>0$. Their identification would evidently give definite information regarding the relative positions of $^2\Sigma_g^+$ and $^2\Pi_u$.[20]

In correspondence, Mulliken has suggested that $a^1\Pi$ may be the lowest of the Rydberg states (derived from $^2\Pi_u$ by the addition of a σ_g electron). Nearly all bands involving higher terms would then probably be masked by stronger absorption (cf. above). On the other hand, were o' (Table IV) the lowest state, identification of higher terms would appear feasible, although even here most of them would be expected to fall below λ797 where they would not show to advantage on my plates. A cursory survey of this possibility has yielded no conclusive results.

Hopfield's Rydberg Series

For certain large energies of excitation, analogous term series are predicted for N_2 and the

TABLE III. Values of $\Delta G'(\frac{1}{2})$, for the Rydberg terms.

m	$\Delta G'(\frac{1}{2})$	m	$\Delta G'(\frac{1}{2})$
3	2180	11	(2176)
4	2179	12	2174
6	(2174)	14	2174
9	2172	15	2174
10	(2178)	16	2174

[24] W. E. Curtis, Trans. Faraday Soc. **25**, 694 (1929).

[25] Y. Tanaka and T. Takamine, Phys. Rev. **59**, 613 (1941). The work was done at Berkeley on the spectrograph described above, but the helium continuum was employed as source.

[26] In Fig. 2, the notation (m_v) refers to Rydberg bands other than those of the main series.

[27] This interpretation revises an earlier grouping of some of the bands (ref. 1) [cf. *Group o'*].

united atom Si I (14 electrons).[21,22] Examination of the known singlet terms of Si I[23,28] shows that only those of the $3pns\,{}^1P_u$ series bear a close resemblance to the excited states of Hopfield's absorption bands.[29] By considering the (two) singlet molecular states derivable from a term of the atomic series, in conjunction with the configuration of the $^2\Sigma_u^+$ state of N_2^+ approached by the terms of Hopfield's series, it appears that the upper states of these bands have the configuration

$$KK(\sigma_g 2s)^2(\sigma_u 2s)(\pi_u 2p)^4(\sigma_g 2p)^2 \cdot(ns\sigma)\,{}^1\Sigma_u^+, \quad n=4, 5, 6, \cdots.$$

Mulliken[6] had already suggested that the excited orbitals may be $ns\sigma$, but that if so, Hopfield's data start with $n=5$, whence another band would be expected at longer wave-lengths. This band should have an unresolved rotational structure ($r_e' \sim r_e''$) and should show a single head ($^1\Sigma - {}^1\Sigma$). With my high dispersion plates, it seemed worth while to look for it, even though Hopfield's other bands—diffuse in nature due to pre-ionization and situated in a region of general absorption—were not in evidence. By setting $m=1$ in the Rydberg formula[30] $\nu_m = 151{,}249 - R/(m+0.907)^2$, the calculated wave-length is found to be 825.94A. Two or three heads lie very near this position, and at least one (λ825.98) is of a suitable character except for its low intensity. However, by the analogy with Si I, the band sought would be displaced toward longer wave-lengths. This consideration as well as that of intensity leads me to favor the narrow band with a single, sharp head at λ828.55 (H—Fig. 2).

Besides the series in absorption, Hopfield[4] reported one in emission. This series is also clearly in evidence on the more recent plates of Tanaka and Takamine, as well as in an earlier reproduction.[5] The fact that corresponding absorption and emission bands approach each other and possess the same series limit,[31] together with the close analogy that exists between the terms of the latter series and the $3pns\,{}^3P_u$ terms of Si I,[32] suggests that the upper states of both series arise from the same electron configuration. As n increases, progressive uncoupling of the spin of the excited electron is expected, and the distinction between the predicted $^1\Sigma$ and $^3\Sigma$ states would diminish. Absence of low pressure absorption to the $^3\Sigma$ states may be attributed to selection rules, which would still operate to some extent. At the same time, the emission bands may be accounted for by supposing that conditions in the source—a condensed discharge in helium, with traces of nitrogen present—result in the transfer of N_2 molecules to the hybrid $^3\Sigma$ states. It would be of interest to examine other regions of the spectrum from the same source to detect if possible transitions between the proposed $^3\Sigma$ terms and known triplet states of N_2. The procedures developed by Kaplan[33] to investigate metastable states might also be of use in testing my suggestion.

NON-RYDBERG BANDS

In the region λλ995–818 are a large number of discrete bands that are stronger and far more prominent than those of the Rydberg series, excepting $c \leftarrow X$. Although likewise shaded toward longer wave-lengths, these bands show in most cases a comparatively open rotational structure, indicative of a large internuclear distance in the excited states. As would be expected, many of these bands appear to form vibrational progressions. The assignments, however, could not be made with assurance by means of the usual criteria, for besides the shortness of several progressions, and an extensive overlapping in the region λλ940–870, the values of $\Delta G'$ were often irregular. At large energies, where many electronic states lie close together, and where a transition toward case d' coupling may in some instances result in an unusual band structure,[34] this is not surprising. It was very fortunate, therefore, that the rotational constant B', which should be uniform for bands of one progression, could often be determined. Above λ865, nearly all of the groupings of Fig. 2, designated by small letters in accordance with precedent,[7,1] have been

[28] A. Fowler, Proc. Roy. Soc. London A**123**, 422 (1929).
[29] Including the new band (below), the effective quantum numbers in Si I exceed those in N_2 by 0.20, 0.23, 0.24, 0.23, 0.24, (0.18) for $n=4$ to 9. (Ref. 1, p. 59.)
[30] This formula reproduces Hopfield's observations ($m=2$ to 6) with residuals of +11, −9, 0, 0, (+38) cm^{-1}.
[31] The formula $\nu_m = 151{,}244 - R/(m+0.107)^2$, with $m=3$ to 6, yields residuals (Hopfield's data) of −55, +1, 0, 0 cm^{-1}.
[32] For the $^3P_1$ levels, the effective quantum numbers are nearly identical (ref. 1).
[33] Joseph Kaplan, Phys. Rev. **54**, 176 (1938).
[34] Cf. ref. 21(b, c), §F3.

TABLE IV. Probable vibrational progressions of N_2 absorption bands.

Group	State	B'	ν_k	$\Delta\nu_k$	Group	State	B'	ν_k	$\Delta\nu_k$
i	(Pl. *B*45)	—	98,486	669	*p*	$^1\Pi$	—	(107,655)	(715)
		—	9,155	671			1.21⁻	8,370	749
		—	9,826				1.21	9,119	712
k,	$b\,^1\Pi$	1.41	101,454	698			—	9,831	
		1.41	2,152*	709	*q*	$^1\Pi$	—	(109,831)	(697)
		1.40	2,861*	693			1.11	10,528	681
		1.41₂	3,554*	588			1.09	1,209	663
l	(text)	1.48₄	4,142	560			1.07	1,872	63₃
		1.47	4,702				—	2,51₀	62₂
m	(text)	1.36	105,347	764			1.05?	3,132	572
		1.35	6,111	(822)			—	3,704	55₀
		—	(6,933)				—	4,25₄	
n	$b'\,^1\Sigma$	1.18	106,640*	686	*r*	$^1\Sigma$	—	(110,943)	(639)
		1.16*?	7,326	672			—	(1,582)	(657)
		1.19⁻	7,998	(691)			1.07	2,239	670
		—	(8,689)				—	2,909	633
o'	(text)	—	(105,693)	(1962)			1.06⁻	3,542	629
		—	7,655	1918			1.05⁻	4,171	607
		—	9,573	1885			1.06⁻?	4,778*	592
		—	11,458				1.08	5,370	

More doubtful progressions

s	$^1\Sigma$	1.11	116,683*	522	*u*	$^1\Sigma$	1.07	120,583	533
	$^1\Sigma$	1.06	7,205	479			—	1,116	519
	$^1\Pi$?	0.96?	7,684				—	1,635	
t	$^1\Pi$?	1.1₆?	118,486	482	*v*	—	—	121,245	923
	—	—	8,968	460			—	2,168	928
	$^1\Sigma$	1.04	9,428	(460)			—	3,096	
	(text)	—	(9,888)						

* Calculated from rotational data.

substantiated by this test. The groups *o'*, *s*, *t*, *u*, and *v* are, as will be explained later, more questionable, but including these, it will be seen that very few bands are unaccounted for.

The assignments to progressions are shown in Table IV.[35] Where possible, the probable type of excited electronic state is indicated, and values of B' for individual bands are listed. Except for the *o'* group, or for bands affected by case *d'* coupling, $\nu_k - \nu_0$ is not expected to exceed 6 cm^{-1}; $\Delta G'$ is then given very closely by the interval between heads ($\Delta\nu_k$). The unusual smallness of these intervals will be considered later.

Determination of the Rotational Constant B'

Even with excellent definition, the rotational structure was not sufficiently resolved to permit an accurate determination of both B_v' and B_0'' by applying combination differences in the usual manner.[36] From selection rules, however, either a two-branch or a three-branch band structure is expected, while, because of unit nuclear spin of the *N* atom, there is an alternation of intensity in each branch, strong lines being associated with an even parity of J''.[21,22] The simplicity of structure, combined with the feature of alternation as a guide in assigning *J* values, made it possible to evaluate the *difference* $B_v' - B_0''$ with considerable assurance. B_v' was then obtained from the previously known value of B_0''.[37]

As an illustration of the data available, Table V gives the measurements on one band of type $^1\Sigma - {}^1\Sigma$, and one of type $^1\Pi - {}^1\Sigma$.[38] It will be seen that for the most part, these data represent the positions of blends formed by two branches that run parallel in $^1\Sigma - {}^1\Sigma$ bands, or nearly parallel in $^1\Pi - {}^1\Sigma$ bands. This feature is typical, and the procedure usually followed in evaluating $B' - B''$ is based on the assumption that the measurements represent mean positions of the components in such blends or "line-pairs".[39] Only occasionally was it feasible to measure isolated branches, such as the *R* branch in bands of group *k*, or *Q* lines in one of the *p* bands.

[35] The (rounded) data for Table IV, and for Table VI below, were obtained in the course of rotational measurements (Table V), when the cross hair was set on the estimated position of head-forming lines. These wave numbers of heads are consistently 1 to 3 cm^{-1} lower than those given in Table I.

[36] To effect a complete rotational analysis would doubtless require photographing the spectrum with a six-meter grating, ruled 30,000 lines to the inch, and surfaced for high reflectivity [G. B. Sabine, Phys. Rev. **55**, 1064 (1939)].

[37] In this paper, the value 1.992 cm^{-1} is used for B_0'' [F. Rasetti, Phys. Rev. **34**, 367 (1929)]. The value 1.998 cm^{-1} given by Watson and Koontz (ref. 7) was obtained from measurements of partially fused lines, with Λ-doubling neglected, while the value 1.994 cm^{-1} given by Tschulanowsky (ref. 8) depends on a long extrapolation.

[38] For more complete measurements, see ref. 1. (Estimates of line intensities given there in a few cases refer, actually, to the relative contrast of neighboring lines or blends.)

[39] Although the components were seldom resolved over the measurable range, their (computed) separation averaged about ten times the least count of the comparator. Hence mean positions could be read quite reliably, at least in that majority of cases in which the components were of equal parity in *J*, and thus of comparable intensity.

A preliminary value of $B'-B''$ was found from the slope of a plot of first differences, so adjusted as to reduce to zero near the band head. The procedure is illustrated in Fig. 3 for the $^1\Sigma-{}^1\Sigma$ band listed in Table V. Since $B''>B'$ in all these cases, the positive quantity $-C\equiv B''-B'$ is used. This graphical solution, as well as Eq. (1), below, assumes that terms beyond J^2 in the rotational energy functions may be neglected. The second difference in the wave numbers of any branch of a band is then $2(B'-B'')$, or $2C$.[40]

The final values of $-C$ listed in Table I were usually obtained algebraically, as follows. Let $\Delta\nu(J)$ represent the observed difference corresponding, in the case of $^1\Sigma-{}^1\Sigma$ bands, to the combination difference $\Delta_2F'(J)$, while the integer m gives the relative numbering of the lines in a blend ($J_R=J_P+m$ for any line-pair). $\Delta\nu(J)$ may then be equated to the mean of the differences $R(J)-P(J)$ and $P(J-m)-R(J+m)$. By substituting the usual quadratic expressions for the wave numbers of P and R lines,[41] and eliminating B' in favor of C, one finds

$$-C=\Delta\nu(J)/m(2J+1). \qquad (1)$$

The value of m, needed for application of Eq. (1), is most easily determined by noting that the appearance of a band as regards intensity alternation can be predicted from the preliminary value of $-C$. The alternation will be pronounced for m even, but hardly detectable for m odd. For exact coincidence, the width of blends, namely,

$$\Delta_{RP}(J)\equiv R(J_P+m)-P(J)$$
$$=[2B''+C(m+2)](2J+m+1),$$

must vanish. The values of $-C$ for the pertinent cases are: 0.996 and 0.664 for $m=2$ and 4, respectively; 0.797 and 0.569 for $m=3$ and 5. In the band λ991.9, for example, $-C\sim0.55$ cm^{-1} (Fig. 3) and as no intensity alternation is observed one sees that m can only be 5. A tentative assignment of $J\equiv J_P$ is made by equating some specific first difference, taken from the plot, to the separation of successive lines in the P branch, namely, $P(J)-P(J+1)=2B''-2CJ$. Alternation, if present, furnishes a partial check, but in any case a correct assignment should lead by Eq. (1) to a series of consistent values of $-C$. The results found in this way not only provide a refinement upon the graphical solution, but give an indication of the uncertainty as well. Thus, in the example cited, a mean of 0.545 cm^{-1} was obtained with residuals averaging 0.005 cm^{-1}.

As a final check, or as a means of detecting questionable data, values of the band origin may be calculated from the revised value of $-C$ and the mean wave number, ν_J, of blends. For R–P pairs, with $J\equiv J_P$,

$$\nu_0=\nu_J-CJ(J+m+1)$$
$$-[(m+1)/2][2B''+C(m+2)]. \qquad (2)$$

Referring again to the band λ991.9, the 17 measurements of ν_J gave $\nu_0=100{,}816.1$ cm^{-1} with an average deviation of 0.4 cm^{-1}. The head should be formed by $R(2)$, 5.4 cm^{-1} beyond. Hence $\nu_h^{calc}=100{,}821.5$ cm^{-1}, as compared to $\nu_h^{obs}=100{,}821^-$ cm^{-1} (Tables I and V).

TABLE V. Sample rotational measurements.
λ991.87, $^1\Sigma-{}^1\Sigma$. No intensity alternation of $R-P$ blends: $J_R=J_P+5$.

J_P	ν^{obs}	Remarks	J_P	ν^{obs}	Remarks
—	100,819.9	Head.	12	110,698.3	
3	801.0	indistinct owing	13	80.9	
4	792.9	to strength of	14	62.7	components
5	84.9	absorption	15	43.9	barely
6	76.1		16	24.1	resolved
7	66.0	sharp	17	02.6	
8	54.6		18	579.3	
9	42.0		19	56.2	
10	29.1		$R(21)$	625.5	
11	14.6		$P(16)$	618.7	

λ965.65, $^1\Pi-{}^1\Sigma$. Marked intensity alternation of $P-Q$ blends: $J_Q=J_P+2$. R branch resolved for $J_R\geq18$. (s designates a strong blend or line.)

J_P	ν^{obs}	Remarks	J_P	ν^{obs}	Remarks
—	103,557.4	Head.	24	103,127.5	s
(10)	455.7	blended with $R(15)$	25	(094.3)	mean (below)
			26	59.3	s
(11)	39.7	blended with $R(16)$	27	—	
			28	102,987.3	s
(12)	23.6	blended with $R(17)$	$Q(27)$	103,096.2	trace
			$P(25)$	092.3	trace
12	25.7	s			
13	07.6		J_R	ν^{obs}	Remarks
14	388.6	s			
15	68.2		18	103,399.8	s?
16	46.6	s (broad)	19	79.4	
17	23.4		20	58.0	s?
18	299.5	s	21	36.3	
19	73.9		22	12.2	s?
20	47.6	s	23	287.2	
21	19.2		24	61.2	s?
22	190.2	s $\Delta_{PQ}\sim$ 4.0 cm^{-1}	25	31.0	
23	59.3				

[40] Cf. ref. 21, 22, or W. Jevons, *Report on Band Spectra* (The Physical Society, London, 1932).

[41] If the terms involving D' and D'' are included (ref. 40), the right-hand side of Eq. (1) will contain the correction $-2(D'-D'')J(J+1)$. Except for the k-group bands (below), there was no clear evidence for the need of such a term, but for $D'>D''$, its neglect will in general cause the value of $-C$ to be somewhat too large.

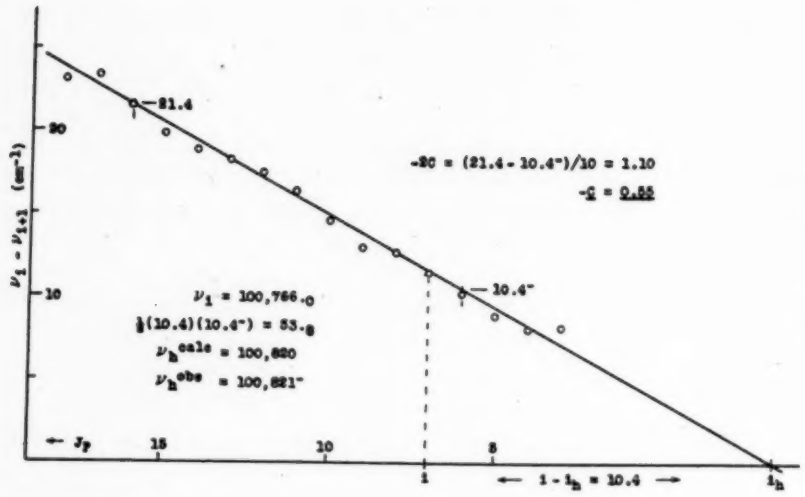

FIG. 3. First differences of $R-P$ blends for λ991.9($^1\Sigma-{}^1\Sigma$). The locus is tested by extrapolation to ν_h from an observed blend, ν_i, as illustrated:

$$\nu_h=\nu_i+\tfrac{1}{2}(i-i_h)\Delta\nu_{i-1}.$$

The J numbering may be obtained after approximating $-C$ from the slope (text).

The procedure for $^1\Pi-{}^1\Sigma$ bands was similar, although more involved. In this case, the graphical solution is subject to the ambiguity introduced by Λ-doubling,[40] and by the fact that the Q branch actually forms a different parabola from the P or R branch. Most frequently, measurable blends consisted of P–Q pairs,[42] and while P and Q lines do not run parallel at low J values, the algebraic method could be applied to advantage over the range encountered, usually $J_Q\sim10$ to 25. Let $\Delta\nu(J)$ again represent the observed difference, equated in this case to the mean of $Q(J)-P(J)$ and $P(J-n)-Q(J+n)$, where n gives the relative numbering of the components in a blend ($J_Q=J_P+n$). In substituting the expression for P and Q branches, one now distinguishes between the two sets of rotational levels due to Λ-doubling by using B_d' and B_e', respectively. When these two constants are eliminated in favor of $q=B_d'-B_e'$,[22] and of $-\bar{C}$, the mean of $B''-B_d'$ and $B''-B_e'$, one finds

$$-\bar{C}+(q/4)(n+1)/J=[\Delta\nu(J)-nB'']/2nJ. \quad (3)$$

It is significant that for the values of J_P involved, the q term may be neglected without appreciable error, and that to this approximation $-\bar{C}$ is independent of the Λ-doubling.

The width of blends is in this case given by

$$\Delta_{QP}(J)=2B''J+2\bar{C}(n+1)(J+n/2)-q[J(J+n)+n(n+1)/2],$$

while band origins were computed from

$$\nu_0=\nu_J-\bar{C}[J(J-1)+(n+1)(J+n/2)]+B''J+\tfrac{1}{2}q(n+1)(J+n/2), \quad (4)$$

where, as usual, J refers to the P component of a blend. The values of $-\bar{C}$ that minimize Δ_{QP} are here given only approximately ($J_P\gg n$, $q=0$). For $n=2$ (pronounced alternation), $-\bar{C}\sim0.66$, while for $n=1$ (alternation absent), $-\bar{C}\sim1.00$. It can be seen that in certain instances the slope of the first-difference curve, together with the presence or absence of alternation, not only gives the value of m or n for use in Eqs. (1) or (3), but provides a criterion of the band type—whether it is $^1\Sigma-{}^1\Sigma$ or $^1\Pi-{}^1\Sigma$.

The procedures just described are based on rotational formulae for bands involving states in which the coupling is not unusual. It is therefore of interest to note that in most cases they were found to be quite appropriate. In fact, it was only by the use of Eq. (3) that a reliable value of $-\bar{C}$ was found for bands of the prominent k group, of which λ965.6 (Table V) is the best example. Here the individual values found from Eq. (3) showed a pronounced trend with J, and only the average was in agreement with the plot of first differences. Since the J numbering was almost certainly correct ($J_Q=J_P+2$, with even parity for strong blends), the observed trend could only be explained by including the term $DJ^2(J+1)^2$ in the rotational energy functions—a refinement that was applied only in the case of these intense bands, where the values of J encountered were

[42] Difference in intensity of the components would render the method inaccurate for $R-Q$ pairs.

rather large ($J_Q=12$ to 32). The significant correction to Eq. (3) consists of a term $-2(D'-D'')J^2$, to be added to the right member,[43] so that if the values originally found are plotted against J^2, they extrapolate to $-\bar{C}$ at $J^2=0$. In this case, $-\bar{C}$ was found to be 0.580 cm^{-1} instead of the original estimate of 0.61 cm^{-1}.[44] The slope, $2(D'-D'')$, was 5.3×10^{-5} cm^{-1}, in reasonable agreement with the harmonic oscillator approximation[22] of 3.4×10^{-5} cm^{-1}. The Λ-doubling in the upper state appears to be small, as a measured estimate of 4.0 cm^{-1} for $\Delta_{QP}(22)$ gave for q the rough value -0.001 cm^{-1}.

The same band, λ965.6, afforded a nice external check of consistency. As is seen in Table V, a number of resolved R-branch lines could be measured, and with these one may form the combination differences

$$R(J-1)-P(J+1)=\Delta_2F''(J)$$
$$=(2J+1)[2B''-D''(2J+1)^2].$$

Values of $P(J+1)$ were obtained from observed frequencies of P–Q blends corrected by $\frac{1}{2}\Delta_{QP}$, and the small constant D'' was taken as 0.6×10^{-5} cm^{-1} (harmonic oscillator approximation). The six available differences gave $B''=1.990$ cm^{-1}, with residuals averaging 0.008 cm^{-1}, in complete agreement with Rasetti's value of 1.992 ± 0.005 cm^{-1}.[45]

The v' Progressions

Before giving a brief account of the individual groupings of Table IV, it should be noted that an unambiguous correlation with known singlet states of N_2, Fig. 1, seemed rather unlikely. A large internuclear distance for the excited states led me not to expect the 0−0 band in most cases; yet except for state b' (a is not considered here because of the lower $a\leftarrow x$ transition probability), levels with $v'>0$ had not previously been identified. Nevertheless it was found that a number of the bands could be attributed to vibrational levels of states b and b'. In order to present most simply the basis of correlation, and also to facilitate reference,[1] it has seemed best to retain the original group designations (k, l instead of b; n instead of b') in the following discussion. At the end, it is shown that two isolated bands of compact structure may probably be assigned to levels f and h.

Group i consists of three bands that appeared faintly only at perhaps twice the pressure used to photograph the other bands. Measurement of rotational structure was not feasible, but the intensities and intervals suggest the grouping.

Group j. The band at λ991.9 has been cited as an example of a $^1\Sigma-{}^1\Sigma$ transition. Although of moderate intensity, it is left uncorrelated with any other band, since the weaker one at λ985.6, designated j originally,[1] is here assigned to the k group.

Group k is the most prominent progression in the entire spectrum. It was just the high intensity of the bands that prevented measurement at intermediate J levels and thus led at first to erroneously large values of $-\bar{C}$. The appropriate correction explained for λ965.6 was applied to the other two strong bands, with satisfactory but less precise results.[46]

It may be seen in Fig. 2 that the head of the strongest band, λ972, is very diffuse. The absorption in fact extends some 50 cm^{-1} beyond the calculated position of the head, which agrees with the position shown on a plate taken at a reduced pressure. This distance seems too great to attribute to the wings of head-forming lines ($J_R=1$, 2, 3), but the peculiarity remains unexplained. A minor irregularity was observed also in the band λ978.9, where an unexpected line at 101,823 cm^{-1} appears to be $R(25)$, in abnormal strength.

The high intensity of the k bands suggests that in their case the 0−0 transition should be observed, in spite of the large value of r_e'. The weaker band at λ985.65, while it does not fit perfectly into the usual sequence of ω_v and B_v

[43] Following Herzberg (ref. 22), I have taken $D>0$.

[44] In view of the approximations involved in my treatment, least-squares solutions seem unjustified. However, if the corrective term is added to each apparent value of $-\bar{C}$, deviations from 0.580 cm^{-1} average less than 0.002 cm^{-1}. Use of the refinement in calculating ν_0 from the pairs $J_P=12$ to 26 led to values with an a.d. of only 0.2 cm^{-1}.

[45] In two bands of $^1\Sigma-{}^1\Sigma$ type, *viz.*, λ890.9 and λ857.0, combination differences were applied directly. In these cases B'' averaged 1.990 cm^{-1}, but the mean average residual was 0.025 cm^{-1}.

[46] The ratio of theoretical intensities (ref. 21) for the Q and P components of a pair was plotted for blends in the range of measurement, and found to vary between extremes of 1.8 and 0.6. Thus a quantitative basis for the use of mean wave numbers, above, was established for bands of the k group.

values,[47] is of nearly the strength expected. Its correlation with the k group would be of unusual significance, as its position agrees with that calculated by Birge and Hopfield[3] for the origin of the b–X system (985.52A). Three of the strongest bands in the entire spectrum would by this identification involve the levels $v'=1$, 2, and 3 of state b.

Group l. Relative intensities suggest that this pair of bands is a continuation of group k which otherwise would terminate abruptly. The original segregation of the l bands[1] was based on a sharp break in the sequence of ω_v and B_v values and on the fact that these bands, in contrast to those of group k, do not show intensity alternation in the rotational structure. Both effects, however, may be explained in terms of a perturbation resulting from the near approach of two electronic states of the same species.[22] The magnitude of Λ-doubling is in fact indicative of a perturbation. First attempts to analyze the band λ960.2 failed, but use of Eq. (3) to obtain the average of B_c' and B_d' with but slight dependence on doubling led to remarkably consistent results.[48] An estimate of pair widths then gave approximately -0.02 cm^{-1} for q. This large value would account for the observed absence of intensity alternation as it implies the blending of P and Q lines of different parity ($J_Q=J_P+3$). The band intensities, together with these considerations, thus make it reasonable to identify the upper terms of the l bands with the $v'=4$ and 5 levels of state b.

The perturbation may perhaps be attributed to $c^1\Pi$, as its potential curve, near minimum, is expected to approach closely that of state b near $v'=3$ (Fig. 4). There are still slight irregularities in the values of ω_v and B_v below $v'=3$, and the unprecedented intensity distribution reported by Birge and Hopfield[3] for the b–X emission bands ($v'=0$) remains unexplained. It should be remarked that the emission bands appear to be very narrow,[3,8] whereas the value of r'/r'', Table I, suggests a pronounced shading.

Group m. The two measured bands, although of but moderate strength, show intensity alternation. However, the type of transition is still ambiguous, as the value of $-C$ shows that lines of the same parity (P and R, or P and Q) would form blends whether the upper state is $^1\Sigma$ or $^1\Pi$. Inclusion of a faint third band is plausible, but implies a large irregularity in $\Delta G'$ (Table IV).

Group n. The value of $-C$, taken in conjunction with the appearance of blends and the regularity of structure at low J values, clearly indicates a $^1\Sigma-{}^1\Sigma$ band type. It was found that the wave numbers of heads are in essential accord with predicted vibrational levels of state b', shown in the upper row of Table VI. These values were obtained by using Birge and Hopfield's[3] calculated position of the 0–0 band, in conjunction with Tschulanowsky's[8] vibrational function, *viz.*, $G(v')=745.42v'-4.16v'^2$. In the lower row, the wave numbers for $v'=2$ and 3 are those of levels d and e,[49] and the remaining four values represent n bands.[50] While the agreement is poor at $v'=4$, this may probably be attributed to inhomogeneity of the data, especially as the vibrational function is itself based on the work of different observers.[7,8] My designation of the upper state as $^1\Sigma$ is in accord with Tschulanowsky's analysis of emission bands from the levels $v'=0$ and 1, but my value for B' is a few percent *larger* than his. Although the correlation is very plausible, it is to be noted that whereas the intensity at $v'=4$ would lead one to expect a band at smaller wave numbers, I find no indication of a head corresponding to $v'=3$, even on a plate ($B45$) taken at a higher pressure.

Group o'. Two of the bands formerly assigned[1] to a group designated o are now identified with vibrational terms of state c. The remaining two are included in group o'. This new arrangement is favored by a more uniform variation of intensity, while the large values of $\Delta G'$ are, as before, consistent with compactness of rotational structure.[51]

Group p. The first unobscured band, at λ922.7,

[47] The faintness of λ985.6 prevented a reliable evaluation of B_v'.

[48] For $J_P=9$ to 17, the *spread* in calculated values of ν_0, Eq. (4), was but 0.2$_5$ cm^{-1} (least count of comparator).

[49] I have extrapolated levels d, e, g, f, and h from Watson and Koontz' data (ref. 7), by use of a least-squares solution for $\Delta G''$.

[50] The wave number of the last n band is presumably a few units smaller than that of the Rydberg head $R_1(2)$ used here. Note that an unassigned head at 108,712 cm^{-1} does not fit the n progression (Table IV).

[51] As r_e' is not much greater than r_e'', the o' minimum, Fig. 4, was located by assuming $v'=0$ for the strong band λ928.9. However, a much weaker band at λ946.1, since it about fits the progression, may well be the 0–0 band. If so, the minimum should be lowered to 104,700 cm^{-1}, while $\omega_e\sim2000$ cm^{-1}.

TABLE VI. Vibrational terms of state b'.

$b'\,{}^1\Sigma,\ v'$	0	1	2	3	4	5	6	7
$\nu_{calc}-10^5$	3678	4419	5152	5877	6593	7301	8001	8692
$\nu_{obs}-10^5$	—	—	5147	5868	6640	7326	7998	(8689)

provided rather complete measurements, from which the II character of the upper state was established. Near the head, P, Q, and R lines were blended ($J_Q=J_P+1$, $J_R=J_P+3$), but beyond $J_P=10$ the Q branch was resolved from R–P pairs. From the latter, $-C_d\equiv B''-B_d'$ was computed by Eq. (1), while with the added measurements of Q lines, $-\bar{C}$ could be found as well. Comparison indicates small Λ-doubling, as the values of $-C_d$ and $-\bar{C}$ were nearly equal. An unexplained feature is the intensity of some Q lines as compared to neighboring R–P blends, for in about half the cases, the computed ratio was inverse to that observed. In the next band only two or three Q lines were resolved, but a regular fluctuation in the first differences of measured blends could be attributed to alternation of intensity in the Q branch. The last band was fitted only by its intensity and position.

Group q. Although of but moderate intensity, these bands form a regular and fairly long progression. The strongest, at λ904.7, consisted of a series of blends of moderate intensity ($J_Q=J_P+1$), between which were faint but measurable traces of sharp lines (R branch). While it was not feasible to evaluate $-C_d$ accurately or to form a reliable estimate of q, measurements of R lines were used in connection with those of P–Q blends to confirm the value of $-\bar{C}$ given by Eq. (3). Measurements were carried out on three weaker q bands, but in these, a resolved R branch was not observed. Generally speaking, the computed intensities of successive blends agreed with observation.

Group r. At least six bands, several of them quite strong, comprise this group. The high intensity of the last two members, however, seems to be due to other, overlying absorption. A long parallelism of branches, and the values of $-C$ coupled with the width of blends and the alternation of intensity, point clearly to a ${}^1\Sigma-{}^1\Sigma$ band type. P and R branches were in fact measured separately in one case (λ890.9), but a precise determination of both rotational constants was not feasible.[45]

There is a marked perturbation of rotational structure in the band at λ880.7, that had not formerly been traced in detail. Diminished intensity, and confusion due to a q band at λ883.9, prevented following the branches beyond $P(20)$, but the sharp lines $R(17)$ and $P(19)$ both indicate a deviation of 10 cm^{-1} for the level $J'=18$ (term value $\sim 113{,}900+10\ cm^{-1}$). However, when deviations of P and R lines were plotted separately against J', a considerably more rapid and larger rise was obtained for the R than for the P branch. Such an effect is not consistent with a single set of levels in the upper state, yet it seems to be too pronounced to attribute to incomplete resolution.[52]

The well-developed band at λ875.9 shows a few peculiarities. Besides two or three very faint irregular lines, and a broadening of the blend $R(17)$–$P(15)$, the pair $R(21)$–$P(19)$ is about twice the expected intensity, while $R(22)$–$P(20)$ is weakened. An overlapping q band prevented following the branches further. Measurements at low J values were not feasible in the case of λ871.4 due to overlying absorption, and the analysis of observable blends was unsatisfactory in that values of $-C$ consistent with the width of blends showed a distinct trend [Eq. (1)]. The average is lower than expected, and while the value of ν_h computed from it fits the ω_v sequence (Table IV), it is some 20 cm^{-1} larger than the apparent wave number. However, an analysis of resolved lines in the tail of the last r band corroborates the drop in $-C$, and in this case the observed and calculated heads agree closely.

Group s. A detailed examination of these three bands throws considerable doubt on the earlier grouping.[1] Whereas the first two can be analyzed as ${}^1\Sigma-{}^1\Sigma$ transitions, the third consists of a strong branch that appears to be formed by superposed P and R lines ($J_R=J_P+2$; $-C_d\sim 1.00$),

[52] The perturbation was in evidence at the pair $R(15)$–$P(13)$, for which $\Delta_{RP}(\nu_R>\nu_P)$ was noticeably larger than expected. The increasing shift causes $R(17)$ to resemble an added line between $R(16)$–$P(14)$ and the blend ($\nu_P>\nu_R$) formed by $P(15)$ with $R(18)$. Finally, the intensity of $P(16)$ indicates near coincidence with $R(19)$. The deviation of $R(19)$ would then be about 30 cm^{-1}, whereas a smooth trend in the P branch predicts 15 cm^{-1} for $P(21)$. Besides these shifts, two or three irregular lines are doubtless to be attributed to the perturbation.

and of a weaker branch, presumably of Q type ($-C_e \sim 1.06$). This interpretation of the third band is supported by combination differences involving B'', but it implies a very large Λ-doubling and gives for ν_h^{calc} a value 30 cm^{-1} less than ν_h^{obs}.[53] These features suggest that the upper state may be of modified Π type (transition toward case d' coupling).[34]

In the second band, λ853.2, an abrupt termination of the strong blends is attributed to predissociation, with breaking off of the rotational levels at $\sim$117,740 cm^{-1}. It appears that a narrow band, still in evidence on a plate taken at a lower pressure, obscures the pair $R(21)$–$P(19)$, but the P branch could be traced as far as a broadened line corresponding to $J'=22$.

Group t. Marked dissimilarities of structure suggest that the three or four bands involved[54] may not represent a true progression. Thus, blends in the first band are narrow in the tail, and broaden rapidly toward the head, while the next band is conspicuous for its remarkably incoherent appearance.[55] In contrast, the band at λ837.3 presents a beautifully simple structure that could be analyzed as a close blending of P and R lines.[56] However, the appearance of the last four unobscured lines in the tail [$P(17)$ to $P(20)$] indicates that the rotational levels of the upper state teminate with $J'=19$ (term value $\sim$119,825 cm^{-1}). The lines in question are weaker and sharper than the preceding blends, and as they are displaced to lower wave numbers by about 3 cm^{-1} ($\frac{1}{2}\Delta_{RP}$), it seems clear that the R component is absent. It may be noted, also, that the blend $R(16)$–$P(14)$ is of half-normal intensity.

Group u. Rotational measurements were carried out for the band at λ829.3, and an open structure is evidently associated with one of the heads near λ825.6. A third head appears faintly on another plate ($B45$), from which its position has been estimated.

Group v. If intensity is any guide, a progression is indicated by the strong band at λ818.5. At the same time, incompletely resolved branches suggest an intermediate value for $\Delta G'$. The grouping of Table IV is thus plausible.

g, f, and h levels. These terms of Watson and Koontz[7] remain for possible correlation with absorption bands. Since the distribution of intensity among the emission bands from level g indicates that r_e' does not differ greatly from r_e'', the 0–0 band might be expected in absorption—but no head is found at the position predicted (108,950 cm^{-1}).[49] On the other hand, there is good agreement between the f level (110,190 cm^{-1}) and the weak band with indication of fine structure at 110,198 cm^{-1}. This is true also of the h level (112,770 cm^{-})[1] and the unassigned band with poorly resolved structure at 112,778 cm^{-1}. However, as intensities among the $h-X$ emission bands lead one *not* to expect the 0–0 transition in absorption, h appears to be a vibrational term with $v'>0$.

Absorption, $\lambda\lambda$818–800. It is clear that a part of the strong and seemingly diffuse absorption at $\lambda\lambda$813, 807, and 801, Fig. 2, is due to overlapping, as additional heads are revealed when the pressure is reduced.[25] On the other hand, there is no clear indication of rotational structure below λ818 (cf. Table I, $\lambda\lambda$814.5, 807.5), a circumstance that may be attributed to insufficient resolving power only in those cases where $r_e' \sim r_e''$ (e.g., Rydberg bands). The diffuseness may then be due in part to photo-dissociation into repulsive states of N_2, while a possibility that the absorption at say λ801 (most diffuse) represents ionization into the $^2\Pi_u$ state of N_2^+ cannot yet be ruled out.[20]

Absorption below λ796. Even on my own plates, there are many measurable bands in this region (Table I). Only the weak $v'=1$ Rydberg bands ($\lambda\lambda$790–785, Fig. 2) have been interpreted, but some of the others are probably related to the non-Rydberg bands (see discussion). An adequate treatment of the absorption here would evidently require plate material obtained at a reduced pressure, in this case by use of either the Lyman or the helium continuum.[12]

DISCUSSION[57]

A number of instances of peculiarities in rotational structure have been noted, particularly for

[53] I refer here to the strong head at λ849.7, rather than to the weaker one at λ849.3 given in ref. 1.

[54] The fourth (see ref. 1), λ834.1, appears to be the Rydberg band $v'=2$, $m=3$, as noted previously.

[55] This may be due in part to overlapping (cf. Table I, λ841.9). In any case, there is an abrupt drop of intensity in the rotational structure at 118,644 cm^{-1}.

[56] An earlier suggestion (ref. 1) is incorrect.

[57] I am indebted to Professor Mulliken for suggesting many of the features brought out in this discussion.

bands of the r, s, and t groups. While some of these anomalies arise from perturbations or from predissociation, it is reasonable to suppose that others, of a more intrinsic sort, are manifestations of case d' coupling in the upper electronic states. It will be recalled that the higher members of the Rydberg series also give evidence of this type of coupling.

An unexpected feature of nearly all the progressions (we shall exclude here the Rydberg terms and state o') is the smallness of $\Delta G'$, or ω. The values are in fact about one-third that of the normal state, and on the whole ω decreases somewhat with increasing energy (Table IV). At the same time, the values of r_e' for these terms are 20 to 40 percent larger than in the ground state,[58] and the increase with energy is quite pronounced (Table I).

It is true that the r bands can be rearranged into two progressions such that every other band falls into one of them. (λ919.8 and λ907.5 (f) would be added to one group, and λ860.5 to the other, while λ870.7 would replace λ871.4.) The alteration would double ω, but the revised values are hardly as consistent as before, and as this was the only case where larger intervals seemed feasible, the modification is not favored.

In the case of state b, further evidence for a small value of ω is provided by the rotational structure, as the value found for D' (k bands) would agree very poorly with the theoretical expression, $4B^3/\omega^2$, if ω were doubled.

States having unusually small ω_e and large r_e are known for other molecules, e.g., for the upper state ($^1\Sigma_u^+$) of the Lyman bands of H_2. In discussing this case, Mulliken[59] has pointed out that the behavior is to be expected if the state is derived from two ions. Mulliken,[60] and Mulliken and Rieke,[61] have also shown that transitions characterized by a net transfer of charge between atoms may be expected to have high intensity, provided (diatomic molecules) the jump is of parallel type, i.e., with $\Delta\Lambda = 0$. Transitions from atomic to ionic (bonding to anti-bonding) orbitals

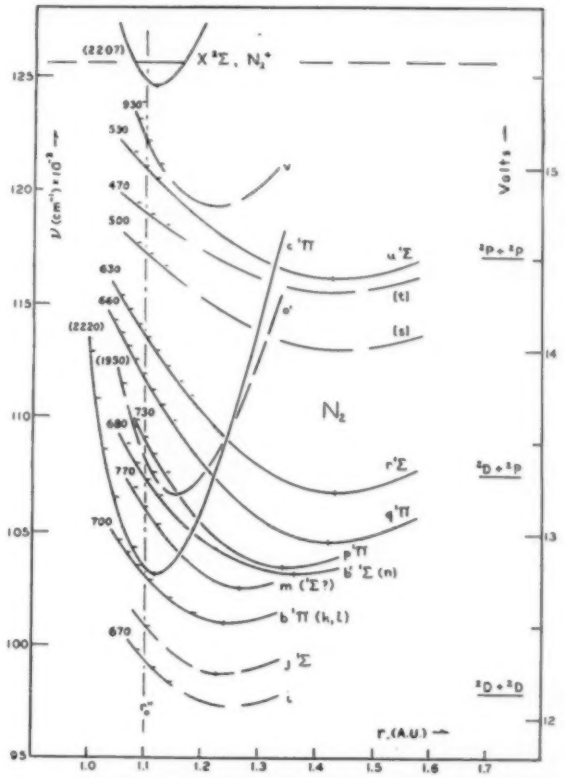

FIG. 4. Highly excited singlet states of N_2. The potential curves for states c and o' (ref. 51) were calculated by Dunham's method (ref. 62) on the basis of reasonable assumptions regarding B_e and α_e. At the left (parentheses) is shown the probable value of ω_e. Levels corresponding to observed bands are indicated by short, horizontal lines. In addition to c, there are of course the other, similar Rydberg states, converging to $X\,^2\Sigma$ of N_2^+. The shallower curves (except for i, j, and v) were sketched from a rough approximation in which only the first term of Dunham's expression was retained, with ΔG_v (shown at left end of curve) and B_v used in place of ω_e and B_e, respectively. Here v refers to the preferred levels ($r'_{\min} \sim r_0''$), with respect to which the minima have been located, vertically. Horizontally, I have arbitrarily used $0.95r_e$ for r_e (short, vertical line). These curves were treated alike, save that for b' the minimum was raised to obtain conformity with Table VI. No correction was needed for b, the only case that permitted a direct check.

are of just this type, and the intense Lyman bands provide a classical example.

From these remarks, it appears that the $^1\Sigma$ states of N_2 considered here are similar to the ionic $^1\Sigma$ state of H_2. However, the ratio ω/B is in the latter case nearly the same as for the normal state of the molecule, whereas in N_2 it is less than half as great in some instances. These deviations from the empirical Birge-Mecke rule imply an unusual anharmonicity, such as occurs in the ionic $^1\Sigma^+$ state of LiH and of KH, where a unique combination of circumstances[59] results in nega-

[58] Cf. F. A. Jenkins and R. E. Worley, Phys. Rev. **57**, 252A (1940). In the next to last line, "four times" should read "1.4 times."

[59] R. S. Mulliken, Phys. Rev. **50**, 1028 (1936).

[60] R. S. Mulliken, J. Chem. Phys. **7**, 14, 20 (1939).

[61] R. S. Mulliken and C. A. Rieke, *Reports on Progress in Physics* (The Physical Society, London, 1941), Vol. 8, p. 231. (Cf. §§4, 5.)

tive values of $x_e\omega_e$ and of α_e. The situation is not without precedent however in N_2. From an analysis of a considerable number of $b'-X$ emission bands, Tschulanowsky[8] found $\omega/B\sim 650$ for state b', as compared to ~ 1100 for the five lowest states of N_2. Although $x_e\omega_e$ and α_e appear to be positive for $b'\,{}^1\Sigma$, my results (Table IV) indicate that $x_e\omega_e$ is negative for some of the other states.

Thus it appears that most of these non-Rydberg terms of N_2 possess both ionic characteristics and an unusual anharmonicity. Presumably they dissociate, or tend to dissociate, into ions $N^+ + N^-$, and are strongly influenced at large r by a Coulomb law of force. Although the detailed shape of the potential curves is not known, I have included a diagram, Fig. 4,[62] to illustrate their main features. The shallowness of the curves and the large values of r_e, as compared to the Rydberg states, is striking. I have not attempted to indicate the nature of the anharmonicity (see caption), nor to consider the mutual influence of neighboring terms, although such influence is doubtless pronounced in some instances.

It is remarkable that in a comparatively small energy range there should be so many states of ionic character, and it may be that some of those energetically farthest apart are configurationally similar (derived from atomic terms that differ only in n). On the other hand, one may suppose that the large values of r_e' are in some cases due to the excitation of *two* bonding electrons. The smaller stability at higher energies (Fig. 4), which led to an earlier suggestion[1] that the excited terms form series whose limits are unstable states of N_2^+, could be explained in this way. However, even though two-electron jumps may be quite strong in molecules,[60, 61] it is doubtful whether they would account for the intense absorption observed here.

Professor Mulliken informs me that the strength of the $^1\Pi-{}^1\Sigma$ bands cannot be explained in the way suggested above for the $^1\Sigma-{}^1\Sigma$ bands. Perpendicular type transitions ($\Delta\Lambda\neq 0$) are expected to be intense only under special circumstances, as for instance when they bear a similarity to the strong atomic s–p jump. It is noteworthy, however, that in the present case, the $\Sigma-\Sigma$ and $\Pi-\Sigma$ transitions, both of which introduce a large change in the molecular bond, are well developed at the same, low pressure of nitrogen.

In conclusion, I wish to express appreciation to Professor F. A. Jenkins for valuable criticism in presenting the results; also to Dr. C. R. Jeppesen for experimental suggestions. For her help in preparing the manuscript, I am grateful to my wife.

[62] Calculated by Dunham's method, see J. L. Dunham, Phys. Rev. **41**, 713, 721 (1932). [Cf. also J. Chem. Phys. **9**, 61 (1941).]

PHYSICAL REVIEW VOLUME 64, NUMBERS 7 AND 8 OCTOBER 1 AND 15, 1943

The Channel of the Spark Discharge*

J. W. FLOWERS
High Voltage Engineering Laboratory, General Electric Company, Pittsfield, Massachusetts
(Received July 6, 1943)

The luminous channel of the spark discharge and the discharge current are simultaneously measured. It is concluded that the spark discharge in air attempts to establish a channel in which the current density is a constant value of the order of 10^3 amperes/cm^2. During the formation of the channel, which takes place by an expansion process producing a pressure or sound wave, the current density is much greater. Throughout most of the formation time and the subsequent history of the channel, the light energy which is radiated is proportional mainly to the current within the channel. From potential measurements and the photographic records, the energy requirements for development are considered, and some possible relations of these requirements to the electrical circuits are discussed. The data are also discussed in relation to the progression of streamers. The pilot streamer theory of the lightning discharge is indicated to be unsatisfactory by comparison with measured discharge characteristics, and the associated roles assumed for diffusion and recombination processes in the spark discharge channel do not appear valid.

THE spark discharge in air at atmospheric pressure is characterized by a sudden electrical transition accompanied by the radiation of light and sound. Although the channel which provides the electrical conduction is often considered to be indistinct and varies greatly in size, Beams[1] has shown that with a suitable photographic system the luminous source during at least part of the development of the discharge has a definite boundary which expands with the development. The photographs obtained by Lawrence and Dunnington,[2] and Dunnington,[3] using a different method, also show a clearly defined channel with the same characteristics in the development over the complete path observed. Suits[4] has considered the expanding luminous channel observed with exploding wires as the source of the sound wave similar to that originating from the spark in air, and has indicated that the sound energy may be much greater than the light energy. To determine more fully the significance of the luminous channel, an investigation has been made of a wide range of spark discharges which are known to be the sources of both intense sound and light.

PHOTOGRAPHY OF THE DISCHARGE CHANNEL

The photographic methods used are schematically shown in Fig. 1. In Fig. 1a, a suitable slit is placed before the discharge path and perpendicular to its direction. The slit image is recorded upon a moving film with the direction of the image perpendicular to the direction of the motion of the film. The length of the recorded image of the slit provides a measure of the channel width at any time, and a known time resolution is provided by the values of the slit image width and film speed when precautions are taken with respect to the film exposure and the density developed. A more flexible method is shown in Fig. 1b. The discharge currents have been provided by various arrangements of high voltage and high current impulse generators of large capacitance. The circuit connections and the cathode-ray oscillograph methods are essentially standard.

A number of photographic records for which simultaneous current measurements were obtained are shown in Fig. 2. Measurements from these individual records which were obtained by the method of Fig. 1a are given in Table I with corresponding measurements from the current oscillograms. Examination of the images reveals that the discharge channel manifested by the intense light is relatively small at the beginning of the intense light, and is expanding at a velocity much greater than that of sound in the sur-

* Part of the experimental results presented here have been reported at the Cambridge, Massachusetts meeting of the American Physical Society, February, 1941 [Phys. Rev. **59**, 685 (1941)].

[1] J. W. Beams, Phys. Rev. **35**, 24 (1930)..

[2] E. O. Lawrence and F. G. Dunnington, Phys. Rev. **35**, 396 (1930).

[3] F. G. Dunnington, Phys. Rev. **38**, 1535 (1931).

[4] C. G. Suits, Gen. Elec. Rev. **39**, 430 (1936).

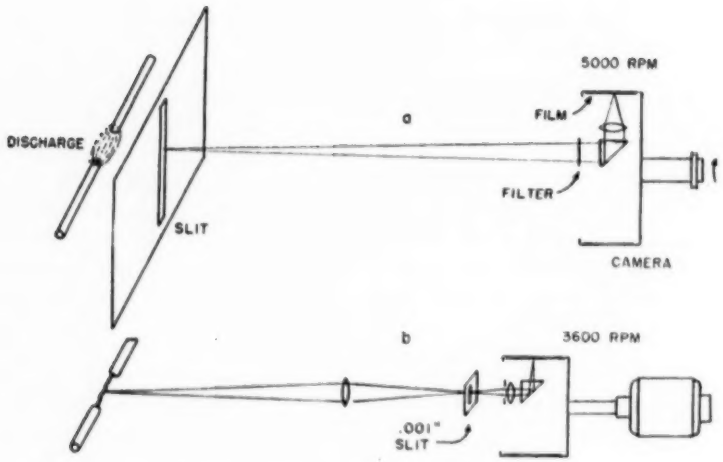

FIG. 1. The photographic systems. The distribution and the intensity of the light emission of the discharge may be recorded as a function of the time.

rounding air. The expansion appears to continue after the current has attained a maximum value although at a reduced rate, and the channel size appears to be larger for higher current values.

To provide additional information about the maximum channel size, it is necessary to sustain the currents by circuits with large time constants. This is accomplished by inserting the necessary resistance in the discharge circuit. In Fig. 3 are shown representative records of the sustained discharges obtained by the method of Fig. 1b. It is evident from Fig. 3 that an essentially constant channel size is attained for a given current after the initial expansion process has taken place. By this method the channel diameters have been investigated for current values from 10 to 10^5 amperes although for values above 10^4 amperes the time constants become insufficient to permit the maximum channel size to be attained. Discharge paths of 8- to 9-cm length allow freedom from electrode vapor near the central portion of the path for times of the order of 100 μsec.[1,2] This is greater than any time which has been found necessary for the expansion.

Upon the assumption that the luminous boundary and the current conduction boundary are the same, the average current density in the channel may be obtained. For sustained channels conducting from 100 to 10^4 amperes, the current densities so determined are very nearly equal. Complete results are given in Fig. 4 where a linear relation is indicated between the current and the channel cross section. Above 10^4 amperes the observational points should fall upon the straight line with sufficient additional generator capacitance. Below 100 amperes uncertainty exists because of reduced image sizes and low film densities obtained with a fixed resolving time and optical reduction. However, below some value of the current, the current density may be expected to decrease because of the increasing fraction of current carried by a surface layer of fixed depth in which the surrounding gas produces

TABLE I. Correlation of data obtained from the photographs of the channel as shown in Fig. 2 and from the corresponding current oscillograms. The diameter measurements give the channel size when the current has attained the maximum value. The current densities also correspond to the time of maximum current.

Discharge film no.	Maximum current amp. $\times 10^3$	Channel diameter cm	Current density amp./cm^2	Time to maximum current sec. $\times 10^{-6}$	Average expansion velocity cm/sec. $\times 10^4$
*33	17	1.6	8,500	8.0	10
*34	18	1.4	12,000	6.0	12
*38	22	1.3	17,000	3.3	20
20	25	1.5	14,000	5.0	15
*26	26	1.8	10,000	8.0	11
23	38	2.7	6,700	16	8.5
37	39	3.2	4,900	35	4.6
28	40	3.2	5,000	35	4.6
39	53	1.9	19,000	5.6	17
7	94	2.3	23,000	5.0	23
**8–1	94	2.1	27,000	5.0	21
8–2	94	2.4	21,000	5.0	24
27	90	3.5	9,400	17	10
**35	90	4.3	6,200	17	13
29	100	3.2	13,000	17	9.4

* Damped wave.
** Probably two channels formed.

disturbances. The measurements given in Fig. 4 are average values and relatively free from effects associated with variable film densities. When the exposure time of a spark photograph extends over a period during which the channel is greatly changing, variations in the film density brought about by altering the photographic speed can greatly alter the image size. This is the usual situation when long sections of sparks are photographed upon a moving film. When this is the case, a fixed channel boundary with maximum contrast cannot be determined. Only by sufficient time resolution can a boundary be determined which is relatively free from reasonable changes in exposure. The transverse slit arrangement greatly facilitates attaining the necessary resolution. The significance of the boundary then determined is indicated by the condition of approximately constant current density within the channel. From the slope of the line drawn in Fig. 4, an average value of 1.1×10^3 amperes/cm^2 is obtained for the current density. This value is within a range of values derived by Ollendorff[5] from a theoretical treatment of a steady state equilibrium. However, his assumptions lead to a channel with a constant radius of the order of 1 cm rather than to a constant current density.

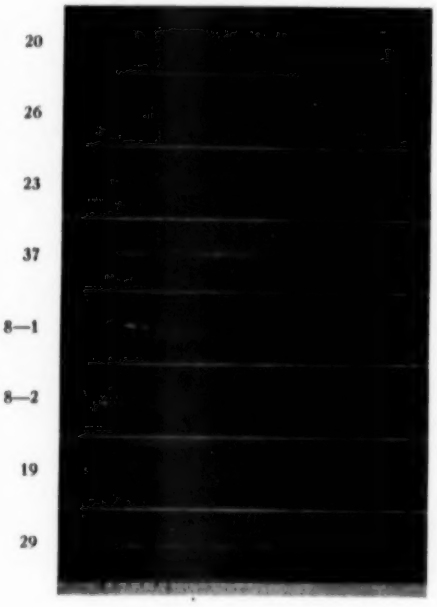

FIG. 2. Luminous channels of high current discharges obtained by the method of Fig. 1a. Increasing current from top to bottom. No. 26 does not oscillate. No. 19 is a discharge in vacuum. Additional data is given in Table I.

[5] F. Ollendorff, Archiv. f. Elektrotech. **27**, 169 (1933).

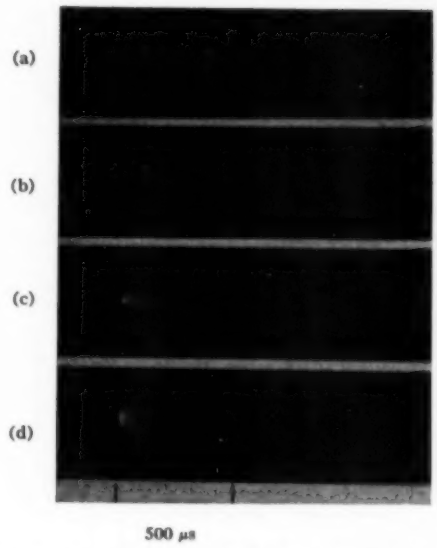

FIG. 3. Discharge channels in air with sustained currents obtained by the method of Fig. 1b. (a) 78 amperes sustained by the discharge of 6 μf and 1150-ohms series resistance. (b) 350 amperes, 6 μf and 255 ohms. (c) 940 amperes, 6 μf and 95 ohms. (d) 2900 amperes, 6 μf and 31 ohms. Current values obtained from oscillograms.

From Fig. 2 and the data of Table I, it is evident that the current density decreases during the expansion of the channel. In Fig. 5 the current density at maximum current is given as a function of the average rate of current rise. High current densities are associated with high rates of current rise. The expansion velocity as a function of the rate of current rise shows a similar characteristic which indicates proportionality between current density and expansion velocity as can be seen in Table I. No noticeable variations are observed for spherical or pointed electrodes. Also electrode spacings of five cm and one cm produce no noticeable difference.

LIGHT RADIATION FROM THE CHANNEL

Uniform development of the records permits some investigation of the light intensities in the channels. The exposures of the films were carefully controlled so that maximum film density values of about 2 were usually obtained. In Fig. 6 is given a density analysis for the central region of each of two images shown in Fig. 2. Image No. 19 is that from a discharge in commercial high

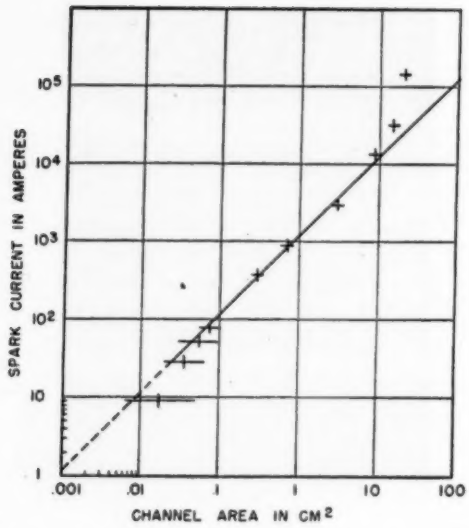

FIG. 4. The relation of current and maximum channel cross section for the spark discharge in air. The maximum channel attained for any current value is such that the current density attains an average value of 1.1×10^3 amperes/cm².

vacuum between copper electrodes with approximately the same current as given for the air discharge No. (8–2). From the roughly known photographic characteristic it is possible to transform density values to linear light intensity values. This has been done in Fig. 7 for some of the discharges. It is evident from Fig. 6 and Fig. 7 that the light intensity, i.e., the radiation per unit of channel surface, is much greater during the expansion process than subsequently. This is the case for all of the air discharges although it is less noticeable for low rates of current rise. From both the calculated time resolution and the analysis of the vacuum discharge which is known to deionize rapidly, it is also evident that for the air discharge the light radiation persists in the channel when the current has ceased momentarily during the oscillation. This persistence is more noticeable as the frequency is increased. In the region of 200 kc only the vacuum discharge is resolved.

A comparison of light intensity and current in Fig. 7 makes it clear that a direct proportionality between the two is not attained. The nearest approach is for discharge *E* of Fig. 7 which is the lowest frequency and which also has the lowest rate of current rise and expansion velocity. This suggests that the expansion process and the associated channel variation is also of importance in the departure of proportionality and that if the total radiation from the channel is used, i.e., the product of intensity and channel surface, the proportionality with current should be much closer. That this is the case is shown in Fig. 7 by the arbitrary ratios between current envelopes and intensity envelopes. The ratios vary with time in the same manner as the channel radii. This is to be expected if proportionality between total radiation and current is the case since the total radiation is related to the product of channel radius and intensity. Additional support for the proportionality of current and total radiation is given by the analysis of photographic records of lightning for which current values are also known,[6] and where the recorded image size is such that the total light radiation of the stroke is measured. The total radiation of light from the channel can also be considered to be in phase with the current where the proportionality exists between total radiation and current magnitude. This follows from experiments with the electro-optical shutter[1–3] where the light radiation and the potential wave from a spark are known to be closely related at very short times of measurement. Thus, the beginning of the luminous expanding channel as recorded corresponds essentially to the beginning of the main current wave. However, a probable condition, unobservable here, will be discussed later for the start of current flow where other factors enter.

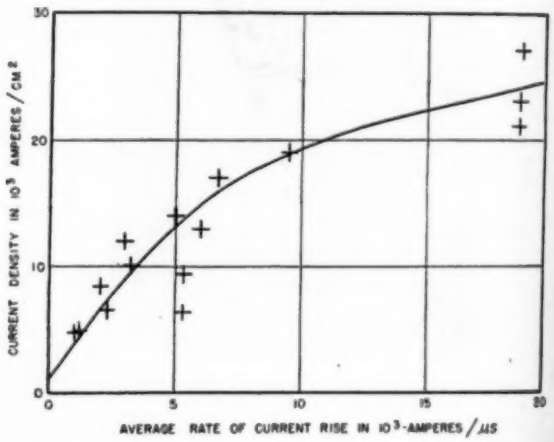

FIG. 5. Current density at maximum current as a function of the average rate of current rise in attaining maximum current in the channel.

[6] J. W. Flowers, manuscript in preparation.

VOLTAGE GRADIENTS IN THE CHANNEL

To supplement the observations of the channel, the potentials between the electrodes during some of the discharges have been recorded. In view of the times and path lengths involved and the usual range of velocities associated with streamers, such measurements provide some information about the voltage gradient in the channel. Various difficulties occur in the measurement of the potential, particularly for lower values. Important phase relations between voltage and current have been determined from oscillograms of voltage as a function of current obtained by applying voltage deflection and current deflection to the perpendicular axes of the oscillograph. This procedure is capable of revealing measurement difficulties which are not readily apparent in the ordinary oscillogram.

In Fig. 8 separate voltage and current oscillograms are shown for a high current oscillatory discharge and in Fig. 9 for a damped discharge. From these and other measurements it is apparent that higher voltage gradients exist during the time of the channel expansion, and that considerably more energy is furnished during this time than at any other.

ENERGY REQUIREMENTS IN THE CHANNEL DEVELOPMENT

The formation of the channel requires considerable energy. There can be scarcely any doubt that the sound wave originates from the expansion process. The view of Ollendorff,[5] which proposes to relate channel explosion and current interruption, cannot be accepted since it is readily observed in the laboratory that enormous sound differences exist for different current magnitudes although the currents decrease slowly to negligible values. The radiation of light and other losses require a continuous supply of energy, but not necessarily greatly more during the development time. During this time, however, the energy required for the ionization must be considered. The current conduction can be considered to take place mainly by the movement of free electrons under conditions of essentially equal positive and negative charge densities. This, at least, must be nearly the case for streamers of great length such as in lightning, otherwise unreasonable space charges become involved. The current is then given by

$$I = \pi r^2 N e v,$$

where r is the channel radius, N is the electron density or ion density, e the electronic charge, and v the electron velocity. The energy of ionization is that required to form $\pi r^2 N$ ion pairs. Very little is known about the ion density. Lawrence and Dunnington[2] give a value of $10^{19}/cm^3$ which must be considered high where appreciable expansion has occurred. Although r and I may be determined, it is necessary also to determine v in order to fix the value of N. Estimates of v are difficult, and estimates obtained for N are unreliable where there is directly or indirectly implied the condition of thermal equilibrium with an associated temperature. Experiments with arcs show that a time of 1000 microseconds is required for thermal equilibrium to be approached in the arc.[7] Thus, the beginning of the bright channel corresponds to a highly transitory

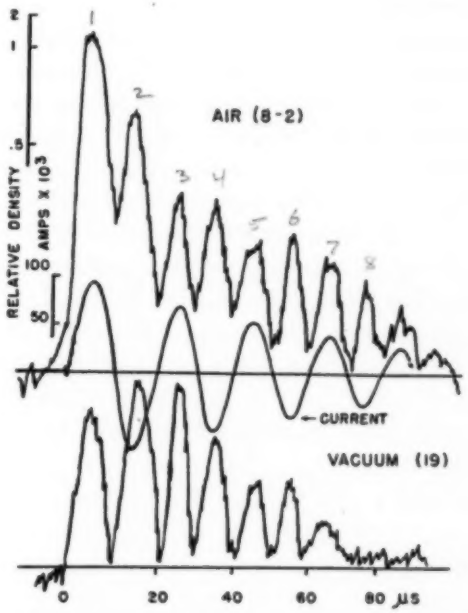

FIG. 6. Photometric analysis. The vacuum discharge, Fig. 2(19), exhibits no noticeable expansion process and the light radiation falls essentially to zero value with the current in contrast to the air discharge, Fig. 2(8–2). The current oscillogram is that obtained for the air discharge. The current was not measured for the vacuum discharge, and differences in impedance may have slightly altered the current magnitude.

[7] C. G. Suits, Gen. Elec. Rev. 38, 194 (1936).

condition and steady state assumptions such as made by Ollendorff[5] and others are not permissible at this stage.

In view of some of the limitations it is nevertheless of value to calculate the energy required to attain the maximum current in an oscillatory discharge. For the case of the discharges Nos. 8–1 and 8–2 listed in Table I and shown in Fig. 2, the generator capacitance stores 9700 watt-seconds before the discharge. At maximum current of 94,000 amperes, attained in 5 microseconds, 7700 watt-seconds remain in the generator inductance. To develop this current in the circuit and 8.5 cm of discharge path requires 2000 watt-seconds. From the average decrement of the current oscillogram shown in Fig. 6, a value of 0.044 ohm is obtained for the effective resistance of the circuit, excluding the first cycle from the measurements. This resistance dissipates 990 watt-seconds which may be considered to account for circuit losses as well as light radiation and diffusion losses in the discharge path. The energy required in ionization for a path length of one cm is $\pi r^2 NW$, where W is the effective ionization potential. Using a value of 10^{19}/cm^3 for N, 15 volts for W, and 1.2 cm for r as given in Table I, one obtains a value of 920 watt-seconds. For the sound wave, the energy may be approximated by considering the displacement of the air by the expanding channel.[4] The energy of the expansion is $\frac{1}{2}MV^2$, where M is the mass of air displaced and V the expansion velocity. The value of M will depend upon the change in density from a non-conducting condition to the conducting one. This is probably sufficiently great so that for estimation, M may be calculated from the density of air at room conditions. For a velocity of 2.4×10^5 cm/sec. and a channel diameter of 2.4 cm as given in Table I, a value of 130 watt-seconds is given for the sound energy. The three calculated values provide 2040 watt-seconds which essentially accounts for the measured value of 2000 watt-seconds. Extended discussion of possible variations in these values is of no particular point. Uncertainties in voltage and current produce greater uncertainties in energy values. Relative to the ionization, N may be high, but W is likely to be too low to be complete. Also, the sound wave front probably extends outside the luminous boundary, thus providing a larger value for the sound energy. While all the values are rough, they indicate some of the energy requirements in the formation of the channel. The relation between the possible energy requirements and the electrical characteristics are expressed in

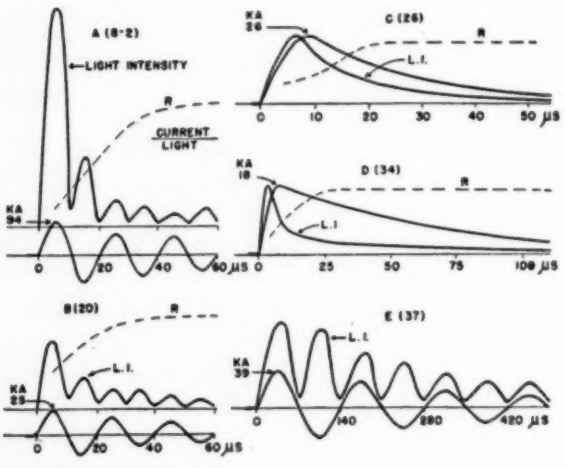

FIG. 7. Light intensity and discharge current. Intensity values are arbitrary and not based upon any common value of current.

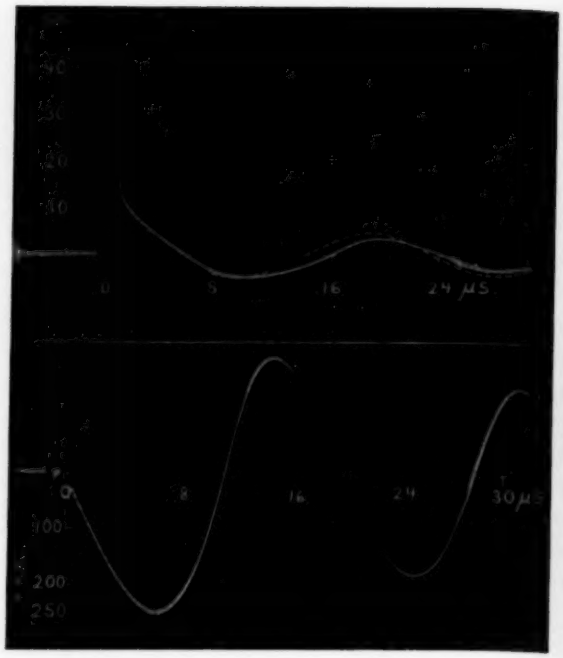

FIG. 8. Cathode-ray oscillograms of voltage and current for a discharge between 0.5″ square brass rods separated 8.8 cm. The induced voltage obtained from a separate oscillogram and a short-circuited gap has been drawn in the correct phase position. The maximum voltage attained but not shown by the voltage oscillogram is 100 kv. Oscillogram axes are slightly oblique.

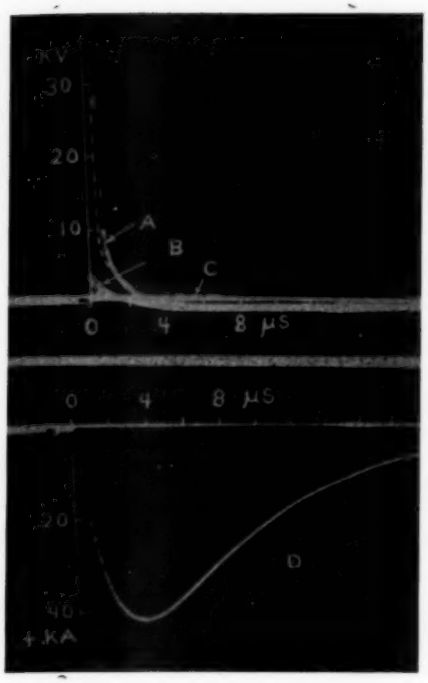

FIG. 9. Cathode-ray oscillograms obtained with a damped discharge between 0.5″ square brass rods separated 8.8 cm. (*A*) recorded voltage; (*B*) induced voltage or distortion; (*C*) discharge voltage free of distortion derived from the difference of (*A*) and (*B*); (*D*) current.

Fig. 10 from an analysis of the oscillograms of Fig. 8. Part of the measured voltage as in Fig. 8 and Fig. 9 is produced by extraneous effects such as induction in the measuring leads and some unbalanced conduction along the leads. This voltage is separately determined for the short-circuited condition of the discharge gap. Voltage contributing to the light radiation and diffusion loss is considered to be in phase with the current throughout, while the third component, necessitated by the ionization and the sound, constitutes the remainder of the voltage after the induced and light components are accounted for. For the 250,000-ampere discharge in the 8.8 cm path, the maximum power is of the order of 800,000 kw.

DISCUSSION

The Bright Channel

It would appear that the spark in air at atmospheric pressure is characterized by a bright channel which always starts as a narrow thread expanding radially. The formation of this channel requires that energy be supplied at a very high rate. Although the field strength may vary widely depending upon the current variations and the corresponding channel energy requirements, the bright channel is characterized by low field strengths in comparison to initiating values. The beginning of the bright channel in any portion of a gap indicates that the field strength is decreasing in that portion. The current in the bright channel is indicated, at least roughly, by the rate of energy radiated in light. The rapid expansion of the channel produces the sound wave of the spark. This expansion is the result of additional energy imparted to the gas in the spark path. It would appear that, for a sustained current, an equilibrium is attained when the channel radius reaches such a value that the rate of energy supplied is equivalent to the losses from the channel boundary. For a wide range of current values, this equilibrium is attained when the current density is reduced to 10^3 amperes/cm^2. However, other slower changes may take place to alter this value gradually. To attain thermal equilibrium within the channel may require appreciable time. Eventually, conditions are completely altered by vapor from the electrodes.

The Progression of Streamers and the Breakdown of Air Gaps

The progression of a bright streamer either in a gap of a few millimeters length or in the lightning discharge may be considered as the progressive development of the bright, expanding

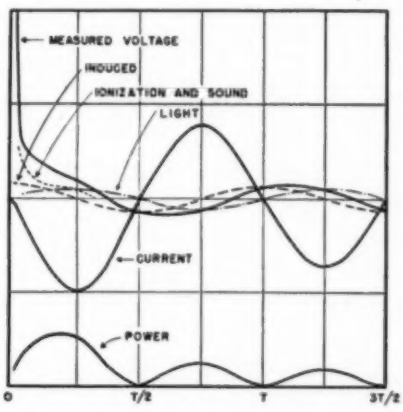

FIG. 10. Analysis of the development voltage. The measured voltage is considered to have three components, the induced voltage, the light voltage, and the sound and ionization voltage. The current oscillogram is shown inverted in the manner similar to record of Fig. 8.

channel. Associated with the streamer is a progressing potential wave with the high field strengths near the tip of the streamer. This view is supported by experiments on the propagation of potential waves in discharge tubes at lower pressures where the luminous wave travels with essentially the same velocity as the potential wave.[8] Maximum fields extend in front of the bright tip by virtue of the space charge carried with the tip by conduction in the bright channel. In the high field before the tip, the current must be considered both as a displacement current and as a conduction current afforded by a few high velocity ions. Sufficiently far ahead of the tip and for long paths, only the displacement current exists. Some of the possible relations are expressed in Fig. 11 for a streamer which has partially traversed the path between two electrodes. Figure 11 is a modification of the picture given by Rudenberg,[9] and provides for the expanding characteristic of the luminous channel as well as the more complete view of conduction current.

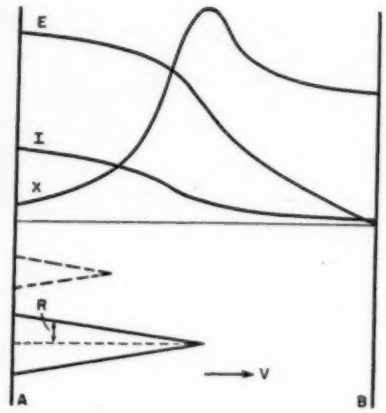

FIG. 11. Diagram of a bright streamer which has partially traversed the path between two electrodes A and B. E, the potential distribution between electrodes; X, the axial field strength; I, the conduction current. The bright channel at an earlier stage is also shown.

The breakdown of an air gap, that is, the fall of potential at the gap electrodes, depends not only upon the process which occurs in the air gap but upon the electrical circuit as well. Thus, the termination of a bright streamer resulting in the luminous bridging of a gap does not necessarily correspond to the breakdown of the gap although this is the usual and perhaps, in general, the practical consideration, since the termination probably marks the time when the impedance mechanism of the complete gap undergoes the greatest transition. However, if one considers a circuit of zero internal impedance and unlimited storage, that is, an infinite bus, no fall of potential would occur; instead an unlimited development of the discharge channel should set in. This condition cannot be realized, but consideration of it points to the dependence of the potential characteristic upon the electrical circuit as well as to the mechanism within the gas. The dependence of the potential characteristic upon the circuit is demonstrated in the experiments of Allibone and Meek[10] who employed circuits of the opposite extreme. For such circuits, with high series resistance and gap electrodes of small capacitance, the fall of potential must occur before the streamer has progressed an appreciable fraction of the gap. The fall may be only temporary, and after preliminary breakdowns and recoveries, the gap may be finally bridged. However, the intermittent streamer process is conditioned by the circuit and does not necessarily apply to all spark discharges. The interrupted streamer effects are probably associated with the limitations of energy, since energy requirements for the establishment of any channel may have considerable influence upon the overall behavior of the system in which the discharge occurs and upon the apparent discharge mechanism. The measurements of Allibone and Meek using the high resistance circuits show that relatively high currents are attained in the intermittent process as compared to the maximum current through the resistance. The discharge circuit elements effective in the formation of the transient current do not establish a small current. Instead, a channel is started as a streamer conducting such a current that the energy available from the charged electrodes is not sufficient to extend the streamer completely and form the channel between the electrodes. The subsequent surges which extend the streamers do so by virtue of the partial recharging of the electrodes and the channel characteristic which permits the storage of energy in the channel for a limited

[8] L. B. Snoddy, J. R. Dietrich, and J. W. Beams, Phys. Rev. **52**, 739 (1937).
[9] R. Rudenberg, Wiss. Veroff, Siemens-Konz. **9**, 1 (1930).
[10] T. E. Allibone and J. M. Meek, Proc. Roy. Soc. **A169**, 246 (1938).

time. From Fig. 10 it is apparent that the first half-cycle of current requires by far the greatest expenditure of energy as compared to subsequent half-cycles. This indicates that energy is stored in the channel during the first half-cycle and less is required from the circuit subsequently. The storage of energy is also revealed by the persistence of luminosity. Thus, where the intermittent streamer or stepping process occurs, most of the available energy is used in extending the streamer, that is, in forming the new step. Thus, the main circuit is able to supply in steps the energy for the whole channel while it is unable to do so in one step at the rate demanded.

Processes Preceding the Bright Channel

In the procedure of the discharge process, it is unlikely that the initial conduction path is of the same character as the bright expanding channel. The initial ionization must develop in a region of high field strength while the bright channel signifies a reduced field. Evidence for high field conduction as represented in Fig. 11 is given in the observation of Dunnington[3] of the faint haze preceding the bright channel. The experiments of Slepian and Torok[11] and Torok and Fielder[12] also suggest a faint channel of a diffused nature while the current which causes high voltage breakdown to depend upon the generator circuit as shown by Hagenguth[13] probably flows by means of such a channel. The conduction before the formation of the bright channel very likely accounts for the condition which permits the formation of cloud-chamber tracks as observed by Flegler and Raether[14] and others.

The faint channel is difficult to observe or photograph because it is usually obscured by the bright channel. There appear to be several reasons for this obscurity. For a given current, the total number of ions in a unit path length is less in the faint channel than in the bright channel since the field strength and ion velocities are greater in the faint channel. From the assumption that the light radiation depends upon the number of ions,[6] it follows that the light radiation for a given current is less from the faint channel. The current density in the faint channel is probably much smaller than that in the following bright channel while the current is also smaller. Together all of these factors may easily produce a brightness ratio of 100 or more. Finally, the short time involved makes an extremely short time resolution necessary for the observation.

Upon the initiation of the discharge, ionization probably spreads rapidly in the region of sufficiently high field strength by a photoelectric process. The necessity of a photoelectric mechanism has been discussed by Loeb[15] and others. However, it seems necessary to consider that many ion pairs are created by photons emitted by electron avalanches shortly after the initiation, rather than to consider that the channel forms by the continued development of one or two avalanches. Those pairs of ions which are formed within the high field region do not alter the field by their presence but only by their subsequent movements which start many individual avalanches and create the faint channel. The continued development of the avalanches eventually results in the bright expanding channel with the associated decreasing field strength. As the tip of the bright streamer forms, the centrally located avalanches of the faint channel probably merge and lose identity, while the outer ones are suppressed as the field reduces and become lost by recombination. The high field is carried forward by the progressing space charge which is maintained by the good conduction of the bright streamer channel while space charge effects within the bright channel are relatively small. Concerning the differences between positive and negative streamer development which have been observed,[10,11] there is the possibility that such differences are associated with the transition from the faint channel to the bright channel tip and with the sign of the space charge carried by the tip. The differences between positive ion and electron mobilities suggest that the positive streamer formation may have the more efficient process since the electrons are gathered by the positive tip. In the negative streamer, they are driven away with the resultant lower density of

[11] J. Slepian and J. J. Torok, Elec. J. **26**, 107 (1929).
[12] J. J. Torok and F. D. Fielder, Trans. A. I. E. E. **49**, 352 (1930).
[13] J. H. Hagenguth, Trans. A. I. E. E. **60**, 803 (1941).
[14] E. Flegler and H. Raether, Zeits. f. Physik **99**, 635 (1936).
[15] L. B. Loeb, *Fundamental Processes of Electrical Discharge in Gases* (John Wiley and Sons, New York, 1939), p. 429, 430.

ionization ahead of the negative streamer. Thus, the bright positive streamer progresses into a region of higher energy density and therefore requires less energy expenditure to progress.

The Pilot Streamer Theory

In an attempt to account for measured velocities associated with the progression of luminosity in the lightning stepped leaders, Schonland[16] has proposed an unrecorded pilot streamer which is considered to precede the luminous tip of the leader. Subsequent assumptions have been made by Meek,[17] and the general picture described by Loeb[18] and Loeb and Meek.[19] The proposed pilot streamer and its associated leaders have assumed channel characteristics which are greatly different from those of the spark channel. Since there appears no reason to suspect any difference between the channel of the lightning discharge and the laboratory spark when the transient currents are the same, it is well to consider carefully some of the assumptions in the pilot streamer theory. Among the difficulties in the theory, the most specific are concerned with the relation between electron diffusion and channel size, with the role of the recombination of ions and with the energy relations within the discharge channel.

Electron diffusion is assumed to be the controlling factor in determining the channel size of the pilot streamer[17,18] as well as subsequently formed bright streamers.[18] The effect of diffusion is assumed to be determined from the cloud chamber observations of Raether.[20] However, if it is necessary to invoke photoelectric processes to explain the progression of the ionization as observed in the cloud chamber,[15] as it seems to be, then it appears doubtful that by such experiments the effects of electron diffusion or electron mobility can be separately distinguished. Moreover, the bright channel of a spark is clearly limited in diameter in a manner which cannot be accounted for by diffusion alone. Other factors, in addition to diffusion, probably enter to determine the size of any possible faint channel. Thus, the derivation of a channel diameter of 0.6 cm for the pilot streamer[17,18] is questionable. Also, this channel is considered to conduct a current of 0.1 ampere; yet, a bright channel of the same diameter conducts a current of over 300 amperes or 3000 times this amount as can be observed from Fig. 4. The great difference between the pilot channel and a bright channel is clear. It may not be argued that the pilot channel is of the nature of the faint channel previously discussed because the pilot streamer is assumed to have reduced field strengths during part of its history. It does not seem reasonable that for a sustained current the field strength can drop without the formation of the bright expanding channel, so that the faint pilot streamer with its sharp drop in field strength followed by a slow rise does not fit into any of the channel characteristics which have been discussed.

It is assumed that in the pilot streamer channel, and in the bright leader channel as well, the resistance increases because of the depletion of ions by recombination.[17] This is proposed as a fundamental process to account for the intermittent character or stepping of the streamers. Such a controlling process does not appear to occur and is discounted by Bruce and Golde.[21] In addition to raising questionable energy relations, such a role would make the necessary changes in total ionization within a channel difficult to explain. In Fig. 8 and Fig. 9, there is little doubt that the ionization increases after the initial fields are greatly reduced. It is unreasonable that a discharge could predetermine and provide the necessary number of ions at a high field that are to be employed by current surges that follow at lower fields. The radiation of light roughly in proportion to the current supports these statements. The assumption of Schonland[16] and others that the intense light in streamers is associated with intense ionization at high field strengths followed by a decay of luminosity because of recombination and channel aging does not appear to be valid. The luminosity decays because the current decays. For some conditions of photography the luminosity may appear to decrease because of the changing image size associated with the expanding channel.

[16] B. F. J. Schonland, Proc. Roy. Soc. **A164**, 132 (1938).
[17] J. M. Meek, Phys. Rev. **55**, 972 (1939).
[18] L. B. Loeb, *Fundamental Processes of Electrical Discharge in Gases* (John Wiley and Sons, New York, 1939), p. 544, 549.
[19] L. B. Loeb and J. M. Meek, *The Mechanism of the Electric Spark* (Stanford Press, 1941), p. 98.
[20] H. Raether, Zeits. f. Physik **107**, 91 (1937).
[21] C. E. R. Bruce and R. H. Golde, J. I. E. E. Part II, **88**, 487 (1941).

The law of energy conservation would appear to be violated within the spark channel for conditions proposed in the recombination theory of Meek and Loeb.[17–19] The assumption of constant current and increasing resistance demands an increasing rate of energy supplied to the channel. It is difficult to account for this increasing energy as mentioned by Szpor.[22] The increasing energy rate is more than necessary to maintain the original ion density proposed, yet it is assumed that the ion density decreases. Thus, a channel of slowly varying diameter, decreasing ion density, and decreasing light radiation provides no adequate reservoir for such energy as would be added. This conception of a discharge of constant current and a rising field strength without increased ionization[16–18] appears to be incorrect. Once current is established by an ionized path any increase in field strength produces an increase in ionization and a greater increase in current. The experiments of McCann and Clark[23] using long duration discharges with superimposed surges reveal the rise in field strength associated with the surges. Only when the electrical circuit is unable to maintain the required field strength does the ionization decay.

Schonland's difficulty in explaining the high leader velocities would seem, in part, to arise from the assumption of a limited or fixed field strength. Since the breakdown of a gap, in general, begins with the bridging by a streamer, it can be inferred from the usual reduction of breakdown time with overvoltage that the velocity of a streamer is dependent upon field strength. The experiments of Snoddy, Dietrich, and Beams show directly the dependence of the streamer velocity upon the applied potential, while this can also be deduced from the experiments of Allibone and Meek where potentials are undoubtedly rapidly reduced at the discharge electrodes upon the start of a streamer and relatively low streamer velocities are attained. In the case of the initiation of a streamer at the surface of an electrode of considerable size and adequate regulation, it is not unreasonable that the field strength should tend to increase as the streamer projects from the surface as would be expected if a wire or metallic conductor were projected.[9] The potential regulation of the point of initiation and the distribution of potential upon the surface are obviously important factors, and a cloud electrode is difficult to consider in such a respect. However, the assumptions leading to the constant velocity pilot streamer to explain lightning streamer velocities would seem to be far more doubtful than the assumption that the field strength at the streamer tip has a tendency to depart from a fixed initial value.

In conclusion the author wishes to express his appreciation of the efforts of Mr. A. F. Rohlfs, Mr. I. B. Johnson, Mr. C. McIntosh, Jr., Mr. R. A. Johns, and Mr. R. B. Gustafson in obtaining the data in the High Voltage Laboratory.

[22] S. Szpor, Bull. Assoc. Suisse Elect. **33**, 6 (1942).
[23] G. D. McCann and J. J. Clark, Trans. A. I. E. E. **62**, 45 (1943).

The Factors Influencing the Plateau Characteristics of Self-Quenching Geiger-Mueller Counters

W. D. B. SPATZ
New York University, University Heights, New York, New York

(Received May 24, 1943)

Investigations of factors influencing the starting potential and plateau slope of self-quenching G-M counters show: I. Impurities such as air or oxygen increase the plateau slope and starting potential of argon-alcohol counters. II. Operation of the counter causes changes in plateau characteristics as follows: (a) Immediately after use, the plateau slope increases slightly. (b) With continued use the plateau slope becomes steeper. (c) For moderate use the counter recovers when inactive, but never to the original characteristics. (d) With further use, the counter loses its plateau and does not recover. (e) The pressure in an argon-alcohol counter was observed to increase as a function of the total number of counts recorded. III. For argon-alcohol counters the useful life in these experiments was found to be about 10^9–10^{10} counts; for argon-methane, 10^7–10^8 counts. The observed changes of characteristics are presumably due to the decomposition of the organic vapor by the discharge.

INTRODUCTION

WHEN a G-M counter of the self-quenching type is connected to the usual external recording circuit, the relationship between the counting rate for a given source as a function of the counter voltage is given by the familiar "plateau" curve. The plateau characteristics are the starting potential and the slope of the plateau. The starting potential is the minimum voltage at which the pulse is of such size as to be able to actuate the external apparatus, and its value will depend on the nature and pressure of the gases used and upon the sensitivity of the amplifier. The slope of the plateau is defined as the percentage increase of counts per volt of counter potential. A perfect counter would be one for which the plateau slope is zero, i.e., the counting rate is independent of the voltage. A flat plateau is not possible because of the occurrence of spurious counts which originate inside the counter, often as a result of the discharge itself.

The problem here discussed is to determine what factors influence the plateau characteristics. Two conditions are desirable: (a) the starting potential should be as low as possible without affecting the efficiency of the counter, and (b) the plateau should be as nearly flat as possible over a considerable voltage range, so that the counting rate be independent of voltage fluctuations.

Many articles have appeared on the problem of the preparation of alcohol-argon counters and on the effect of the preparation on the plateau characteristics.[1–6] Care in preparation reduces the spurious counts and, therefore, the plateau slope. Experiments on the temperature coeffi-

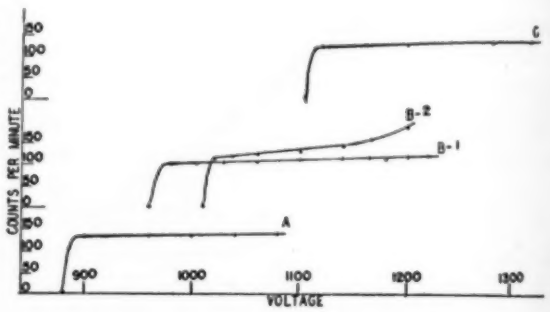

FIG. 1. Comparison of plateau characteristics of alcohol-argon counter having a total pressure of 10 cm of Hg with different mixtures. (*A*) 5 percent alcohol vapor: starting potential 840 volts, slope less than 0.01 percent per volt. (*B*-1) 10 percent alcohol vapor: starting potential 940 volts, slope 0.025 percent per volt. (*B*-2) 10 percent alcohol vapor and 2 percent air; starting potential 1000 volts, slope 0.15 percent per volt. (*C*) 20 percent alcohol vapor: starting potential 1080 volts, slope 0.05 percent per volt.

[1] S. C. Curren and V. Petrzilka, Proc. Camb. Phil. Soc. **35**, 309 (1939).
[2] H. V. Neher, J. Strong's *Modern Physical Laboratory Practice* (Prentice-Hall, Inc., New York, 1941), p. 268.
[3] F. R. Shonka, Phys. Rev. **55**, 24 (1939).
[4] G. L. Locher, Phys. Rev. **55**, 675 (1941).
[5] C. H. Collie and D. Roaf, Proc. Phys. Soc. **52**, 186 (1941).
[6] F. J. Davis and L. F. Curtiss, J. Research Nat. Bur. Stand. **29**, 405 (1942).

cient[7] show that in the case where the quenching constituent is a vapor, temperature has a decided effect on the plateau characteristics because of the temperature dependence of the vapor pressure.

APPARATUS

The conventional multivibrator, scale-of-8, and mechanical recorder circuit were used for recording the counting rate during plateau runs. A two-megohm leakage resistance was used in all tests described below. Counters were of the thin-walled glass type[8] of 15-cm length, 2-cm diameter with 4-mil tungsten center wire. The silvered portion extended for a length of 8 cm with the thin-walled section 6 cm long. The glass thickness varied considerably but was of the order of 10^{-2} cm. A circular manifold held 6 counters parallel and equi-spaced at a distance of 7 cm from the center, where a radium source was placed during the continuous operations. The source was of such strength as to give about 100 counts per second. All tests were made on 6 counters, and in most cases the counters were evacuated and refilled a second time and the tests repeated.

OBSERVATIONS

Test of Dependence of Flatness of Plateau on Argon Purity

A manifold of 6 counters was filled with a mixture of 5 percent alcohol vapor and 95 percent argon, which latter gas was 99.8 percent pure, to a total pressure of 10 cm of Hg. The counters were found to require 24 hours for complete mixing and diffusion of gas and vapor. The state of complete equilibrium was verified by checking the starting potential at intervals of several hours; the starting potential being a function of the percentage of vapor present. A beta-source weaker than the one mentioned above was placed 20 cm from the counters in all plateau runs; this yielded about 150 to 200 counts per minute depending on the individual wall thickness. The counting rate was observed for an over-voltage of 200 volts, in steps of 20 volts. At each voltage step a sufficient number of counts was recorded

TABLE I. Dependence of plateau slope and starting potential on argon purity and alcohol content.

Percent alcohol vapor	Argon purity	Starting pot. volts	Plat. slope percent/v
5	99.8	840	0.01
10	99.8	960	.02
10	98.0	1000	.15
10	90.0	1125	.25
20	99.8	1080	.05
20	90.0	1220	.35

[7] S. A. Korff, W. Spatz, and N. Hilberry, Rev. Sci. Inst. **13**, 127 (1942).
[8] Silvered thin-walled type made by Eck and Krebs of New York.

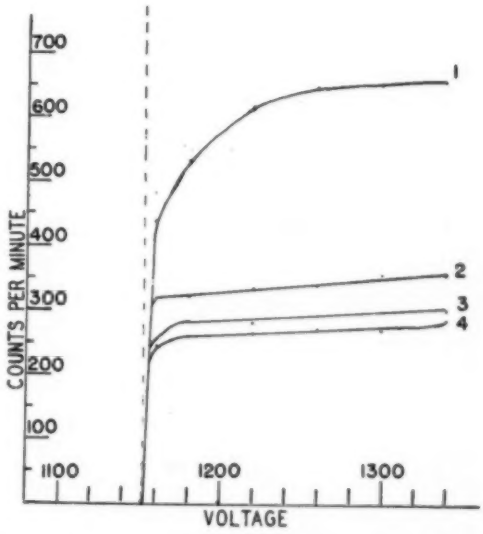

FIG. 2. Recovery of the plateau of an alcohol-argon counter after an exposure of 125 hours (5×10^7 counts). Immediately after exposure and one day later the counting rate was too high for the mechanical recorder and is represented by the broken vertical line. Curves 1–4 represent the plateau after a rest period of 2, 3, 4, and 5 days, respectively.

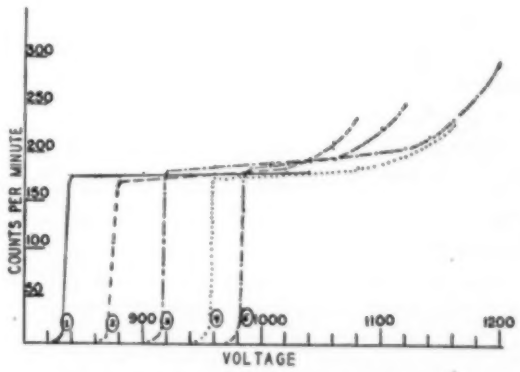

FIG. 3. Plateau characteristics of alcohol-argon counter after exposure at a rate of the order of 4×10^5 counts per hour (1) before exposure, (2) one day after 34-hr. exposure, (3) one day after 63-hr. exposure, (4) one day after 97-hr. exposure, and (5) four days after 169-hr. exposure.

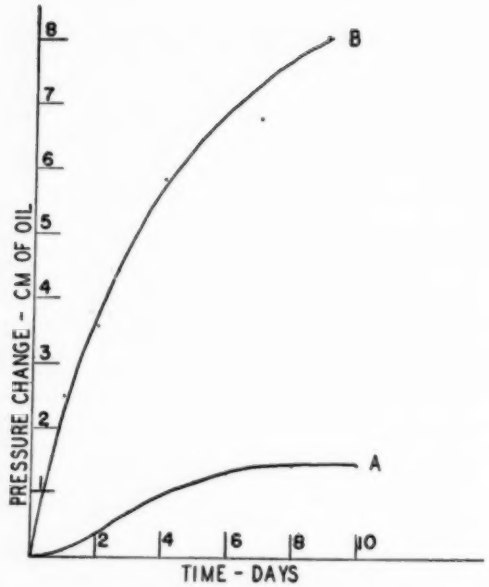

FIG. 4. Pressure change for alcohol-argon (*B*) and methane-argon (*A*) with exposure time. Differential manometer attached to the manifold contained Apiezon *B* oil. Counting rate was of the order of 10^7 per day.

so as to have the statistical fluctuations (based on the square root of the total count) below 3 percent. The plateau slope in all cases was less than 0.01 percent per volt.

The process was repeated with mixtures of 10 percent and 20 percent alcohol vapor at the same total pressure. The effect of contamination, produced by adding 2 percent and 10 percent of air, was examined. Typical curves in Fig. 1 show the effect of increased alcohol vapor and of air contamination. Table I gives a comparison for these mixtures. In all cases 6 counters were used so as not to be influenced by the possible peculiarities of any one counter.

Aging Tests

The manifold was filled with a mixture of 5 percent alcohol and 95 percent argon to a total pressure of 10 cm of Hg, and the characteristic curves taken. A radium source was placed at the center of the manifold and the counters connected to the high potential with an over-voltage of 60 volts. The pulse size was noted for this over-voltage, which was maintained by checking the pulse size every 6 hours. The counters were operated for a period of 24 hours, and then the plateau was measured by using the same beta-source and geometry. Immediately upon removal, the counters exhibited counting rates much higher than those previously recorded for the given source and geometry, but, after 24 hours during which the counters were inactive, they again showed plateau characteristics. With each successive period of use the slope of the plateau changed very little, but the starting potential increased steadily. When the counters had been subjected to prolonged use (over 100 hours), it was noted, as before, that immediately after removal the counters had no plateau, and it took several days for them to recover. This recovery effect in the case of 125 hours use is shown in Fig. 2. The change in starting potential is shown in Fig. 3, in which plateaus were determined after progressively greater use. In each case the counter was allowed to recover fully before the plateau was measured.

Pressure Variation

It was observed in a preliminary test that the pressure in the counter increased with use. The above aging process was repeated for a mixture of 20 percent alcohol and the same total pressure. In this case a differential oil manometer was attached to the manifold to measure the pressure variation as a function of the counter's use. The results are shown in Fig. 4.

The question was raised as to whether the change in the starting potential could be ascribed to a change of both composition and total pressure of the quenching vapor in the counter. This was experimentally determined by observing the starting potential-pressure curves under the following conditions. The manifold was initially filled with a 20 percent alcohol mixture at a total pressure of 10 cm of Hg and the starting potential change was noted for pressure change when: (1) the total pressure of the mixture increased, (2) the manifold with the original mixture was subjected to use at the high counting rate, and (3) the total pressure was changed by the addition of hydrogen to the original mixture. Figure 5 shows the results of these tests.

There was no measurable pressure change during the recovery period when the counter was not in use.

Increasing Photosensitivity with Use

It was noticed that alcohol-argon counters became photosensitive to visible light after long use.

Tests on Methane Counters

Experiments on methane-argon counters have not been carried out as extensively as those for the alcohol-argon type. Previous experiments[7] on temperature coefficients show that over the range of temperature studied (−22°C to 85°C), the methane-argon counters showed no appreciable change in plateau characteristics. In general, methane-argon counters have a higher starting potential and greater plateau slope, and preliminary tests did not show the recovery effects observed in the case of the alcohol-argon counters. Figure 4 shows the comparison of pressure increase between the two types of counters under identical operating conditions. It is estimated that an alcohol-argon counter undergoes about 10^9 to 10^{10} discharges before losing all plateau characteristics. Methane-argon counters, on the other hand, have a useful life of approximately 10^7 to 10^8 discharges, but this estimate is based on incomplete data at present.

DISCUSSION

When the alcohol-argon counter is operated continuously at the high rate described, the above-mentioned phenomena were observed as length of time of use progressed. We shall see how these effects can be explained on the basis of the breakdown of the alcohol molecule by the action of the avalanche discharge.

As indicated earlier, the avalanche discharge in the counter is believed to be initiated close to the center wire. The electrons in the avalanche have sufficient energy to ionize the argon and alcohol molecules in this region. Probably the discharge also causes the alcohol molecules to disintegrate into ions of lower atomic mass. Cummings and Bleakney[9] subjected ethyl alcohol to electron impacts and measured the mass and relative abundance of the ions formed. The essential part of their results is shown in Table II. However, their experimental procedure was to separate the various ions immediately after bombardment, and as many of the resultant ions are unstable, one cannot assume that all the types of ions are present in the case of the similar electron impacts occurring in the discharge process of the Geiger counter. A similar disintegration of methane has been observed by L. M. Yaddanapalli.[10] In this case hydrogen and heavy hydrocarbons are also the products of the disintegration process.

The relative abundance of alcohol in the disintegration products is only 4 percent, the rest being of lower atomic number. In this way the alcohol present in the counter is gradually decreasing with increased operation time of the counter, and it is to be noted that two of the final products are oxygen and hydrogen, both

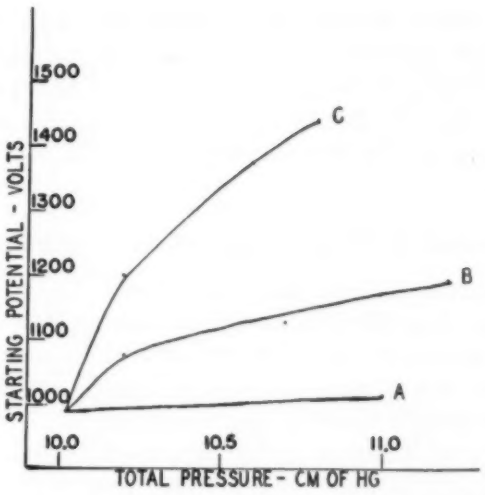

FIG. 5. Variation of starting potential of an alcohol-argon counter originally at a total pressure of 10 cm of Hg using a 20 percent alcohol mixture under the following conditions: (*A*) increase of total pressure of original mixture; (*B*) increase of total pressure resulting from exposure of original mixture; (*C*) addition of hydrogen to the original mixture.

TABLE II. Table of decomposition products of alcohol vapor in a discharge, from the data of Cummings and Bleakney.

Mass	Ion	Relative abundance	Mass	Ion	Relative abundance
46	C_2H_5OH	100	26	C_2H_2	110
45	C_2H_4OH	242	17	OH	3.9
31	CH_2OH	986	16	CH_4 & O	9.6
29	HCO	293	12	C	18.7
28	C_2H_4	390	2	H_2	30.4
27	C_2H_3	272	1	H	4.7

[9] C. S. Cummings and W. Bleakney, Phys. Rev. **58**, 787 (1940).

[10] L. M. Yaddanapalli, J. Phys. Chem. **10**, 249 (1942).

of which increase with operation time. This would seriously affect the slope of the plateau inasmuch as the percentage of organic vapor is less and the percentage of non-quenching gases is greater. The decomposition would be a gradual one.

Increase of Pressure and of Starting Potential

If the alcohol molecule breaks up to form other constituents, the total pressure will increase in accordance with the law of partial pressures. Also, for a given number of alcohol molecules originally available, one would expect that the pressure increase would not be constant with time of operation, but would tend to reach a steady value. This is observed in Fig. 4 for both alcohol and methane; as the length of time of operation increases, the total pressure tends to approach a constant value which would be that for complete disintegration. The fact that the change in pressure for methane is considerably less than for alcohol is explainable on the basis of the observations of Yaddanapalli[10] that heavy polymers are formed in the disintegration of methane thus reducing the number of atoms in the gaseous state.

The resultant increase in the pressure of the gases in the counter automatically brings about an increase of the starting potential. However, the starting potential is also a function of the type of quenching gas. If the increase of pressure is due to merely an increase of alcohol (which is unlikely on the disintegration hypothesis), the starting potential-pressure relationship is far below that actually observed in Fig. 5. On the other hand, if hydrogen is assumed to be the only disintegration product, the starting potential-pressure relationship is above that observed. It is well known that, in general, hydrogen is a "high starting potential" gas, and if 1 cm of hydrogen is added to a given mixture of alcohol-argon, the resultant increase in starting potential is greater than that for an addition of 1 cm of alcohol. The actual observed relationship between starting potential and pressure probably arises from a mixture of organic gases, as suggested in Table II. Just what the mixture composition is and how it changes with time is not known at present, but it evidently does change with time of operation.

Increase in Plateau Slope and Recovery

A change in the plateau slope takes place after the first aging run of 24 hours but does not change much with subsequent use, except for the fact that, as the counter is used more and more, the time required for the plateau to recover also increases. Abrupt change of the plateau does not seem to occur until the time of use is of such length as to destroy the self-quenching completely. This will presumably occur when the percentage of hydrogen present has increased, with the decrease of organic constituent, to the point where the amount of organic constituents is insufficient for complete quenching.

Effect of Percentage of Alcohol on the Plateau Slope

Tests on the correlation between plateau slope and percentage of alcohol indicate that, with increase of alcohol, an increase in the plateau slope results. If the alcohol is contaminated, as by the absorption of air, we would have a possible source of spurious counts due to negative ions whose quantity is dependent on alcohol content. Such a possibility is indeed present if the alcohol is not degassed after transfer to the mixing system. This had not been done in the present experiment. Calculations based on the known solubility of air in alcohol show that the contamination, for the percentage of alcohol used, would be of the order of several tenths (0.7 percent for the 20 percent alcohol mixture) of one percent. The large increase in plateau slope produced by admitting a 2 percent contamination of air has been found to be 0.15 percent per volt, and thus for the estimated 0.7 percent contamination in the case of the 20 percent alcohol mixture one would expect to find a slope of 0.05 percent per volt, as is observed. The exact agreement may, of course, be fortuitous.

The author wishes to express his appreciation to Dr. S. A. Korff for his invaluable suggestions and aid given during the course of this research.

Thermal and Electrical Conductivities of Tungsten and Tantalum*

MARTHA COX**
Department of Physics, Bryn Mawr College, Bryn Mawr, Pennsylvania

An investigation was made of the variation with temperature of the resistance, thermal conductivity, and Wiedemann-Franz ratio of pure tungsten and tantalum wires. Measurements were made of the resistance, as a function of power input, of the wires suspended in vacuum and thermostated at 77°K, 90°K, 273°K and 373°K. The resistivity of the wires was determined from the resistance at zero power input. A method was developed for calculating the thermal conductivity from the resistance at zero power input and the slope of the resistance *versus* power input curve. Limitations were found on the method, particularly lack of available data on the emissivity of tantalum at the temperatures used. An anomaly was observed in the variation with temperature of the resistance of tantalum.

INTRODUCTION

SOME preliminary measurements made in this laboratory[1,2] on the thermal conductivity of tungsten at temperatures below room temperature, as well as the results of other workers on various metals, indicate that the Wiedemann-Franz law does not hold for low temperatures. A search of the literature reveals a need for data on electrical and thermal conductivities of pure metals at moderately low temperatures. Several values have been published for tungsten[3–16] but these show very little agreement with one another, particularly on thermal conductivity. Only two published values have been found for the thermal conductivity of tantalum[8,17] at these low temperatures. The purpose of the present work was to measure more precisely than has previously been done both the electrical and thermal conductivities of pure tungsten and tantalum at temperatures ranging from 77°K to 373°K so as to find the nature of the variation with temperature of the Wiedemann-Franz ratio, and check as far as possible modern theories of the conductivity of solids.

The method of measurement was similar to that used by Kannuluik,[18] Roberts,[14] Michels and Cox,[2] and Raines[19] in measuring thermal conductivities and accommodation coefficients. Kannuluik and Roberts developed the theory of the heat losses from an electrically heated wire with its ends and surroundings thermostated at a known temperature. Michels and Cox extended the theory for application to a wire supported by springs. Raines added a correction for the variation of resistivity along the wire. In this paper the equation for the wire is further corrected and a rigorous and explicit solution found for the thermal conductivity.

THEORY OF HEAT LOSSES FROM A WIRE

A wire of length L and radius a is supported in an evacuated tube and immersed in a constant temperature bath so that the ends of the wire and the walls of the tube are maintained at a temperature T. A current i is sent through the wire causing any point in the wire to be raised to a

* From a dissertation submitted in partial fulfillment of the requirements for the degree of Doctor of Philosophy at Bryn Mawr College, Bryn Mawr, Pennsylvania.

** Now at Newcomb College, Tulane University, New Orleans, Louisiana.

[1] W. C. Michels and G. White, Phys. Rev. **47**, 197A (1935).

[2] W. C. Michels and M. Cox, Physics **7**, 153 (1936).

[3] L. Holborn, Ann. der Physik **59**, 145 (1919).

[4] F. Henning, Zeits. f. Physik **5**, 264 (1921).

[5] W. Geiss and J. Vam Liempt, Zeits. f. anorg. u. allgem. Chemie **128**, 355 (1923).

[6] W. E. Forsythe and A. G. Worthing, Astrophys. J. **61**, 146 (1925).

[7] W. Meissner, Physik. Zeits. **29**, 897 (1928); Zeits. f. Physik **61**, 191 (1930); W. Meissner and B. Voight, Ann. der Physik **7**, 892 (1930).

[8] T. Barratt, Proc. Phys. Soc. **26**, 347 (1914).

[9] S. Weber, Ann. der Physik **54**, 165 (1917).

[10] E. Gruneisen and E. Goens, Zeits. f. Physik **44**, 615 (1927); E. Gruneisen, Zeits. f. Physik **46**, 151 (1927); E. Gruneisen and H. Adenstedt, Ann. der Physik **29**, 597 (1937).

[11] W. G. Kannuluik, Proc. Roy. Soc. **141**, 159 (1933).

[12] W. J. de Haas and J. de Nobel, Physica **5**, 449 (1938).

[13] W. D. Coolidge, quoted in *Handbook of Chemistry and Physics* (Chemical Rubber Publishing Company, 1937), twenty-second edition, p. 1385.

[14] J. K. Roberts, Proc. Roy. Soc. **135**, 192 (1932).

[15] I. Langmuir and J. B. Taylor, Phys. Rev. **50**, 68 (1936).

[16] H. Bremmer and W. J. de Haas, Physica **3**, 672 (1936).

[17] A. G. Worthing, Phys. Rev. **4**, 535 (1914).

[18] W. G. Kannuluik, Proc. Roy. Soc. **A131**, 320 (1931).

[19] B. Raines, Phys. Rev. **56**, 691 (1939).

temperature t above the surroundings, t being a function of x, the distance from one end of the wire. Let ρ be the resistivity of the metal at the temperature $T+t$, e the total emissivity at that temperature, and K the thermal conductivity. Let ρ_0, e_0, and K_0 be the values of these quantities at the temperature T, α and β the temperature coefficients of electrical and thermal resistance, respectively, and σ the radiation constant. R and R_0 are the resistances of the wire at the temperatures $T+t$, and T, respectively.

If, in a section of wire of length dx the power input is dW, the heat lost by conduction dQ_K, and the heat lost by radiation dQ_R, then

$$dW=dQ_K+dQ_R, \tag{1}$$

or

$$i^2\rho_0(1+\alpha t)dx/\pi a^2=-\frac{\pi a^2K_0}{1+\beta t}\frac{d^2t}{dx^2}dx + 2\pi ae\sigma[(T+t)^4-T^4]dx. \tag{2}$$

This is a differential equation of the form

$$d^2t/dx^2+B-At-Ct^2-Dt^3-Et^4-Ft^5=0, \tag{3}$$

where

$$A=8\sigma eT^3/K_0a-i^2\rho_0(\alpha+\beta)/\pi^2a^4K_0,$$

$$B=i^2\rho_0/\pi^2a^4K_0,$$

$$C=(12\sigma eT^2+8\sigma eT^3\beta)/K_0a-i^2\rho_0\alpha\beta/\pi^2a^4K_0,$$

$$D=(8\sigma eT+12\sigma eT^2\beta)/K_0a,$$

$$E=(2\sigma e+8\sigma eT\beta)/K_0a,$$

$$F=2\sigma e\beta/K_0a.$$

In previous work it has been assumed that the terms Ct^2, Dt^3 etc. were negligible compared with the first three terms of the equation. The equation was solved by neglecting these terms, and definite experimental values of the current i and the corresponding average temperature rise $\bar{t}$ were inserted in the solution. K_0 was then calculated by successive approximations. In the case of the wires used in this experiment, the coefficient A is very small for any reasonable value of i, and may be comparable with Ct. Thus it is a very poor approximation to keep the term At and neglect the term Ct^2 if the solution is to be applied to a wire with a definite power input. In the limiting case, however, as the power input in the wire is made very small and the temperature rise t becomes correspondingly small, the ratio Ct^2/At approaches zero and the equation describing the temperature distribution along the wire does approach the form

$$d^2t/dx^2+B-At=0. \tag{4}$$

This is the differential equation which has been solved by previous workers, but it must be kept in mind that it is valid only for a wire in which the power input is very low. The method of solution shown below allows a calculation of the thermal conductivity from the limiting case of zero power input, and justifies the use of the approximate differential equation, as well as simplifies the calculations.

Integration of the equation with the boundary condition that $dt/dx=0$ at $x=L/2$ gives

$$(dt/dx)_{x=0}=B(\cosh LA^{\frac{1}{2}}-1)/A^{\frac{1}{2}}\sinh LA^{\frac{1}{2}} =BLF(LA^{\frac{1}{2}}), \tag{5}$$

where

$$F(x)=(\cosh x-1)/x\sinh x =(e^x+e^{-x}-2)/x(e^x-e^{-x}). \tag{6}$$

If the total power input in the wire is W and the heat losses from the entire wire by conduction and radiation are Q_K and Q_R,

$$Q_K=2\pi a^2K_0(dt/dx)_0=2i^2\rho_0LF(LA^{\frac{1}{2}})/\pi a^2, \tag{7}$$

$$Q_R=2\pi ae\sigma\int_0^L[(T+t)^4-T^4]dx =8\pi ae\sigma LT^3\bar{t}, \quad \text{for } t\ll T, \tag{8}$$

$$W=\int_0^L i^2\rho_0(1+\alpha t)dx/\pi a^2=i^2\rho_0L(1+\alpha\bar{t})/\pi a^2. \tag{9}$$

We may set $\bar{t}=W(dR/dW)/(dR/dt)$, since R varies linearly with both power input and temperature over ranges much larger than are assumed here. Also

$$W=Q_K+Q_R, \tag{10}$$

or

$$F(LA^{\frac{1}{2}})=1/2\{1-8\pi ae\sigma T^3L(dR/dW)/(dR/dt)\}\cdot \{1+(W/R_0)(dR/dW)\}. \tag{11}$$

But A is a continuous function of W, and $F(LA^{\frac{1}{2}})$ a continuous function of A so that

$$\lim_{W\to 0} F(LA^{\frac{1}{2}}) = F(\lim_{W\to 0} LA^{\frac{1}{2}}) = F(LA_0^{\frac{1}{2}}), \quad (12)$$

where

$$A_0 = 8\sigma e T^3/K_0 a. \quad (13)$$

Taking the limits of both sides of Eq. (11) one obtains

$$F(LA_0^{\frac{1}{2}}) = 1/2\{1 - 8\pi a e \sigma L T^3 (dR/dW)/(dR/dt)\}. \quad (14)$$

The quantity dR/dW must be evaluated at $W=0$. This is possible because, when measured values of R are plotted against the values of W used in an actual experiment, the points fall on a straight line. This constancy of dR/dW over a relatively large range of power input makes possible a precise determination of its value at zero power input. Use of the limiting equation for $W=0$ insures the validity of the approximate form of the differential equation which is used.

The value of $F(LA_0^{\frac{1}{2}})$ can be calculated from Eq. (14). $LA_0^{\frac{1}{2}}$ is then found graphically or from tables, and from this is found A_0, and therefore K_0 from Eq. (13).

At the lower temperatures, (77°K and 90°K), the term to be subtracted from 1, in Eq. (14), becomes so small and the value of $F(LA_0^{\frac{1}{2}})$ so close to $F(0)=\frac{1}{2}$ that the calculation can not be made in the same way. For this case let $LA_0^{\frac{1}{2}}=x$ and let $8\pi a e \sigma T^3 L(dR/dW)/(dR/dt)=y$. Equation (14) becomes

$$(\cosh x - 1)/x \sinh x = (1-y)/2. \quad (15)$$

Expansion of the hyperbolic functions into power series yields

$$1-y = (1+x^2/12+x^4/360+\cdots)/(1+x^2/6+x^4/120+\cdots)$$
$$= 1 - x^2/12 + x^4/120 - 17x^6/20160 + \cdots. \quad (16)$$

Neglecting terms in x^4 and higher powers of x, we find

$$x^2 = 12y. \quad (17)$$

In the case where this solution is used, x^2 is about 5×10^{-8}, so that the approximation is completely justified. In intermediate cases, where this expression is not quite correct, another term may be kept in the expansions and the resulting quadratic equation in x^2 solved, giving

$$x^2 = 12y(1+1.2y+\cdots). \quad (18)$$

Thus for very low temperatures Eq. (17) holds and K_0 is obtained from the equation

$$K_0 = L(dR/dt)/12\pi a^2 (dR/dW), \quad (19)$$

which does not depend on the emissivity of the metal. When x^6 is very small but x^4 is considerable, Eq. (18) gives

$$K_0 = L(dR/dt)/12\pi a^2 (dR/dW)(1+1.2y). \quad (20)$$

In the latter case y and therefore the emissivity comes in only as a small correction term. Equation (20) was found valid for tungsten at 273°K and was used to check the calculation there, but it is not valid for tantalum at that temperature.

EXPERIMENTAL METHOD

The metal used was in the form of drawn wires 0.010 inch in diameter and about 40 cm long. The tungsten wire was contributed by Dr. W. E. Forsythe of the General Electric Company. Dr. Forsythe sent the wire in 1939 and stated that it was the highest purity tungsten wire that had then been made. The tantalum wire was obtained from the Fansteel Corporation, and according to their report had a purity of 99.9 percent.

In order to eliminate supporting springs, which complicate the calculations and increase the uncertainty of the results, the wire was hung in a glass tube bent so that its axis was a catenary. This method of support allowed the wire to expand and contract without being strained or touching the tube, but allowed the thermostating bath to surround the wire over its entire length. The experimental tube with an ionization gauge attached was sealed off at a pressure of less than 10^{-6} mm of Hg after the glass and metal parts had been cleaned up on a vacuum system. The wire to be measured was first heated with direct current so that it could be kept away from the walls of the tube with a magnet while it was first being brought up to the temperature at which it would hang freely in the tube. After the wire had

TABLE I. Experimental values and emissivity ϵ.

Tube	T (°K)	R_0 (ohms)	dR/dW (ohms/watt)	dR/dt (ohms/°K)	ϵ[a,b]
Tungsten No. 2	77.4	0.05588±0.00013	5.62±0.10	0.001509	
	90.2	0.075754±0.000092	6.18±0.14	0.001629	
	193	0.2635±0.001			
	273.2	0.417613±0.000054	6.804±0.020	0.0018682	0.01579
	372.8	0.613195±0.000048	5.569±0.017	0.0020032	0.02389
Tungsten No. 8	77.36	0.049830±0.000043	5.159±0.048	0.001472	
	90.2	0.069518±0.000080	5.760±0.072	0.001590	
	273.2	0.408953±0.000011	6.7414±0.0020	0.0018672	0.01579
	373.1	0.603460±0.000033	5.6787±0.0085	0.0020175	0.02392
Tantalum No. 3	77.33	0.194403±0.000045	49.82±0.13		
	273.2	0.979331±0.000070	24.99±0.10	0.0037587	0.055±0.005*
	373.4	1.355954±0.000068	11.841±0.083	0.0037587	0.067±0.005*

[a] See reference 24 in text.
[b] See reference 20 in text.
* Extrapolated.

acquired its proper catenary form all heating was done with 60-cycle alternating current.

The wire was aged by passing through it as high a current as was possible without evaporating the metal. A slight amount of evaporation did take place during the determination of this highest safe current, but not enough to change the diameter of the wire beyond the uncertainty of the measurement of the diameter. Tungsten tube No. 2 was aged at temperatures of 2400°C and 2600°C, tungsten tube No. 8 at 2300°C and tantalum tube No. 3 at 1800°C and 2000°C. The aging was interrupted at intervals and a determination made of the resistance of the wire as a function of power input with the tube at 0°C. The resistance at zero power input was plotted as a function of time of aging. The resistance decreased rapidly at first and finally reached a stable value, at which time it was assumed that the wire had acquired a stable crystalline structure. About 370 hours of aging were necessary for tungsten and 2750 hours for tantalum, although the latter time could have been shortened as the first part of the aging was carried out at an unnecessarily low temperature.

After the wire had been aged, the tube was immersed in various baths and readings were taken of voltage across the tube, and current in it, by means of a Queen Gray potentiometer. From these readings resistance and power input could be determined, and then R_0 and dR/dW calculated. A temperature of 273.2°K was obtained by surrounding the tube with finely crushed ice packed down in water in a one-gallon Dewar flask. A second point was found by immersing the tube in briskly boiling water of which the temperature was determined, in some cases with mercury in glass thermometers later calibrated in steam at a measured atmospheric pressure, and in others directly from the barometric reading. The latter method was the more satisfactory providing the water could be kept pure for a long enough time to take the readings. Temperatures of 77.4°K and 90.2°K were obtained by using boiling liquid nitrogen and boiling liquid oxygen. The latter could not be used for the tantalum tube owing to wartime restrictions on the transportation of liquid oxygen. Attempts to thermostat the tubes at intermediate temperatures, in solid CO_2 and in melting tetrachlorethane, were not successful, probably because of the large volume of the Dewar flask used, and because of the high constancy of temperature necessary to make the experimental points lie on a straight line on the R–W graph within the uncertainty of the measurements.

From the values of R_0 at different bath temperatures, dR_0/dT and therefore dR/dt could be found. In the case of tungsten R_0 is not linear in T and the slope of the R_0–T curve is difficult to

TABLE II. Constants of the wires.

Tube	a (cm)	L (cm)	$\sigma \times 10^{12}$[a] (watts/cm² deg.⁴)
Tungsten No. 2	0.01252±0.00002	40.85±0.02	5.75±0.03
Tungsten No. 8	0.01252±0.00002	40.00±0.02	5.75±0.03
Tantalum No. 3	0.01270±0.00006	40.00±0.02	5.75±0.03

[a] *International Critical Tables of Numerical Data* (1929), Vol. 5, p. 237.

estimate at low temperatures. Log R_0 was plotted against log T and the curvature was thus arranged so that it was possible, on a large graph, to estimate $dR_0/dT=(R_0/T)(d \log R_0/d \log T)$ with fairly good precision. In the case of tantalum it was impossible to determine this quantity except at the two higher temperatures.

The diameter of the tungsten wire after aging was determined by means of the screw of a dividing engine, with a dial indicator to bring two blocks together always with the same pressure. A pair of Webber blocks was used both for the calibration of the screw and for the actual measurement, in which two pieces of the wire separated the blocks. The probable error of this determination was 0.2 percent. The diameter of the tantalum wire was specified by the Fansteel Corporation with a tolerance of 0.5 percent.

Attempts to prepare a molybdenum wire for measurement have so far been unsuccessful. Because of the large difference in emissivity between the oxide and the clean surface of this metal, when the wire is first heated up for outgassing that portion of the surface which happens to get rid of its oxide first gets so extremely hot that it is impossible to get the rest of the wire hot enough without burning out that part which is clean. In cleaning up tungsten and tantalum the same phenomenon is observed to a lesser degree, one portion of the wire becoming very bright, but in those cases the bright area soon spreads over the entire wire.

RESULTS

The experimental values of R_0, dR/dW, and dR/dt, together with the values used for the total emissivity are shown in Table I, and the constants of the three wires used in Table II. Table III gives the values for the resistivity, thermal conductivity, and Wiedemann-Franz ratio calculated from the data in Tables I and II.

TABLE III. Values of resistivity and thermal conductivity and $W-F$ ratio.

Tube	T (°K)	K (watts/cm deg.)	$\rho\times10^6$ (ohm cm)	$K\rho/T\times10^8$ (volt²/deg.²)
Tungsten No. 2	77.4	1.86	0.6736	1.62
	90.2	1.82	0.9132	1.84
	193		3.18	
	273.2	1.70	5.034	3.13
	372.8	1.73	7.392	3.43
Tungsten No. 8	77.36	1.93	0.6135	1.53
	90.2	1.87	0.8558	1.77
	273.2	1.69	5.035	3.11
	373.1	1.68	7.429	3.35
Tantalum No. 3	77.33		2.46	
	273.2	0.36±0.04	12.41	1.64
	373.4	0.19±0.17	17.18	0.87

Tantalum

The high uncertainty in the thermal conductivity of tantalum, at 273°K and especially at 373°K, is due to lack of knowledge of the emissivity of tantalum at these temperatures. Malter and Langmuir's[20] data at temperatures from 1000°K to 1500°K were extrapolated to yield the highly uncertain values of e shown in Table I. The magnitude of the term $8\pi ae\sigma T^3L(dR/dW)/(dR/dt)$ is such that a 10 percent error in e, at 373°K, causes a 90 percent error in K while the percentage error in K at 273°K, due to e, is about equal to the percentage error in e.

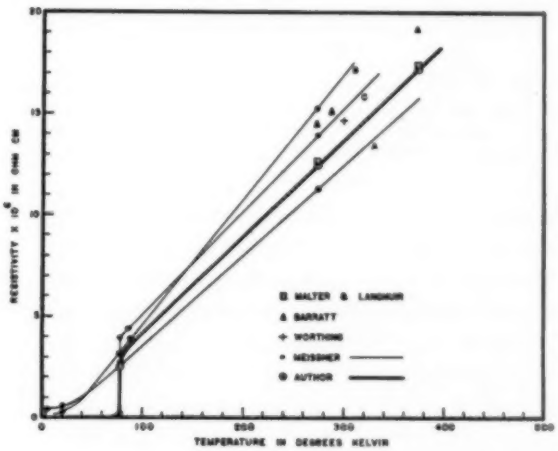

FIG. 1. The resistivity of tantalum. Of Meissner's curves, the curves marked A and B were obtained from lamps of unknown purity, which had been in use for a long time. Curve C was made from a lamp containing Fe_2O_3 and flashed at 2800°K.

At 77°K the second method of calculation is valid for both metals, but at this temperature it was impossible to evaluate dR/dt for tantalum as R does not vary in a regular manner with T throughout the range. As can be seen in Fig. 1, the value of R at 77°K is considerably below that which would be expected from the two upper values. That is, a reasonable curve drawn through

[20] L. Malter and D. B. Langmuir, Phys. Rev. 55, 743 (1939).

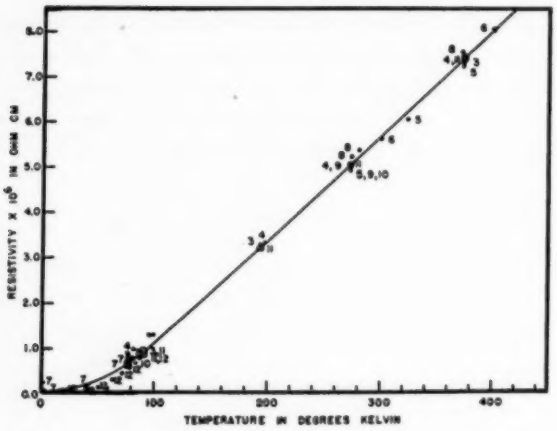

FIG. 2. The resistivity of tungsten. The curve is drawn through the circles, which represent the author's experimental points. The numbers on the other points refer to the footnotes giving the sources of the data shown.

the three points would be concave towards the axis and could not be made to go through the origin or to give a positive resistance intercept. In studying Meissner's[7] data on the resistivity of tantalum in this temperature range it was observed that some of his samples showed a peculiar sudden drop in resistance at low temperatures. Curves for three of his samples are shown in Fig. 1, with the author's points plotted on the same scale. One sample showed this sudden drop at 77°K and another at 4°K. It is unfortunate that liquid oxygen could not be obtained for data on tantalum at 90°K to check this anomalous behavior.

Although the data on tantalum are insufficient for any check on theory, the values given for ρ and the rough value of K at 273°K are thought to be reliable. The values of ρ check very well with those of Malter and Langmuir.[20]

Tungsten

The values of ρ, which are plotted in Fig. 2, show a very satisfactory check with those of other workers.[3–12] Previous measurements of K[8–13] show such wide disparity that comparison is difficult. The values of Barratt,[8] Weber,[9] and Coolidge,[13] however, are probably not reliable as pure tungsten was not available at the time at which their work was done. A good check was found with Kannuluik[11] throughout the range, particularly with one of his samples, and with Langmuir and Taylor[15] at 273°K. The author's values of K are plotted in Fig. 3, with those of other workers.

The theory of conductivity at low temperatures as worked out by Bloch[21] predicts that at temperatures very small compared with the Debye characteristic temperature the electrical conductivity should be proportional to T^{-5} and the thermal conductivity proportional to T^{-2}. Sommerfeld and Bethe[22] point out that the values of K for tungsten measured at 21.2°K and 83.2°K by Gruneisen and Goens[10] are nearly proportional to T^{-2}. But the characteristic temperature for tungsten is 310°K so that it is not to be expected that the T^{-2} law will hold in a range as high as 83°K. The author's values of K at 77°K and 90°K do not obey the T^{-2} law. The values given by de Haas and de Nobel[12] show, also, that the T^{-2} law does not hold for temperatures as high as 80°K. The use of Gruneisen's data by Sommerfeld and Bethe to show $1/K \propto T^2$ does not seem to be justified over such a large range. The good agreement between the author's values and those

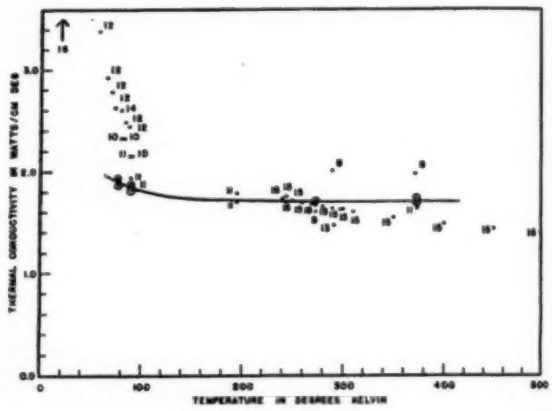

FIG. 3. The thermal conductivity of tungsten. The curve is drawn through the circles, which represent the author's experimental points. The numbers on the other points refer to the footnotes giving the sources of the data shown.

of Kannuluik indicate that the values of Gruneisen and of de Haas and de Nobel for the thermal conductivity of tungsten are probably too high.

Another comparison with theory may be made by considering the variation with temperature of the quantity $K\rho/T$. In the very low temperature range, if $\rho \propto T^5$ and $1/K \propto T^2$ we should expect

[21] F. Bloch, Zeits. f. Physik **52**, 555 (1929); **59**, 208 (1930).
[22] A. Sommerfeld and H. Bethe, *Handbuch der Physik* (1933), Vol. 24, Part 2, p. 535.

$K\rho/T \propto T^2$. The temperatures used do not extend to a sufficiently low range to test this relation. However the extrapolation in Fig. 4, based on a T^2 law, is not inconsistent with the experimental observations.

At high temperatures, $K\rho/T$ approaches a constant value, higher than the classical theoretical value. Mott and Jones[23] show that $K\rho/T$ should have the classical value for temperatures appreciably higher than the Debye characteristic temperature, except for transition metals. The approximations used involve the assumption that $kT \ll \zeta$, where ζ is the Gibbs potential per electron. This is not true for transition metals, in which ζ is very small. Thus in the case of tungsten one should not expect $K\rho/T$ to have the classical value, even at high temperatures. The theoretical calculations have not been carried sufficiently far to predict the correct high temperature value of $K\rho/T$ for a transition metal.

While the results presented are inconclusive in the case of tantalum and not numerous in the case of tungsten, it is believed that the method outlined for the measurement of thermal conductivity of metals is a practical one, especially if it were used in conjunction with measurements of emissivity according to the method of Langmuir and Taylor.[24]

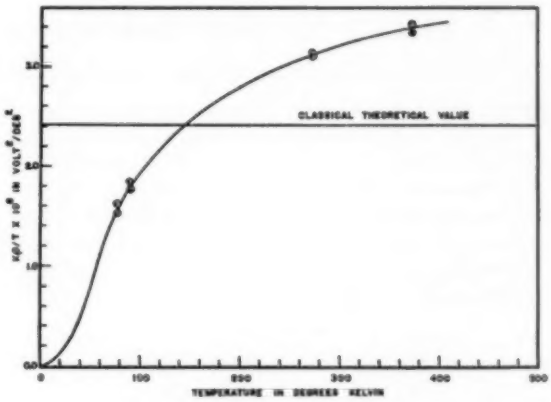

FIG. 4. The Wiedemann-Franz ratio for tungsten.

The author wishes to express sincere thanks to Dr. Walter C. Michels for suggesting the problem and for many helpful suggestions in carrying out the work.

[23] N. F. Mott and H. Jones, *The Theory of the Properties of Metals and Alloys* (Oxford University Press, 1936).

[24] I. Langmuir and J. B. Taylor, J. Opt. Soc. Am. **25**, 321 (1935).

Letters to the Editor

PROMPT publication of brief reports of important discoveries in physics may be secured by addressing them to this department. The closing date for this department is the third of the month. Because of the late closing date for the section no proof can be shown to authors. The Board of Editors does not hold itself responsible for the opinions expressed by the correspondents. Communications should not in general exceed 600 words in length.

Statistical Mechanics of Processes Observed in Cosmic-Ray Phenomena

G. WATAGHIN
University of Sao Paulo, Sao Paulo, Brazil
June 12, 1943

SOME of the processes observed in cosmic rays are obviously irreversible because of the simultaneous or successive creation of many particles, the instability of mesotrons, and the production of neutrinos.[1] We have direct evidence of the successive transformation of the high energy of a primary particle into the energy of many photons and electrons of lower energy (in the cascade showers and in the mesotron showers). Sometimes, in the processes involving emission of neutrinos, an appreciable fraction of this energy escapes any observation.

The statistical laws for such processes are quite different from the usual ones. For some of them only the rate of the irreversible reaction in a given assemblage of particles can be established. At temperatures $T \gtrsim 10^{10}$ degrees ($\kappa T \gtrsim 2mc^2 \sim 10^6$ ev) the thermal equilibrium between photons, electrons, and nuclei will give rise to pair production and radiation processes which we observe in the cascade showers, as well as to processes of "two photons annihilation," and of materialization of two photons.

Let us consider the equilibrium between photons, electrons, positrons, neutrons, protons, and nuclei at $\kappa T > 2mc^2$. Let N_s n_{es} n_{ps} n_{ns} n_{Hs} $n_{As}{}^Z$ be the numbers of photons, electrons, positrons, neutrons, protons, and nuclei of charge Z and atomic weight A, which belong to the momentum-interval p_s to $p_s + dp_s$. We assume the validity of the laws of conservation of charge ($\Sigma_s [n_{ps} + n_{Hs} + Z n_{As}{}^Z - n_{es}$), conservation of energy and conservation of the total number of neutrons and protons. Then, if we indicate by

$$g_s = G(p_s)\frac{8\pi V p_s{}^2 dp_s}{h^3}$$

the number of quantum states (or eigenvalues of energy) belonging to the sth momentum-interval, we obtain in the usual way[2] a set of expressions of the type:

$$N_s = g_s(e^{\beta h\nu_s} - 1)^{-1}; \quad n_{es} = g_s(e^{-\alpha + \beta E_s} + 1)^{-1};$$
$$n_{Hs} = g_s(e^{\alpha + \gamma + \beta E_{Hs}} + 1)^{-1} \quad \ldots \qquad (I)$$

where the factor $G(p_s)$, appearing in g_s, is equal to 1 in the usual quantum mechanics, but is here a function which decreases and vanishes more rapidly than $p_s{}^{-3}$ for values of p_s greater than a critical value $\sim 137mc$.

Let us assume for β and G_s the accepted values $\beta = 1/\kappa T$ and $G_s = 1$. From Planck's formula we find at once that for $\kappa T > E_0 = 10^8$ ev the number N_1 of photons having $h\nu > E_0$ is greater than the number N_2 of photons having $h\nu < E_0$: $N_1/N_2 \sim 4.8/y_0{}^2 > 1$ (where $y_0 = E_0/\kappa T < 1$).

This consequence is in contradiction with the irreversibility of the collision processes taking place for high energy photons. From (1) we see how the usual statistical laws could be modified by introduction of $G(p_s)$ in such a way that the total number of quantum states $\Sigma_s g_s$ results finite. This idea is in contrast with the basic assumption of the equal probability of equal regions in the phase space, but agrees with the assumption of the existence of a new supplementary indeterminacy in the region of high relative momenta.[3] Full account of the modification of the statistical formulae (I) and of the commutation relations will be published elsewhere. Here we limit ourselves to the following remarks: In the collision of particles in which many mesotrons are produced and β-ray processes are taking part, the laws of conservation of energy and momentum become uncontrollable at least insofar as "neutrinos" or gravitational reactions escape our observation. It signifies also that our possibility to distinguish usual quantum states and measure eigenvalues is limited. A Lorentz transformation with a parameter $(1-\beta^2)^{-\frac{1}{2}} > 100$ transforms some low energy particles into shower-producing cosmic rays. Thus one must introduce new groups of transformations in order to satisfy the principle of covariancy for cosmic-ray phenomena.[3]

[1] See Phys. Rev., March 1 and 15, 1943. The main reason of irreversibility lies in the fact that the inverse processes involve ternary or multiple collisions. The frequency of these collisions is negligible for any reasonable concentration of heavy particles (even at nuclear densities).
[2] Phil. Mag. [7], **17**, 910 (1934); Comptes rendus **203**, 909 (1935).
[3] Nature **142**, 393 (1938); Comptes rendus **207**, 358 (1938); *ibid.* **207**, 421 (1938).

Burst Production in a Gas Volume

M. SINHA
Bose Institute, Calcutta, India
May 15, 1943

ONE of the most interesting cosmic-ray phenomena is the production of bursts during the traversal of high energy particles through thick layers of an absorbing medium. Such bursts are usually investigated with the help of a large pressure ionization chamber surrounded by layers of different absorbing materials. The number of ionizing particles created by the burst is estimated from the total ionization produced in the chamber. When the outer shield is of lead of thickness greater than 10 cm, it is assumed that the burst is due to a high energy mesotron which has imparted a large portion of its energy to a knock-on electron or a photon, and either of these two products then starts a cascade process.

In Wilson chamber photographs taken under large thicknesses of lead, these bursts are seen to occur, and they usually emerge from the lead plates placed above or inside the chamber. A photograph is shown (Fig. 1) in which a burst has started inside the gaseous volume of a Wilson chamber. A lead block 17.5 cm thick was placed

above the chamber and another plate 2.2 cm thick inside the chamber. Under the lead block a counter tube arrangement similar in many ways to that used by Bothe and Schmeiser[1] for the investigation of narrow angled penetrating showers, was used to control the expansion of the Wilson chamber. The latter is placed between the upper and lower set of counters.[2] The remarkable thing about the burst is the very short distance, about 2-cm length, in which it has developed, considering that for the gas oxygen with which the chamber is filled the characteristic length is 340 m. Another notable feature is that the particles appear to emerge in all directions, though the majority of them are ejected in a downward direction which is the direction of the incident particle. The core of the burst has again produced a large cascade shower in the lead plate inside the chamber, and it presumably contains a number of high energy electrons and photons. The burst produced must be due to a high energy charged

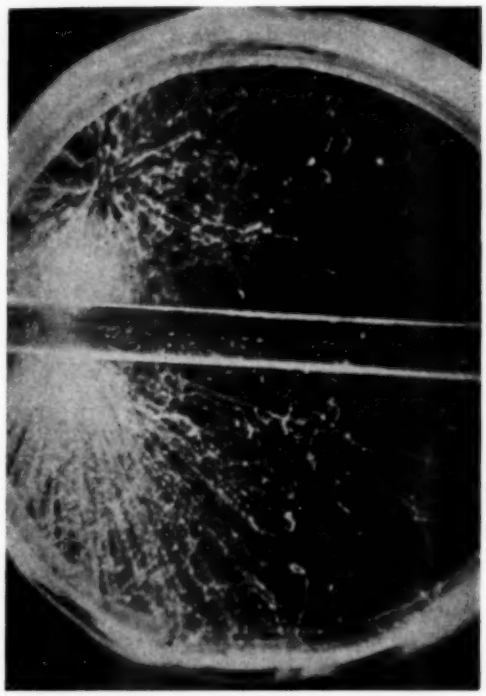

FIG. 1. Photograph of a burst within Wilson chamber.

penetrating particle, presumably a mesotron, which after traversing the lead, either itself or by means of knock-on electron trips the upper counter and produces the burst inside the chamber.

Three different explanations of the origin of this burst are possible. It is due to (1) a cascade process representing an extreme type of fluctuation effect, (2) the simultaneous generation of a large number of high energy electrons, (3) an explosion process of a type envisaged by Heisenberg, about whose mechanism nothing definite can be said. The occurrence of such large multiplication within a short length has been observed in photographic emulsions exposed to cosmic radiation at high altitudes. They usually start from large grains of silver bromide crystals of diameter up to 10μ (equivalent to 3.5-cm air length), and the tracks emerge in all directions, in numbers up to 40. Taylor[3] calls them clusters, to distinguish them from stars—which diverge from points within limited angles, and the number tracks do not exceed seven. Similar clusters have been observed by Miss Bibha Choudhuri of this Institute.

The author desires to record his indebtedness to Dr. R. L. SenGupta for help in constructing the apparatus.

[1] Schmeiser and Bothe, Ann. d. Physik **32**, 161 (1936).
[2] Sinha and SenGupta, Ind. J. Phys. **16**, 129 (1942).
[3] Taylor, Fraser, and Dhabolkar, Nature **141**, 472 (1938).

Corona in Gases at Low Pressures

J. D. CRAGGS AND J. M. MEEK
High Voltage Laboratory, Metropolitan-Vickers Electrical Co. Ltd., Manchester, England

August 24, 1943

THE breakdown processes in air at atmospheric pressure have been studied by Loeb and his collaborators,[1-3] who have clearly differentiated between the forms of corona discharge which take place at voltages lower than the spark breakdown voltage. The corona at pressures <3 cm Hg does not appear to have been studied, and experiments started over a year ago indicate that forms of corona discharge persist at very low pressures (<1 mm Hg) and that the results differ widely with the nature of the gas. Since that time, Weissler's paper[4] has appeared in which, with different techniques and higher pressures, he has clearly shown that various gases, as would be expected, show fundamental differences in their corona discharges. Our results are largely in agreement with those of Weissler, but several new effects have been observed.

The technique adopted, i.e., the use of 50 c.p.s. a.c. in preference to the d.c. used by the above authors, appears to have important advantages in that positive and negative corona are shown together, and the corona is synchronized with the supply voltage. Thus, where rapidly recurrent streamers are observed, they occur at random for d.c. observations and give a confused pattern on an oscillograph with a continuous time sweep, whereas on a.c. they are observed near the crest of each half-cycle. It was necessary to insure that the use of a.c. did not by itself introduce misleading effects, and comparative experiments on d.c. were therefore performed. Any possible effects caused by the sign reversals on alternate half-cycles can be eliminated by the use of half-wave rectified a.c.

A further improvement in technique has been effected by the use of a two-beam oscillograph which enables the tube current to be observed simultaneously with either the tube voltage or a time-calibrating wave.

Owing to present circumstances, facilities for purifying gases were not available, but the impurities present in the commercial-grade gases used are known approximately. We intend to improve the vacuum technique so that the effect of impurities may be further studied.[4] However, the use of different impure gases is of practical importance

and leads to widely differing results which are of considerable interest. We hope to extend this work to pressures of one atmosphere and higher, where it would be difficult to obtain pure gases in sufficient quantities.

Figure 1 is a reproduction of oscillograms which show some of the variations in results. All the effects are accurately reproducible. The figure was taken on a 1/100 second sweep; the voltage rises from zero to its maximum value and then falls to zero again, once for each sweep of either polarity. The maximum corona current corresponds approximately to the maximum tube voltage. Figure 1A shows the current flowing on the positive and negative half-cycles, 1180 volts crest, for a 1-cm gap between a 0.16 cm diameter hemispherically-ended tungsten point and a molybdenum plane in air at 0.57 cm Hg pressure (Apiezon oil manometer). Corona onset was at 670 volts negative and 970 volts positive. The current discontinuities reveal the presence of streamers on both polarities. With a 1-cm gap between a sharp tungsten point and a molybdenum plane in hydrogen at 0.14 cm Hg and an applied voltage of 635 volts crest, the streamers are present on the positive half-cycle only (Fig. 1B), whereas on the negative half-cycle the current is continuous (corona onset at 430 volts negative, 545 volts positive). No streamers are present for a discharge in oxygen at 1.52 cm Hg pressure in a copper cathode Geiger counter, of wire diameter 0.127 cm (tungsten) and cylinder diameter 2.54 cm, at

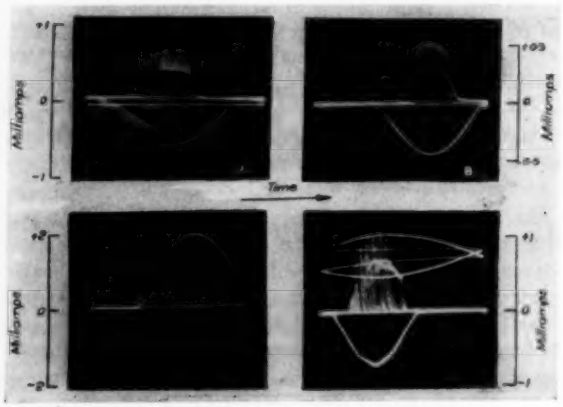

FIG. 1. Reproductions of oscillograms.

2330 volts crest (corona onset at 1370 volts negative, 1190 volts positive), when the discharge is disruptive on both polarities, as seen in Fig. 1C. The form of the discharge in the same counter when filled with CCl_2F_2 at a pressure of 0.69 cm Hg, and a 50-cycle timing wave, are shown in Fig. 1D (1560 volts crest). Many positive streamers are seen to be present whereas with a negative wire, the current is more or less continuous with indications of streamers near the crest (corona onset at 1050 volts negative, 1380 volts positive).

A detailed analysis of the results will be published in the near future.

We wish to thank Dr. A. P. M. Fleming, Director, Research and Education Departments, Metropolitan-Vickers Electrical Co. Ltd., for permission to publish this note.

[1] L. B. Loeb and A. F. Kip, J. App. Phys. **10**, 142 (1939).
[2] A. F. Kip, Phys. Rev. **54**, 139 (1938); **55**, 549 (1939).
[3] G. W. Trichel, Phys. Rev. **54**, 1078 (1938); **55**, 382 (1939).
[4] G. L. Weissler, Phys. Rev. **63**, 96 (1943).

The Multiple Production of Secondary Cosmic-Ray Particles in the Lower Atmosphere

VICTOR H. REGENER
Ryerson Physical Laboratory, University of Chicago, Chicago, Illinois
August 31, 1943

A DETAILED study of secondary processes of the cosmic radiation was made at altitudes between sea level and 14,000 feet. The instrument consisted of 125 counter tubes placed above and between six layers of lead *A* to *F* (Fig. 1), which are 1, 5, 5, 5, 9, 10 cm thick,

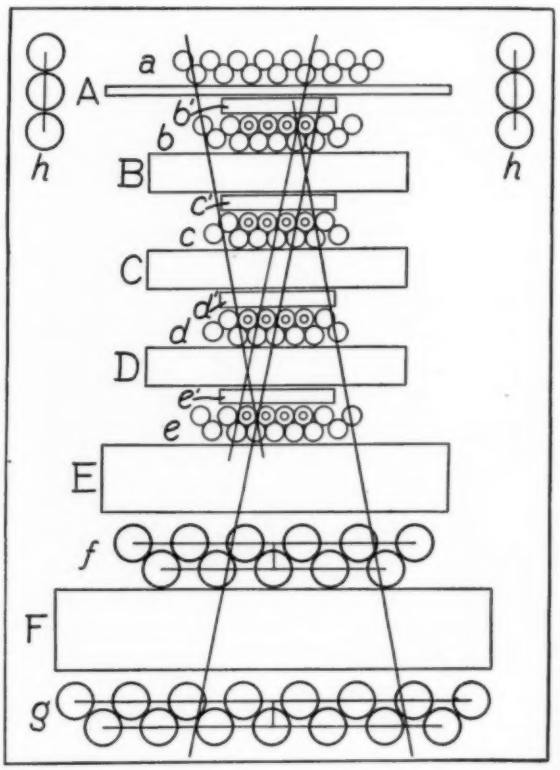

FIG. 1. Schematic diagram of the arrangement of counters and absorbers.

respectively. The counter tubes of groups *a* to *e* are individually connected to one indicating neon lamp each. All neon lamps are arranged on a panel in places corresponding to the actual positions of the counter tubes to which they belong. A "master pulse" flashes a neon lamp for the duration of 0.5 sec., provided that a particle coincident with the master pulse (resolving time 10^{-5} sec.) traversed the counter tube to which the neon lamp belongs. The ring-marked counters and six counters in each group

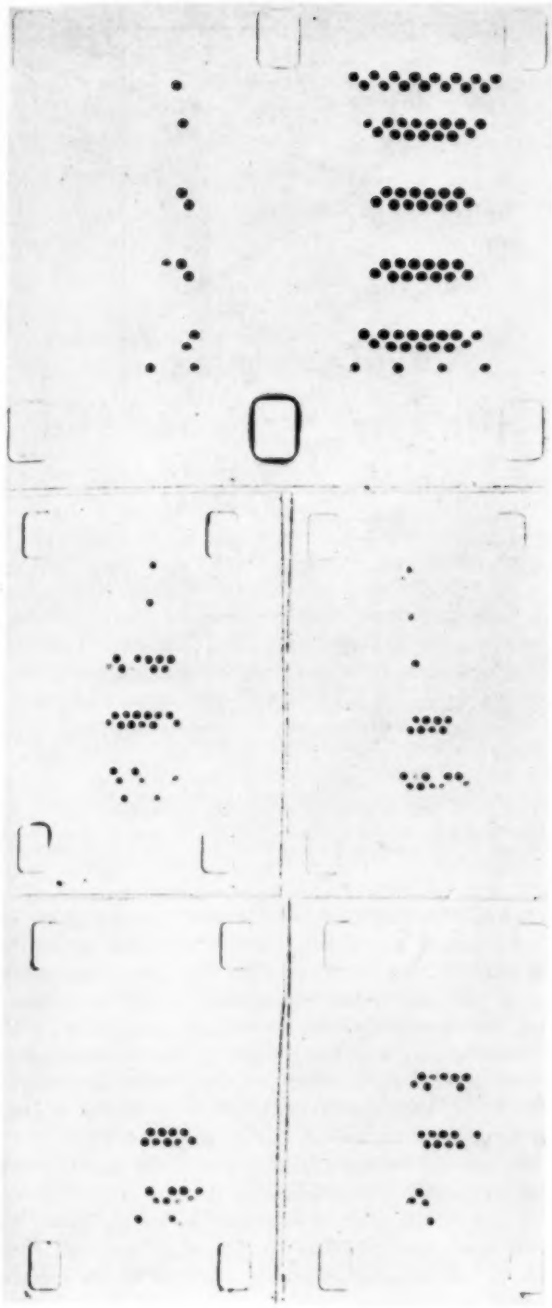

FIG. 2. Photographs of the neon lamps enlarged from 16-mm film. The pictures in the center and at the bottom are typical for the multiple production process.

b' to e' (oriented at a right angle with the other counters) set off a master pulse whenever a vertical particle penetrates at least *one* of the absorbers B, C, or D. The master pulse also operates the automatic camera. Figure 2 (top, right) shows a photograph taken when all neon lamps were flashed artificially. The four neon lamps at the bottom of this picture are connected to counter groups h, f, g, and to an additional tray of counters placed about two meters away from the instrument.

Altogether, 200,000 pictures were taken on Mt. Evans in September, 1941, and between Climax, Colorado (11,500 feet), and Chicago, in January, 1942. Besides single mesotrons (Fig. 2, top, left) and cascade showers, two distinct processes of production of secondary particles were observed.

In the first process, a neutral radiation produces in the top layer A of 1-cm lead *single, non-multiplying* particles mostly of a range below 5-cm lead. A detailed account of this process is given in the following letter.[1]

In the second process, the produced particles invariably come in showers; one-tenth of the observed production processes are initiated by penetrating *ionizing* rays, nine-tenths by penetrating *non-ionizing* rays. Figure 2 (center and bottom) gives typical examples. Production processes initiated by penetrating neutral particles have been reported previously.[2]

Absorbers of 5-cm iron, aluminum, carbon, and paraffin were alternated with lead in positions B and C at Climax. The ratio of the frequency of production in B to the frequency of production in C affords a rough determination of the cross section of the process.[3] The hourly rate (the standard error averages 10 percent) of the production in B and C and the cross sections per nucleus in 10^{-24} cm^2 are:

	Pb	Fe	Al	C	H	Paraffin
B	13.5	18.5	26	20		20
C	10.5	6	15	12		8
Cross Section	1.5	2.7	1.8	2.0	1.5	

The cross sections of light nuclei observed here agree with those observed with fast neutrons as projectiles, but no increase of cross section is observed for heavy nuclei. Processes initiated by ionizing rays show approximately the same cross section, multiplicity, and energy as those initiated by non-ionizing rays. Neutrons and protons may be the particles initiating these processes. The multiple production of mesotrons by ionizing, non-shower-producing particles (protons) reported by Schein, Jesse, and Wollan[4] and discussed by Carlson and Schein[5] may well be identical with the present process (the cross section of the latter is an order of magnitude larger than the one estimated by Carlson and Schein).

The range of the produced particles averages 10-cm lead for those produced in light materials and increases up to 30-cm lead for particles produced in lead. With the data available so far, an unambiguous conclusion as to the significance of this result cannot be reached.

The altitude dependence of the production in lead was measured between Climax and Chicago. The rate of production drops rapidly below Climax to one-third at Idaho Springs (8600 feet), to one-fourth at Denver (5300 feet), and to one-seventh at Chicago. The production cross section for nitrogen and oxygen to be expected from our data would lead to an absorption ten times faster than this. We must therefore assume that these particles are themselves of secondary origin and that they might be identified as neutrons and protons produced by the photons of the soft component.[6]

The writer wishes to express his deep appreciation to

Dean A. H. Compton for the inspiring encouragement and for the generous support given to this work. The writer is indebted to Professor J. C. Stearns of the University of Denver, to Dr. W. O. Roberts of Harvard College Observatory, to Dr. W. M. Powell of the University of California, and to the Climax Molybdenum Company, for their generous assistance rendered in Colorado; to Mr. R. E. Lapp for his untiring help during the winter expedition, and to Dr. M. Schein for enlightening discussions of the results.

[1] V. H. Regener, Phys. Rev. **64**, 252 (1943).
[2] F. R. Shonka, Phys. Rev. **55**, 24 (1939); M. Schein, E. O. Wollan, and G. Groetzinger, Phys. Rev. **58**, 1027 (1940); B. Rossi and V. H. Regener, Phys. Rev. **58**, 837 (1940); V. H. Regener and B. Rossi, Phys. Rev. **59**, 113 (1941).
[3] Since it is rather certain that we have to deal with the production of rays of various energies, the assumption has been made that the cross section for the production process is in first approximation independent of energy.
[4] M. Schein, W. P. Jesse, and E. O. Wollan, Phys. Rev. **59**, 615 (1941).
[5] J. F. Carlson and M. Schein, Phys. Rev. **59**, 840 (1941).
[6] S. A. Korff and E. T. Clarke, Phys. Rev. **61**, 422 (1942); see also reference 1.

Absorption Curve and Production of Slow Cosmic-Ray Protons at Low Altitude

VICTOR H. REGENER
Ryerson Physical Laboratory, University of Chicago, Chicago, Illinois
August 31, 1943

WITH the apparatus described in the preceding letter,[1] the production of single, non-cascade-producing particles by a non-ionizing radiation was investigated. Also, statistics were made of pictures showing ordinary mesotrons and protons stopped by 20-cm lead.

The events represented by the absorption curves in Fig. 1 are those where a particle never showed multiplication upon traversing one cm of lead and successive absorbers. The curves are average curves evaluated from measurements taken on different days with different absorbing materials. A constant factor close to unity was applied to some of the original curves in order to account for changes in intensity due to meteorological conditions.

The upper curve gives the total hourly rate of cosmic rays at Climax, Colorado, (11,500 feet), on a mass scale, with the exclusion of what is generally termed the "soft component" with its multiplicative character. The slope of this curve indicates the well-known presence at this altitude of low energy particles which must have been produced close to the apparatus in the atmosphere. The production of mesotrons by non-ionizing rays as previously reported[2] must be partly responsible for the presence of these particles.

With the apparatus here used a production process was observed which seems to account well for the particles responsible for the steep drop of the absorption curve below 5-cm lead. In the top layer of 1-cm lead and *not* at larger absorber thicknesses, single, non-multiplying particles are produced by non-ionizing rays. The lower curve of Fig. 1 gives the absorption curve of these particles measured after they emerge from the layer of lead in which they are produced. The data for the thickness of absorber include 1-cm lead for the producing layer.

Particles with the short range observed here were detected on Mt. Evans by Powell[3] who identified them in a cloud chamber as protons. There can be little doubt that our particles are identical with the ones observed by Powell and are therefore protons. Nielsen and Powell[4] recently reported the absence of slow mesotrons on Mt. Evans. Paraffin, with its content of free protons, should absorb our protons stronger than mass-proportional. Indeed, the intensities measured below paraffin (Fig. 1) are lower and seem to drop off faster than the others.

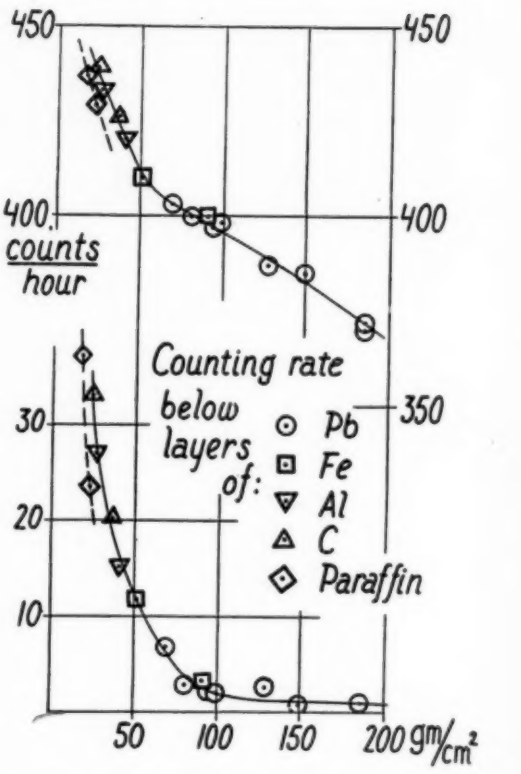

FIG. 1. Above: An absorption curve of non-multiplying cosmic rays at Climax (11,500 feet). Below: An absorption curve of slow protons produced by non-ionizing rays in 1-cm lead at Climax. The experimental error is to be inferred from the scattering of the values about the curves.

The photon seems to be the most likely agent of non-ionizing character responsible for this production process. The case for the photon is supported by the rather frequent occurrence of events where a single, non-multiplying particle can be seen emerging from under an energetic cascade shower.

No cross sections can be computed because the top layer of 1-cm lead saturated the process. When 1-cm iron was substituted for the lead the production was of the same frequency, indicating saturation also in 1-cm iron.

The altitude dependence of this process was measured only for events where particles penetrating more than 6-cm lead (including 1 cm for the producing layer) were produced. The hourly rate was at Climax (11,500 feet) 7, at Idaho Springs (8600 feet) 28, at Denver (5300 feet) 25, and at Chicago 5, with an error of about 15 percent in each case. Because only processes at the high energy end of the energy

distribution are selected here, one cannot conclude that there is a general maximum of this production process at an altitude as low as 8000 feet. But at lower altitude, the center of gravity of the energy distribution is definitely shifted to higher energies.

[1] V. H. Regener, Phys. Rev. **64**, 250 (1943).
[2] M. Schein and V. C. Wilson, Phys. Rev. **54**, 304 (1938); M. Schein, W. P. Jesse, and E. O. Wollan, Phys. Rev. **57**, 847 (1940); see also reference 1 and the papers cited there.
[3] W. M. Powell, Phys. Rev. **61**, 670 (1942).
[4] C. E. Nielsen and W. M. Powell, Phys. Rev. **63**, 384 (1943).

Production of Secondaries in Paraffin by Primary Cosmic-Ray Particles

MARCEL SCHEIN, MARIO IONA, JR., AND JULIUS TABIN
Ryerson Physical Laboratory, University of Chicago, Chicago, Illinois
September 6, 1943

TWO high altitude balloon experiments were recently carried out for the purpose of measuring the secondary radiation which is generated in paraffin by penetrating cosmic-ray particles. Five different 4- and 5-fold coincidence circuits were used in each of these flights. Figure 1 shows the arrangement of the Geiger-Müller counters used in the flight of July 31, 1943. The 4-fold coincidence circuit *ABCD* measured the vertical intensity of cosmic radiation penetrating 8 cm of lead. ("*A*" consists of 3 counters connected in parallel.) The 5-fold set *EFACD* registered showers of 2 or more particles originating in the air above the apparatus. *GBCD* and *LBCD* measured the production of one or more particles in a layer of paraffin of 5 and 10 cm, respectively. Circuit *HKCD* measured the production of two or more particles in 10 cm of paraffin. The coincidences of the various counter sets were recorded by the same method as used in previous balloon experiments by one of the authors (Marcel Schein) in collaboration with W. P. Jesse and E. O. Wollan.[1] The coincidence pulses from the different circuits tripped separate neon lamps. The flashes of these neon lamps were photographically recorded on a sensitive film. Using this method, simultaneous coincidences in several of the counter circuits could be observed easily.

It was found in these experiments that in the upper atmosphere the circuits *GBCD*, *LBCD*, and *HKCD* were frequently tripped in coincidence with circuit *ABCD*. This means that at high altitudes a large fraction of the penetrating ionizing rays are accompanied by secondaries produced in the paraffin. A similar action of the penetrating component at sea level has not been found as yet. That the secondaries below the paraffin did not originate from the air above the apparatus is demonstrated by the fact that less than 3 percent of the coincidences *ABCD* were accompanied by a coincidence *EFACD*. This amounted to less than 7 percent of the multiples observed below the paraffin.

At an altitude corresponding to a pressure of 17 cm Hg, 15 percent of the vertical penetrating rays (*ABCD*) were accompanied by particles through any of the counters *G* and 35 percent by particles passing through any of the counters *L*. Correcting for the difference in solid angle between the counter set for the vertical penetrating rays and the counter sets for the radiation which produces the secondaries in paraffin one can say that 10 percent of the penetrating rays are accompanied by secondaries below 5 cm of paraffin and 20 percent below 10 cm of paraffin. The number of particles registered in circuit *HKCD* (two or more particles necessary for tripping this circuit) in coincidence with *ABCD* is considerably smaller than that in *LBCD*, which definitely shows that the secondaries are emitted in the forward direction with a small angular spread.

At higher altitudes similar measurements were carried out with a counter arrangement of slightly different geometry. The number of secondaries below the paraffin were measured up to an altitude corresponding to a pressure of 5.0 cm Hg. It was found that at a pressure of 6 cm Hg, 25 percent of the penetrating component is accompanied by secondaries below the paraffin, and that as many as 50 percent of the penetrating rays produce secondaries in 10 cm of paraffin. (These figures are again corrected for the difference in solid angle for the different counter telescopes.) This large number of secondaries below the paraffin indicates a cross section for production which is of the order of 10^{-24} cm^2, much larger than expected from the average area of the nuclei in paraffin.

Since the number of secondaries produced by mesotrons or electrons in paraffin is very small, it is obvious that the particles producing the large effect, which has been described above, cannot be of electronic or mesotronic nature. However, it seems highly probable that these particles consist of primaries since their number increases very rapidly with altitude close to the top of the atmosphere. It was previously assumed[2] that a multiple production of mesotrons should occur in nuclear collisions if the majority of the

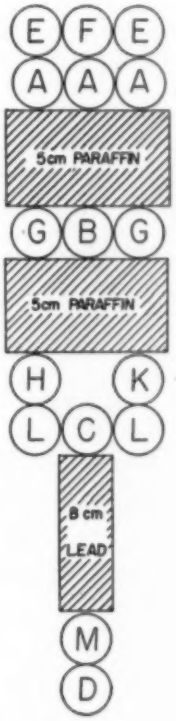

FIG 1. Counter arrangement used in balloon flight.

primaries were protons. This would be in good agreement with the results of the present experiments, which seem to show that at high altitudes part of the penetrating component consists of particles which are accompanied by secondaries after passing through paraffin. The existence of such an effect in paraffin is characteristic for the primary cosmic radiation and is so far the only specific property exhibited by primaries which makes their identification possible.

The evaluation of the present experiments indicates a decrease in proton intensity from the top of the atmosphere (zero pressure) to a pressure of 6 cm Hg by a factor of 2.2 and to a pressure of 17 cm Hg by a factor of 7.5. This decrease leads to an absorption with a cross section of 2×10^{-25} cm^2. This cross section is approximately equal to the area of a nitrogen or oxygen nucleus and shows that the primaries are absorbed in air by nuclear processes.

The authors wish to express their appreciation to Dean A. H. Compton for his continued interest in these experiments.

[1] M. Schein, W. P. Jesse, and E. O. Wollan, Phys. Rev. **59**, 615 (1941).
[2] J. F. Carlson and M. Schein, Phys. Rev. **59**, 840 (1941).

The Origin of Large Bursts Under Thick Shields

R. E. Lapp
Ryerson Physical Laboratory, University of Chicago, Chicago, Illinois
September 9, 1943

A HIGH pressure model C ionization chamber was used to record cosmic-ray bursts containing more than 100 particles. Surrounding the chamber (Fig. 1) was a uniform hemispherical shield of 35 cm of iron equivalent to 12 cm of lead in terms of radiation units. It has been pointed out by several authors that large bursts under 20 radiation units of material are very probably produced by the mesotron component of cosmic rays. Since the high energy mesotrons (energies greater than 10^{10} ev) which produce bursts of more than 100 particles under thick shields show a distribution which is roughly independent of the zenith angle, it is quite necessary to shield the ionization chamber with a uniform hemisphere of material in order to obtain results which are consistent. The scattering of shower electrons in the shielding material likewise makes it imperative that a good geometry be used for the shield.

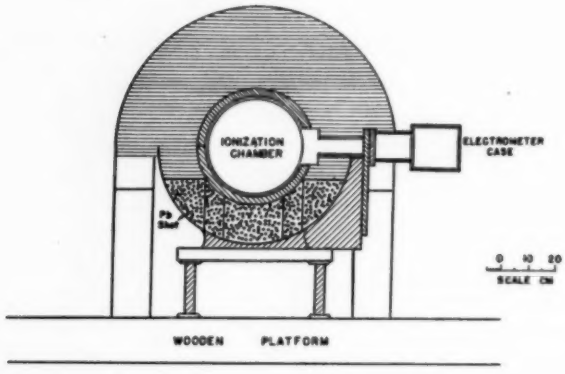

FIG. 1. Details of the 35-cm iron shield.

The burst data in 35 cm of Fe were compared with the burst data of Schein and Gill[1] obtained at sea level with a similar ionization chamber shielded with 12 cm of lead. This comparison shows that the size of large bursts of energy greater than 5×10^{10} ev depends approximately on the square of the atomic number of the shielding material in which the bursts are produced. This is in agreement with the cascade theory of bursts according to which these bursts are described as photon-initiated showers in the chamber shield; the photon initiating the shower is produced by the bremsstrahlung process of the incident mesotron. Christy and Kusaka[2] have shown that for burst production by mesotrons, the bremsstrahlung process is the most probable for mesotrons of energy greater than 5×10^{10} ev.

Recent experiments[3] were carried out in Chicago with an unshielded ionization chamber operated "in coincidence" with 5 sets of G-M counter coincidence units so arranged that each had a high probability of detecting extensive atmospheric (*A* showers) showers. It was found that when there was a negligible amount of heavy material surrounding the ionization chamber practically all the observed bursts of more than 100 particles were accompanied by a simultaneous discharge of the G-M counters. Thus these experiments prove that a large burst observed in the unshielded ionization chamber is in reality the high density region of an *A* shower. According to the theory of *A* showers the dense part (core) of such a shower should contain particles of very high energy. It might therefore be anticipated that at least a large fraction of the core particles in *A* showers should be able to traverse considerable thicknesses of heavy material. The amount of material traversed by these core particles should then give a rough measure of their energy. The experiments carried out with 12 cm of lead around the ionization chamber show that only 4 to 7 percent of the bursts are coincident with *A* showers as detected with G-M counters. While there are thus relatively few *A* showers which produce bursts under 12 cm of lead, there is definite evidence that some of the *A* showers have cores containing particles which traverse 12 cm of lead. An electron or photon must have more than 10^{10}-ev energy in order to traverse 12 cm of lead and appear below that thickness of material as a single particle; if it is to traverse this material and emerge below it with a multiplication of 100 particles, it must have an energy several times 10^{11}. The experiments with the unshielded chamber[3] have shown that *A* showers have particle densities in the core up to 30,000 particles per square meter. If one is to interpret the present results correctly, one must assume that at sea level the great majority of the particles in the core of an *A* shower producing bursts under 12 cm of lead have less than about 10^{11}-ev energy.

Having thus obtained experimental evidence for the nature of the bursts both for the unshielded case and for the 12-cm Pb shielded case, it is necessary to investigate the origin of the bursts which occur under an intermediate thickness of shielding material. It is well known from

transition curves that bursts exhibit a maximum frequency at a thickness of shielding material equivalent to about 7 radiation units. These experiments are in progress with a 12-cm iron shield (about 7 radiation units).

[1] M. Schein and P. S. Gill, Rev. Mod. Phys. 11, 267 (1939).
[2] R. F. Christy and S. Kusaka, Phys. Rev. 59, 414 (1941).
[3] R. E. Lapp, Phys. Rev. 64, 129 (1943).

On the Spin of the Mesotron from Burst Measurements

R. E. LAPP
Ryerson Physical Laboratory, University of Chicago, Chicago, Illinois
September 9, 1943

IN an accompanying Letter,[1] it has been pointed out that the large bursts observed under thick (i.e., 20 radiation units) shields of heavy material are chiefly produced by mesotrons. The contribution of A showers to these bursts is of the order of 4 to 7 percent of the total burst frequency and for the purposes of this discussion, can be neglected. Through the generous cooperation of Dr. Jno. A. Fleming of the Carnegie Institution, the extensive burst data obtained at the Cheltenham Cosmic-Ray Station (72 meters elevation) were made available to the writer. These data were obtained with a Carnegie model C ionization chamber shielded with a uniform layer of lead shot equivalent to a solid 10.7-cm lead shield. From an analysis of the data, an integral size-frequency distribution curve was constructed as shown by the experimental points in Fig. 1. The large amount of data available at Cheltenham allows for a small statistical error for bursts containing even 1000 or more particles; the accuracy of the experimental points is illustrated by the small statistical error drawn for each point. Here the absolute burst frequency N (number of bursts greater than size S per square cm per sec.) is plotted against the product βS where β is the critical shower energy characteristic of the shielding material, and S is the size of the burst in number of particles. On the same graph, three additional curves have been plotted; these are the theoretical curves for burst production by spin 0, ½, and 1 mesotrons, respectively, as calculated by Christy and Kusaka.[2] It is seen that the experimental data are apparently in excellent agreement with the theoretical spin 0 curve. However, certain factors[3] which enter into the theory possibly introduce an uncertainty into the theoretical results so that it is not certain at present whether spin ½ can be eliminated from consideration. For example, the present agreement between theory and experiment is obtained on the basis of an assumed mesotron mass of 177 m_e (m_e=mass of the electron); however, calculation shows that the mesotron mass of 230 m_e would yield a theoretical curve for spin ½ which would be in fair agreement with the burst data.

While it does not seem possible to distinguish between spin 0 or ½ on the basis of the present data, it is possible to state that the existence of a spin 1 mesotron at sea level is definitely ruled out by the experimental evidence. The marked increase in frequency of large bursts as a function

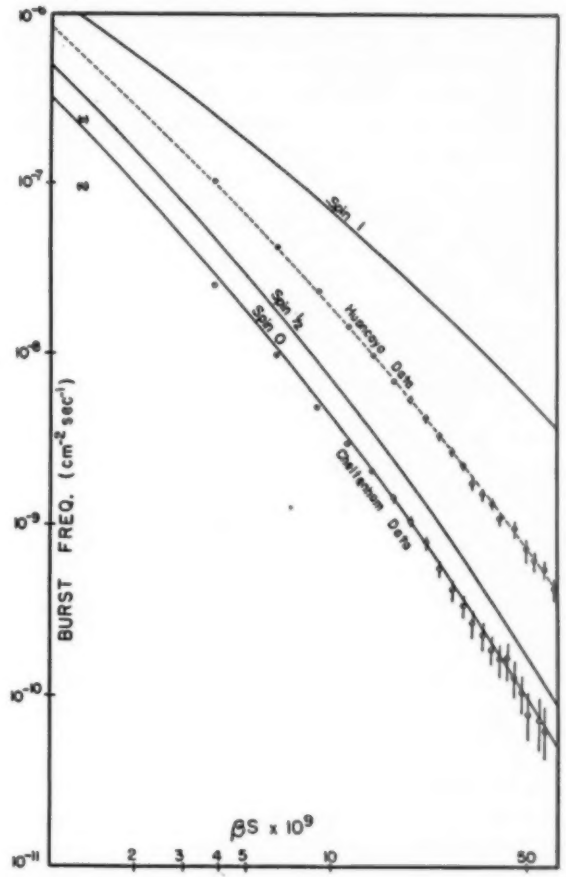

FIG. 1. Integral size frequency distribution curves. The burst frequency per square cm per second is plotted against the product of S where β is the critical shower energy of the shielding material, and S is the number of particles in the burst. The curves labeled spin 0, ½, and 1 are the theoretical curves for burst production by mesotrons as given by Christy and Kusaka.

of altitude has been pointed out by Schein and Gill.[4] An analysis similar to that obtained from the Cheltenham burst data has been carried out for the burst data obtained at the Carnegie station at Huancayo, Peru (3350 meters). From the analysis a size-frequency distribution curve was plotted as shown in Fig. 1. Since the mesotrons giving rise to the bursts under thick shields at Huancayo were due to mesotrons of the same kind as are present at sea level, there should be no increase in the burst frequency with increasing altitude, for the high energy mesotrons are absorbed very little in traversing the atmosphere between Huancayo and sea level and are therefore just as numerous at sea level as at high altitude. There are two explanations possible for this observed increase with altitude. The first and more probable explanation is that at high altitude the cores of A showers (extensive atmospheric showers) penetrate 12 cm of lead and produce the majority of these bursts. This explanation is given additional credence by the evidence presented in the accompanying letter. Furthermore, the marked increase of A showers with altitude as found by Auger and Hilberry indicates that the increase in burst

frequency could be due to this phenomenon. The other explanation[5] is that spin 1 mesotrons are present at higher altitudes in addition to spin 0 $-\frac{1}{2}$ mesotrons, and these give rise to the observed bursts. One assumes that the spin 1 mesotrons are of the fast decaying type, and only the highest energy ones reach sea level.

[1] Phys. Rev. **64**, 254 (1943).
[2] R. F. Christy and S. Kusaka, Phys. Rev. **59**, 414 (1941).
[3] This point is discussed in an accompanying Letter to the Editor by S. Kusaka, Phys. Rev. **64**, 256 (1943).
[4] M. Schein and P. S. Gill, Rev. Mod. Phys. **11**, 267 (1939).
[5] H. Snyder, Phys. Rev. **59**, 1043 (1941). R. F. Christy and J. R. Oppenheimer, Phys. Rev. **60**, 159 (1941).

The Effect of Radiation Damping on Burst Production

SHUICHI KUSAKA
Department of Physics, Smith College, Northampton, Massachusetts
September 20, 1943

IN a recent paper Chakrabarty[1] has repeated the calculation of Christy and the present author[2] on the frequency of burst production by mesons and concludes that the comparison with the experimental data shows that the meson has spin 1, in contradiction to our result that the spin is 0 or 1/2. He states that the reasons for the different conclusion obtained are (1) the difference in the form of the fluctuation assumed, (2) the rough values used for the average number of particles produced in a cascade shower by an energetic electron or photon, and (3) the consideration of the effect of radiation damping on the cross section for bremsstrahlung of spin 1 mesons.

Chakrabarty used the Poisson distribution in preference to the fluctuation formula obtained on the Furry model which we used, and the recent work of Scott and Uhlenbeck[3] indicates that the former is nearer the truth. However, this point does not introduce any appreciable difference since we found that the effect of the fluctuation on the frequency of burst production on our model is to give just about twice as many bursts as calculations based on the assumption of no fluctuation. The Poisson distribution gives smaller fluctuations than the Furry model, and hence it would give results intermediate between the two. Moreover we recognized the fact that the Furry model gave too great a value for the fluctuation and corrected for this by reducing the burst production probability by a factor of $\sqrt{2}$. Thus the difference introduced by the use of the Poisson distribution should at most be a factor of about $\sqrt{2}$.

The second difference is due to the fact that we used Serber's[4] calculation on the cascade theory while Chakrabarty used the recent results obtained by Bhabha and himself.[5] The latter gives for the average number of particles a value smaller than the former by a factor ranging from 1.5 to 2.1 for initial energy between 10^{10} and 10^{12} ev.

Most of the deviation between the two calculations arises from the third difference. Chakrabarty based his calculation on the formula for bremsstrahlung cross section of spin 1 meson with radiation damping obtained by Wilson,[6] but it has now been found that this formula is in error, and hence his conclusions are invalid.

Formula (52) in Wilson's paper for the cross section for scattering of light quantum by a meson with spin 1 initially at rest is incorrect and should read instead[7]

$$\varphi_0=\frac{5\pi}{36}\left(\frac{e^2}{\mu}\right)^2\frac{k_0}{\mu}\,(k_0>>\mu),$$

where k_0 is the initial energy of the light quantum. When the calculation of the cross section for bremsstrahlung is carried out in the same way by using the method of the virtual quanta and Wilson's approximate way of taking into account the effect of radiation damping, the result is

$$\varphi(\epsilon)d\epsilon=\frac{5Z^2\alpha}{144}\left(\frac{e^2}{\mu}\right)^2(2-2\epsilon+7\epsilon^2)Gd\epsilon,$$

where $\alpha=1/137$ is the fine structure constant, ϵ is the fraction of the initial energy, E_0, of the meson emitted in the form of a light quantum, and

$$G=\int_1^{\mu R}\frac{dy}{y}\int_{y\mu/E_0}^{\infty}\frac{dx}{x+(5/288)\alpha^2},$$

R being $a_0Z^{-\frac{1}{3}}=(\alpha mZ^{\frac{1}{3}})^{-1}$ and where we are using units in which $\hbar=c=1$. The effect of the radiation damping appears in the term $(5/288)\alpha^2$ in the denominator. It is negligible for energies such that $(E_0/\mu)^2<<(288/5\alpha^2)$, and its effect becomes appreciable only for energies of the order $E_0/\mu\sim 10/\alpha=1370$. In the limit of very high energies, $E_0/\mu>>10\mu/\alpha^2mZ^{\frac{1}{3}}$, the cross section becomes

$$\varphi(\epsilon)d\epsilon=\frac{\pi}{12}\left(\frac{5}{2}\right)^{\frac{1}{2}}Z^2\left(\frac{e^2}{\mu}\right)^2(2-2\epsilon+7\epsilon^2)\log\left(\frac{137\mu}{Z^{\frac{1}{3}}m}\right)d\epsilon.$$

It must be noted here that there is an uncertainty in the numerical coefficient of the order unity due to the averaging over the angles which was necessary in order to compute the effect of the damping. The above result is essentially the same as that obtained by Gora,[8] and agrees with the general conclusions of Landau[9] and Oppenheimer[10] that the cross section obtained by the perturbation theory should be valid up to energies of the order 137μ. Hence our calculation in which we cut off the frequency integral at 137μ should at least give the lower limit of the burst production by spin 1 mesons.

The improvements in the treatment of the fluctuation and in the cascade theory mentioned above should change our results at most by a factor of 3, and our conclusion that the spin of the meson can be 0 or 1/2, but not 1 is still valid. Comparison of Chakrabarty's results for spin 0 and 1/2 with ours shows that his theoretical burst frequencies are smaller by a factor of about 5. We both used the same value for the meson mass, 177 m, but Chakrabarty fails to mention the value he used for β, the critical energy in the cascade theory, and the additional difference may be due to this.

It should be emphasized again that these calculations for the burst production give the *minimum* estimates in which only the electromagnetic interaction of the meson with the atomic nuclei is considered. Hence it is possible to rule out particles for which our calculations give burst production frequencies greater than the observed values,

but it is not possible to do the same for particles which give smaller burst production.

It is a pleasure to thank Professor W. Pauli for valuable discussions on this subject.

[1] S. K. Chakrabarty, Ind. J. Phys. **16**, 377 (1942).
[2] R. F. Christy and S. Kusaka, Phys. Rev. **59**, 414 (1941).
[3] W. T. Scott and G. E. Uhlenbeck, Phys. Rev. **62**, 497 (1942).
[4] R. Serber, Phys. Rev. **54**, 317 (1938).
[5] H. J. Bhabha and S. K. Chakrabarty, Proc. Ind. Acad. Sci. **A15**, 464 (1942).
[6] A. H. Wilson, Proc. Camb. Phil. Soc. **37**, 301 (1941).
[7] Cf. formula in row IVA of Table IIIA on p. 230 of W. Pauli, Rev. Mod. Phys. **13**, 203 (1941).
[8] E. Gora, Zeits. f. Physik **120**, 121 (1943).
[9] L. Landau, J. Phys. USSR **2**, 483 (1940).
[10] J. R. Oppenheimer, Phys. Rev. **59**, 462L (1941).

The Multiple Production of Penetrating Particles by Cosmic-Ray Protons and Neutrons

WAYNE E. HAZEN
Department of Physics, University of California, Berkeley, California
September 21, 1943

IN a recent paper, Hamilton, Heitler, and Peng[1] have presented the results of calculations for the probability of mesotron production in close nuclear encounters by protons or neutrons. They predict a cascade process for the production of mesotrons in which the incident proton loses energy very rapidly until its energy has fallen to 10^9 ev. For example, a proton with energy 10^{10} ev should produce 3.3 mesotrons in 5 cm of lead, and a proton with energy 10^{11} ev should produce 11 mesotrons in 20 cm of lead. In other words, one mesotron should be produced in roughly every two centimeters of lead. Previously, it has been customary to hypothesize simultaneous production of several mesotrons.

In a cloud chamber containing eight 0.7-cm lead plates[2] operated at 10,000 feet, no events were observed of the cascade type mentioned in the preceding paragraph. On the other hand, four photographs were obtained that showed multiple production, apparently in a single event, of high velocity penetrating particles. The expected number of high energy protons, which are presumed to produce the events, can be estimated from the information given by Hamilton, Heitler, and Peng.[1] Since the number of high energy protons varies as the inverse cube of the depth in the atmosphere, there should be three times as many energetic protons at 10,000 feet as at sea level. The number of penetrating particles increases by a factor of two and hence the relative abundance of energetic protons should increase by a factor of 1.5. Now since 1/12,000 of the rays at sea level produce showers of penetrating particles,[3] 1/8,000 of the particles at 10,000 feet should produce such showers. In the present experiment 13,000 tracks of penetrating particles were observed, and one would therefore expect to observe one or two showers of penetrating particles. As previously mentioned, there did occur four events in which the multiple production in a single event of penetrating particles with range greater than four lead plates was observed. These particles were still traveling with velocity $\backsimeq c$ when they passed out of the chamber, and thus it is possible that they had sufficient energy to produce the penetrating type of shower observed by Janossy.[3]

The showers of penetrating particles were produced both by ionizing and by non-ionizing rays just as in the observations of Janossy. None of the four pictures showed electron showers associated with the penetrating shower. However, this fact does not necessarily indicate lack of association with an Auger shower since there is a probability of at least 1/4 that the cloud chamber was located in a region surrounded by shower particles but itself untouched by shower particles.[4] Janossy[3] concluded that all the penetrating showers observed with no absorber above the first counters were parts of Auger showers, whereas less than 1/3 were associated with Auger showers when 1.8 cm of lead was placed above the first counters; the latter arrangement was comparable with that used by the author.

There does not appear to be any direct experimental evidence for a cascade production of penetrating particles. On the other hand, several cases of multiple production of energetic penetrating particles in a single event (or a cascade confined to a few millimeters thickness of lead) have been photographed both by the author and by other observers.

[1] Hamilton, Heitler, and Peng, Phys. Rev. **64**, 78 (1943).
[2] W. E. Hazen, Phys. Rev. **64**, 7 (1943).
[3] L. Janossy, Proc. Roy. Soc. **179**, 361 (1942).
[4] See L. Janossy and A. C. B. Lovell, Nature **142**, 761 (1938) as an example.

The Diffraction of X-Rays by Binary Alloys

R. SMOLUCHOWSKI
Research Laboratory, General Electric Company, Schenectady, New York
October 1, 1943

IT is generally assumed that binary alloys, apart from those which show a definite periodicity of atomic arrangement, have the two kinds of atoms distributed among the lattice points at random.

In connection with a study of the various types of deviations of the atomic distributions from the purely statistical one, the effect of atomic arrangement on the x-ray diffraction was investigated. It is assumed that no long range order exists so that the periodicity of the lattice is unchanged. However, the average neighborhood of an atom A is in general different from that of a B atom. This statistical preference of like or opposite atoms to be near to each other can be expressed in various ways. Let us consider an A–B alloy in which there are more B atoms than A atoms and let $\alpha(r)$ be the probability that one of the neighbors at a distance r from an atom A is also an A atom and $\beta(r)$ the probability that one of the neighbors at a distance r from an atom B is an A atom. We define the distribution factor $s=s(r)=\beta(r)-\alpha(r)$; it is equal to zero in a random crystal at all concentrations. There are altogether N atoms, and the concentration of atoms A is c_a and of atoms B is c_b. Then the mathematical expectation of the scattering factor of an atom n at the distance r from an atom A is

$$F_n^{\mathrm{A}}=[c_a-c_b s(r_n)]F_{\mathrm{A}}+[c_b+c_b s(r_n)]F_{\mathrm{B}},$$

and similarly

$$F_n^{\mathrm{B}}=[c_a+c_a s(r_n)]F_{\mathrm{A}}+[c_b-c_a s(r_n)]F_{\mathrm{B}}$$

where F_A and F_B are the atomic scattering factors of the atoms A and B, respectively.

The total scattered intensity is

$$\sum_{m=1}^{N}\sum_{n=1}^{N} F_m F_n \exp\left[ik(r_{mn}\cdot\sigma)\right],$$

where r_{mn} is the distance between atoms m and n, k equals $2\pi/\lambda$, and σ is the difference between the unit vectors along the directions of incident and of scattered radiation.

The evaluation of this sum follows the classical method of diffraction theory and gives the result:

$$Nc_a c_b(F_A-F_B)^2\{1-\sum_{n=1}^{N} s_n \exp\left[ik(r_n\cdot\sigma)\right]\}$$

$$+N(c_a F_A+c_b F_B)^2\sum_{n=1}^{N}\exp\left[ik(r_n\cdot\sigma)\right]. \quad (1)$$

It follows that the distribution factor s_n affects only the diffuse scattering and not the sharp diffraction maxima which are given by the second sum in Eq. (1). For $s_n=0$ the formula reduces to that given by Laue for a statistical crystal. For an A_3B alloy a similar formula was derived for powder method and compared with experiment by Wilchinsky,[1] who used a different distribution factor. The purpose of this calculation was to investigate the general case.

In the first sum in Eq. (1) we can group together members which have the same $|r_n|$, thus the same s_n.

$$\sum_{n=1}^{N} s_n \exp\left[ik(r_n\cdot\sigma)\right]=s_1\sum_{n=1}^{N_1}\exp\left[ik(r_n\cdot\sigma)\right]$$

$$+s_2\sum_{n=N_1+1}^{N_2}\exp\left[ik(r_n\cdot\sigma)\right]+\cdots. \quad (2)$$

These sums do not depend upon the distribution factor, and thus they can be easily calculated for a given lattice depending upon its position with respect to the monochromatic x-ray beam. Each sum contributes a pattern of maxima and minima to the background which has a definite relation to the position of diffraction maxima if there are any. In most cases only the few nearest shells of neighbors, maybe only the first shell, have a large s so that the pattern should be rather simple to analyze.

In the case of powder x-ray diagrams, the sums in Eq. (2) reduce to $(\sin kr\sigma)/kr\sigma$ and give concentric rings around the central spot. Of course, all these patterns are superimposed on a rather rapidly changing intensity of the background due to other factors and may be difficult to identify. A more detailed discussion of these patterns will be given later.

[1] Z. W. Wilchinsky, Phys. Rev. **63**, 223 (1943).